SCARAB:

Development of a Rugged, Low-cost, Inspection Class Robotic Platform

M.Sc.(Eng.) Dissertation by THOMAS J. MATHEW

Supervised by TREVOR CLOETE and TRACY BOOYSEN

IN ASSOCIATION WITH

Department of Mechanical Engineering
University of Cape Town

May 2015 – version 1.1

PUBLICATIONS

Some portions of the work in this dissertation have, prior to submission, been published in academic literature. These are:

1. T. Booysen and T. J. Mathew, "The Case for a General Purpose, First Response Rescue Robot," in *Proceedings of the 2014 PRASA, RobMech and AfLaT International Joint Symposium, 2014. [1].*

2. T. J. Mathew *et al*, "The Design of a Rugged, Low-Cost, Man-Packable Urban Search and Rescue Robotic System," in *Proceedings of the 2014 PRASA, RobMech and AfLaT International Joint Symposium, 2014.[2].*

DECLARATION

This dissertation is submitted in fulfilment of the requirements for the degree of Master of Science in Engineering. It has never been submitted before for any degree or examination at this or any other University. I know the meaning of plagiarism and declare that all the work in the document, save for that which is properly acknowledged, is my own.

Cape Town, May 2015

Signed by candidate

Thomas J. Mathew

SUMMARY

INTRODUCTION AND BACKGROUND

This dissertation details the design and development of a prototype of a new robotic platform designed to carry a variety of sensors into environments that are too dangerous or confined for human workers, and forms part of a series of three concurrent M.Sc(Eng) dissertations which will integrate into a complete system. Ultimately this platform will be controlled and transported by the man-wearable harness and control station developed by W.K. Fong, and will gather data using the sensor payloads designed by G. Knox. Each dissertation, however, has independently quantifiable goals and results.

Figure 0.1
A mannequin carries the prototype robot in its harness

An important application area for such a system is Urban Search and Rescue (USAR): the field of work concerned with the discovery, extrication, and treatment of survivors trapped in collapsed struc-

tures. These typically occur as a result of terrorist attacks, natural disasters, or engineering failure. Human workers, often assisted by dogs, are trained in this work but the danger of the working environments make USAR a key area where the use of robotic assistance can make a massive difference in helping to save lives - both those of rescuees and rescuers. A body of existing work, both in the commercial and academic spheres, has been done in this regard, and as a result there is much to be learned from the experiences of others.

The history of robot-assisted USAR work, as well as the existing robots available, is surveyed and critically analysed. Significant challenges are noted: existing systems frequently lack sufficient mobility, are too large, difficult to transport and deploy, difficult to use, and very costly. Their cost has affected the prevalence of their use both as a barrier to acquisition but also during their use; robot operators frequently have their decisions constrained by the financial risk of losing or damaging a robot. Accordingly, it is proposed to develop a small, rugged, low-cost inspection-class robot that can be quickly and easily deployed in a variety of scenarios.

This development work is covered in three sections; the mechanical and industrial design of the platform, its design, manufacture and assembly are considered first. This is followed by a description of the electrical and electronic systems needed to power and control the robot as it conducts inspections in challenging terrain. To protect the robot from damage in this terrain, impact-absorbing wheels are developed. The test-driven iterative design approach followed, as well as the equipment and methods used therein, constitute a large portion of this dissertation and are detailed in their own chapter which can be read as a sub-project within the main project.

The finished prototype is tested against the developed specifications, and from these results conclusions are drawn and recommendations for future work made.

MECHANICAL AND INDUSTRIAL DESIGN

The mechanical and industrial design component of this project is chiefly focused on the development of a uni-body shell that contains the internal components of the robot, combining the functions of a traditional structural chassis holding components in place as well as an outer cladding that protects the robot from damage and contaminants. The design and manufacture of this component is described, along with the assembly and integration of the components and subsystems to form the working prototype.

Figure 0.2
The outer shell designed for the robot

ELECTRICAL

Electrical and electronic systems were developed to manage communication between the robot and base station, interpret these commands, and convert them into appropriate control signals to drive the two geared motors. Feedback is also provided to the operator on the temperature and current consumption of each motor. To achieve this, two motor driver ICs are controlled by a microcontroller upon which embedded software manages and controls the various data inputs and outputs. These are located on a custom PCB located inside the platform. The required battery power and wireless communication hardware are provided by the sub-systems designed by G. Knox.

IMPACT-ABSORBING WHEEL DESIGNS

To protect the robot from falls it may incur during operation and ensure it can be safely deployed by throwing, energy-absorbing wheels are developed. As there was very little useful literature on the topic, and the development of a FEM model and optimisation process would have been out of the scope of this project, an iterative test-driven design methodology is developed whereby the responses of a range of prototype wheels to drop testing are measured, and from these concepts an optimised wheel is iteratively developed.

TESTING

The performance of the completed prototype system is evaluated in a series of tests that assess its ability to drive in a controlled manner,

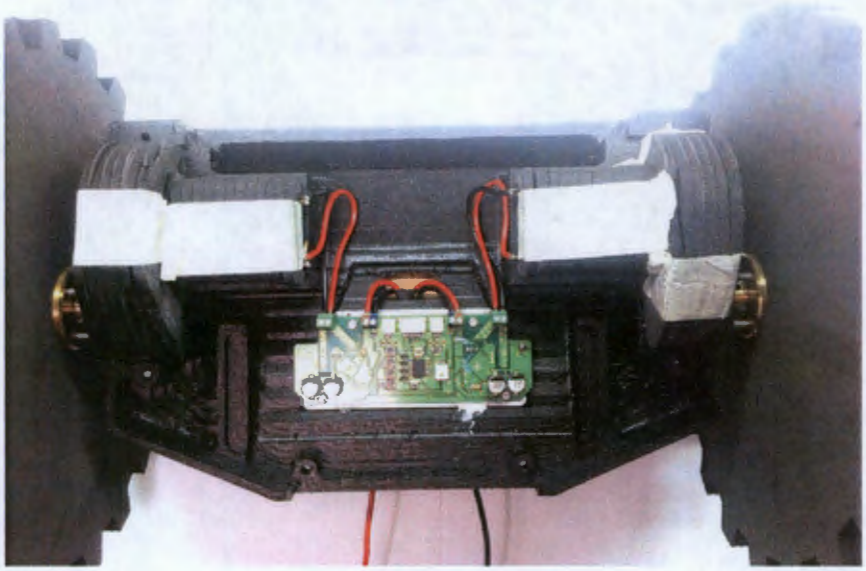

Figure 0.3
The motors and control PCB inside the platform's housing

(a) Straight-spoked wheel **(b)** Curved-spoke wheel **(c)** Composite wheel

(d) "Dreamcatcher" Mesh wheel **(e)** Solid wheel

Figure 0.4
Wheel concept designs

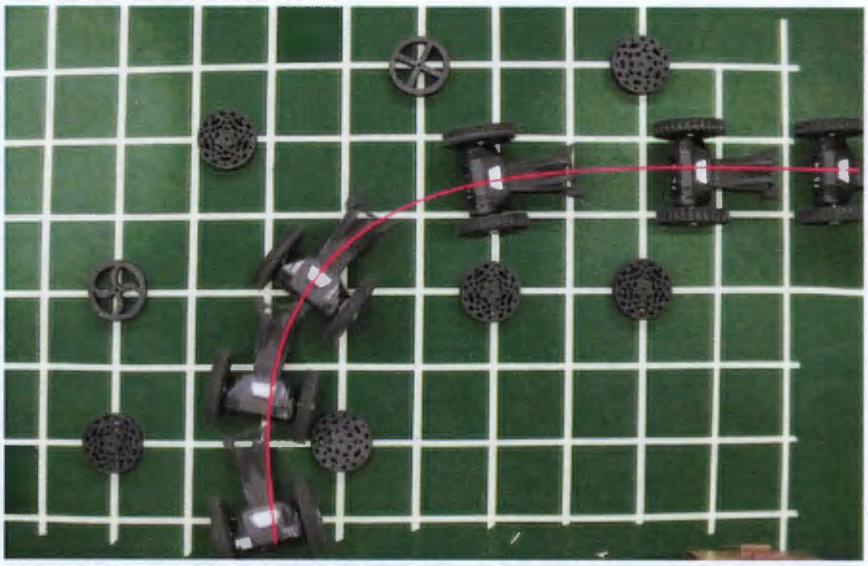

Figure 0.5
The robot performing a sweeping turn through obstacles

surmount obstacles, fall in a safe orientation, and so forth. These test procedures and their results are described. Although not meeting all of its specifications due to challenges and setbacks in the manufacturing processes, these results serve well to inform the recommendations for future work.

CONCLUSIONS AND RECOMMENDATIONS

The results of the testing are analysed and conclusions are presented alongside recommendations for future work. These include both the shortcomings of the prototype (such as its lack of power and flaws in manufacture) as well as the extent of the development work; further analysis of the wheel designs is highly recommended.

A master's dissertation is never complete;
it is merely abandoned.

— Anon

ACKNOWLEDGMENTS

It falls to me here to credit a group of people for whom I am very grateful. Without their contributions, this project could never have been abandoned with such conviction.

To Trevor Cloete, for his technical support, mentorship, always having time for me, and his rarely-welcome but always-needed skepticism. His kind yet exacting guidance has ensured that no stone is left unturned in pursuit of knowledge.

To Tracy Booysen, for her technical support, wit, kindness, and support as the new leader of our lab. This project would never have been finished without her willingness to assist and nurture ideas others would think too ambitious.

To Sam Ginsberg, Reuben Govender and Richard Curry, for their specialist technical support and good cheer.

To Gerald Nurick, for his excellent interim supervision of this project in early 2014.

To Julian Kent; for his love of "unsolvable" problems, for building the first low-cost robot out of two electric screwdriver motors and some old pipe, and for always making me think.

To Stephen Marais, for his support and supervision in the first year of the project, for risking a new idea, and for giving us the space and framework to begin.

To my colleagues Greig Knox and Victor Fong, for their camaraderie, rousing debate, and good teamwork. Well done!

To editor extraordinaire Laura Barnard; joiner of split infinitives, slayer of the comma splice, and all-round excellent human.

To all my other friends and family who have supported and believed in me along the way. I wouldn't be here without you.

A special thanks is given to Jasson Gryzagoridis, whose generous financial support made this work possible.

CONTENTS

LIST OF FIGURES

LIST OF TABLES

GLOSSARY

ADC Analogue-to-Digital Converter, a device or module that digitises signals for interpretation by a computer.

EMI Electro-Magnetic Interference, noise radiated by electronic devices onto other circuitry.

FEM The Finite Element Method

GPIO General-Purpose Input/Output, a pin on a microcontroller that can be used to assert or read voltage levels.

IMU Inertial Measurement Unit, a device containing sensors such as a compass, magnetometer, and accelerometers; used to determine orientation and movement in three-dimensional space.

PSU Power Supply Unit

RARL The Robotics and Agents Research Laboratory, University of Cape Town.

SPI Serial Peripheral Interface, a serial protocol for exchanging data between devices.

UCT The University of Cape Town

UGV Unmanned Ground Vehicle

USAR Urban Search and Rescue

1 INTRODUCTION

1.1 BACKGROUND

It is desired, for reasons that are made clear in the following sections, to design a small, rugged, robotic system equipped with basic sensors suitable for carrying out a range of inspection tasks in environments that are too confined or too dangerous for humans to enter.

The range of applications of such a system, if developed, would be massive and diverse, and it would be impossible to define a single operating environment. However, the field of Urban Search and Rescue (USAR) presents a range of challenges which are arguably among the most diverse and technically challenging of any robotics application, and an existing body of research, test standards and international collaboration is established in the field. As such, this project focuses on USAR as an application area as a robot capable of meeting this high standard would be easily extended into any other field.

USAR as the 'ultimate' challenge of mobile robotics

A number of robotic systems designed specifically for USAR work are available, ranging from simple inspection-class systems to more complex platforms equipped with powerful arms, tools, and specialised sensors. One such example, the RATEL, developed by the UCT Robotics and Agents Research Lab (RARL), is shown in Figure 1.1.

Many of these are also frequently used in military and tactical operations as those environments see robots faced with similar challenges. Although these systems are, on the whole, powerful and successful, they are criticised for their lack of mobility, their complexity, their lengthy deployment times, and their cost.

Cost is a particularly significant factor as it influences both the acquisition and operation of robotic systems in real disaster scenarios. While the research in this project argues that, clearly, every police station or fire department should have small, general-purpose robots on hand to assist rescue operations should disaster strike, the reality is that the cost of these systems — even the most basic offerings — has posed a significant barrier to their implementation. Secondly, those institutions that can afford to purchase a robot frequently under-utilise it, as the financial risk associated with its loss or damage in a disaster environment is too high. As such it is desired that a new system should be cheap enough that the operator's decisions are not constrained by the risk of losing or damaging the robot.

To establish historical context, there is a brief review of the functions of robotic systems and the state of the field to date, leading towards the development of inspection robots for use in hostile en-

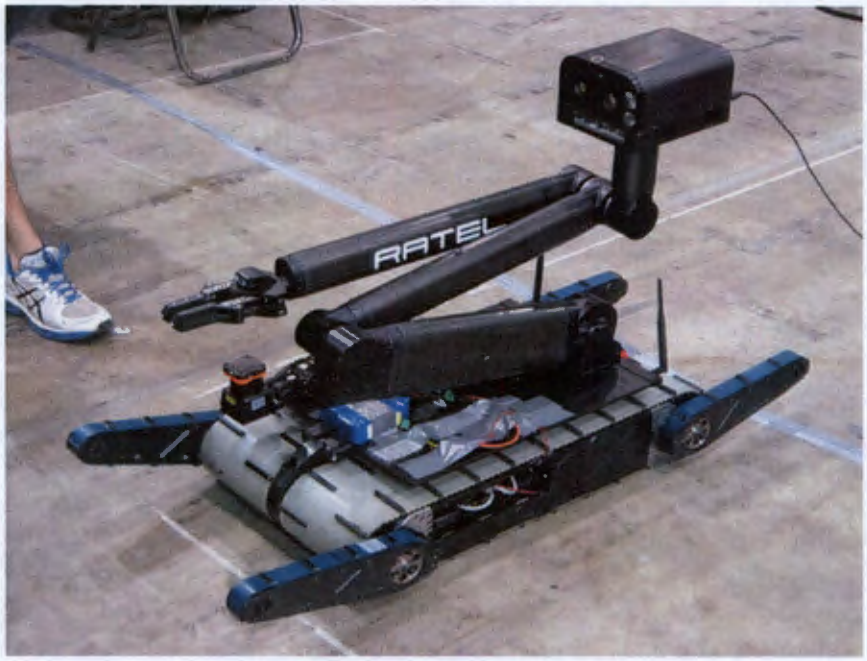

Figure 1.1 The UCT Ratel rescue robot. Photo credit: Julian Kent

vironments. Thereafter, the key points of Robotic USAR research are extracted, before moving on to the scope, limitations, and plan of development of this document. The following chapter will then conduct a deeper investigation into the use of robotic systems in disaster scenarios, and critically analyse existing systems that are available.

1.2 WORKING ROBOTS: A BRIEF HISTORY

Why do we use robots?

Throughout human history, imaginations have been captured by the idea of a machine that can do the work of a human. The Ancient Greeks are often credited with conceptualising (and in some cases even developing) the first automata, as far back as 500BC; however these, as well as early Chinese descriptions from the same era, are mostly for aesthetic or amusement purposes, and their behaviour was not particularly variable or controllable. It took until 1898 to produce the first viable attempt at a device that could be controlled from a distance; Nikola Tesla was awarded US Patent 613809 for his *Method of and apparatus for controlling mechanism of moving vessels or vehicles*[9] (See Figure 1.2).

Massive advances in robotics research in recent decades have brought us to a point where the technologies required to develop robust, capable, tele-operated robots are varied and mature, and a wide range of industrial, educational, recreational and military robots are available to the well-financed buyer. Robots now do a wide range of jobs that are too tedious, too dangerous, or too difficult for human workers. Figure 1.3 shows some examples; a robot designed for IED disposal (dangerous and difficult work), a 'Roomba' household vacuum

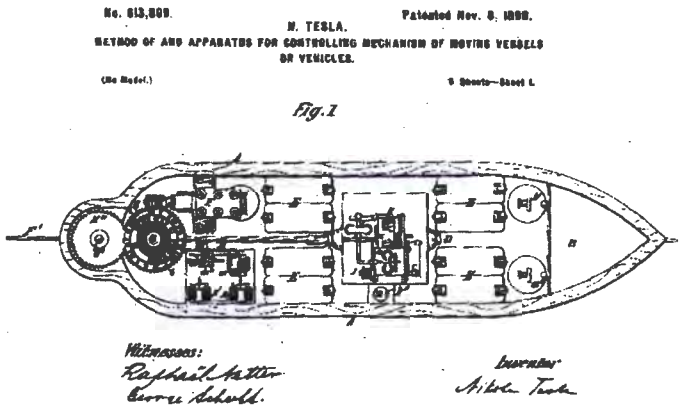

Figure 1.2 Excerpt from Tesla's original patent [9]

cleaner (tedious work) and an industrial robot arm in a foundry (tedious, difficult *and* dangerous work).

1.3 URBAN SEARCH AND RESCUE

> *"...the strategy, tactics, and operations for locating, providing medical treatment, and extrication of entrapped victims."*
> - FEMA 9356.1-PR, 2000[13]

The nature of the high-risk environments in which rescuers work has been a challenge as long as there have been disasters from which to rescue victims. During the Mexico City earthquake in 1985, 135 rescuers died — 65 of these due to flooding in collapsed structures[14]. For many years, rescue workers and fire-fighters have used trained dogs to locate victims trapped in collapsed, burning or unsafe structures — these dogs then lead the rescue workers to the victims' location. Although this strategy is still used today, it has several drawbacks. In the event of a building collapse, uncontrollable fire or gas leak, dogs may die, and although the loss of a dog is considered less devastating than the loss of a human worker, it is nevertheless undesirable. Furthermore, dogs can only lead a worker to the victim — no other information is available on the condition of the victim or their surroundings.

Tragic and preventable loss of human life

Another common method is to use cameras on poles to look into voids and around corners; however the length and inflexibility of the pole severely limits the depth to which these inspections can be take.

It is thus clear that the risks and challenges presented in these environments make them ideally suited to the use of robots to minimise risk to human workers. Robots are able to go into places where humans cannot: environments with low oxygen, extreme heat, high toxicity, or with small entrances are all better suited to robots than hu-

(a) IED Disposal [10]

(b) Roomba[11]

(c) Robot Arm [12]

Figure 1.3 A range of different modern robots

mans. As early as 1996, John Blitch identified USAR as a focus area for robotic research:

> . . .[USAR work] is a very dangerous job for human rescuers, poses an almost infinitely difficult spectrum of challenges, and yet provides an opportunity for robots to play a pivotal support role in helping to save lives.[15]

The first documented use of robots in a USAR operation was in September 2001 in the aftermath of the 9/11 terrorist attacks[16]. At Ground Zero in New York, several teams with a variety of different robots were dispatched to assist in the inspection and clean-up phases of operations[17]. Some of these are detailed in Section 2.3.

In their landmark paper *Human-Robot Interactions During the Robot-Assisted USAR Response at the WTC*, Casper and Murphy[17] morbidly noted that:

> The remains of 10+ victims were found; 5+ during the rescue phase and 5+ during the inspection phase (the nature of the remains makes it impossible to adequately count)

Although the efforts of the robotic USAR deployments in New York failed to retrieve any living victims, this became a strong starting point for USAR robotics as a serious, practical, and relevant research field. Subsequently, robot-assisted rescue missions in the aftermath of Hurricane Katrina in 2005 and the nuclear disaster at Fukushima Daiichi power station in Japan in 2011 have proved the value of robots as members of USAR teams[18][19].

However, this has not been without challenges. As G Anthes states,

> Real disasters are infrequent, and every one is different. The robots never get used exactly the way you think they will, and they keep uncovering new bottlenecks and problems. So it's an emerging technology. [20]

It is this ever changing and challenging environment that creates a significant challenge for rescue robot designers.

RoboCup Rescue and AAAI Urban Search and Rescue competitions have also provided an invaluable resource to robot developers (primarily teams from academic institutions) in the form of competitions which pit robots against each other in a series of challenge arenas that simulate disaster zones. These are based on the *DHS-NIST-ASTM Standard Test Methods for Response Robots*[21] which provide a system of benchmarking the performance of robots designed for these applications. UCT competed in the RoboCup Rescue league in Mexico in 2012, and the knowledge and experience gained there was invaluable. Much of the inspiration for this project comes from RoboCup 2012, and the subsequent IEEE/RAS conference held in Turkey the same year.

1.4 SCOPE AND LIMITATIONS

The broader goal of this project is to produce a prototype of a complete, man-portable, rugged inspection robot system, ready for further testing and refinement. However, as this is a monumentally large task, the project is divided into three parts. Two other concurrent M.Sc (Eng) dissertations, by G. Knox and W.K. Fong, cover the design of the operator control station and transportation sub-systems, and the sensor payloads and battery management sub-systems respectively, and this project focuses on the robotic platform itself.

The development of the robotic platform is divided into three main sections. First, the design of mechanical sub-systems such as the housing, or shell, of the robot, with a focus on ergonomics, aesthetics, and design for manufacture and assembly. These concerns could be grouped under the umbrella term of 'Industrial Design' as they serve to make the final prototype functional, usable and practical in a real-world environment rather than merely developing the required technologies as a laboratory demonstration.

Secondly, the design of electrical, electronic, and software systems must be considered. This is limited to only what is required to receive commands and control the movement of the robot through its environment. It does not include the wireless communications, power management, or battery but rather focuses on developing low-level intelligence in the smallest and cheapest circuits possible, designed to reliably and faithfully execute commands passed from a higher-level controller.

Thirdly, a complex mechanical problem that could not be addressed using known existing methods is explored; the design of impact-absorbing wheels to protect the robotic platform from damage in severe falls and throws. This component of the project aims to provide an initial investigation into the design of said wheels using an iterative test-driven rapid prototyping process, as far too many unknown variables were present to attempt a numerical solution.

1.5 PLAN OF DEVELOPMENT

This dissertation sets out to argue the case for, and then detail the development of, small, general-purpose inspection-class robots. These will be designed to withstand the challenges of USAR work, as it provides well-documented yet deeply challenging technical requirements. As such, the next chapter outlines further research undertaken to understand the circumstances surrounding use of robots in real disaster sites, noting their successes or failures, before moving on to critically analyse a selection of current commercially-available robotic systems that could be seen to meet the needs of these scenarios.

This research informs the creation of a list of goals that a new robotic system should succeed in, and Chapter 3 quantifies these into specifications against which the performance of the designed prototype cam be measured. Chapters 4 and 5 describe the mechanical and electrical design and manufacturing respectively. Chapter 6 then describes a test-driven method for developing shock-absorbing wheels to protect the robot from damage as it traverses challenging terrain, and in so doing, these wheels are developed for use on the prototype robot.

The assembled robot is tested against its specifications: this is detailed in Chapter 7. From these test results, Chapter 8 draws conclusions and, most importantly in a project culminating in the design of a prototype, makes recommendations for future work.

2 BACKGROUND RESEARCH

2.1 INTRODUCTION

This section sets out to explore the available technologies and existing research relevant to the goals introduced in the previous chapter.

As discussed in Chapter 1, the applications of inspection-class robotic technology are naturally very diverse but USAR is chosen as a development area as it poses some of the greatest challenges but is supported by a large body of existing work and standards. Following the previous chapter, where the relevance of robotic technologies in USAR was established, this chapter begins with a survey of the literature describing previous disasters. The challenges presented by these environments are thus assessed and particular areas for development highlighted.

The chapter then goes on to detail, compare, and critically analyse a range of existing systems which perform similar functions or have similar specifications to the aim of this dissertation. This prior work is mostly industrial (rather than academic), and serves as a body of examples from which important lessons can be learned and design inspiration can be drawn. In the latter two sections, specific attention is drawn to challenges presented in using robots for USAR work, and the ways in which existing technologies succeeded or failed in meeting the demands of the environment. These will ultimately define the goals and specifications for this project, which are elaborated in the following chapter.

Note: A significant portion of this chapter was published in the Proceedings of the 2014 PRASA, RobMech and AfLaT International Joint Symposium as *The Case for a General Purpose, First Response Rescue Robot*[1].

2.2 USE OF ROBOTS IN DISASTER SITES

Although many disasters can shed light on the topic of rescue robotics, some of the most illuminating insights come from the aftermath of the World Trade Centre collapse in 2001. Planes flown by terrorists into the buildings caused a massive collapse, leaving a landscape of rubble and twisted metal in which the bodies of survivors and victims were trapped. The scale of the destruction is captured in Figure 2.1, a photograph by photojournalist Jim MacMillan from the morning of September 12th.

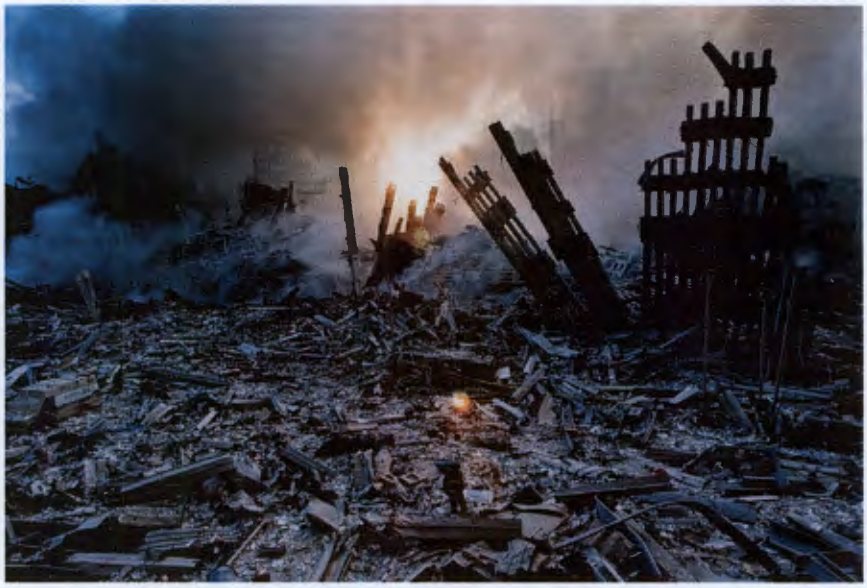

Figure 2.1 A firefighter is dwarfed by the scale of destruction on September 11th 2001[22]

Issues of robot size and terrain

Ten different robot models were deployed to the site, although only three were used[17]. The rubble created terrain too challenging for the robots to traverse, which caused rescuers to have to carry them into the search areas. The difficulty of carrying the larger robots and the fact that the voids were very small meant that most of the robots delivered to the site were too large to be effectively used. The INUKTUN MICROTRACS and VGTV models were the most used robots as they were able to be carried in a backpack to the rescue site. The MicroTracs was used in 7 of 8 drops because it was the smallest in size. A lack of trust in the robotic systems also led rescuers to rely on dogs and other techniques even when using a robotic system would have been faster[17] — and quite possibly safer too.

Difficulties operating complex robots

The operators described numerous problems with many of the robots at the site, including the fact that they were too fragile and that their user interfaces were too difficult to use. The necessity of tether or rope management often left the rescue workers themselves undesirably close to the hazards they were aiming to avoid; this is shown in Figure 2.2. Stressed or sleep-deprived operators working long shifts also experienced reduced cognitive capabilities and as such found the robots more difficult than expected to operate. Furthermore, when footage from the operation was reviewed months later, objects such as human remains and watches were identified that had been overlooked during the actual operation[17].

Failure of complex mechanisms

The Inuktun VGTV was used again during two further disasters, during the 2005 La Conchita Mudslides and after Hurricane Katrina in 2005[24]. The terrain created by the mudslides caused the tracks to fall off the robot and its performance was described as "no better than could be achieved with a simple human operated pole camera"[24].

Figure 2.2
Rescue workers managing a robot's tether[23]

During the Katrina rescue operation, the robot was tasked to investigate partially collapsed buildings to look for survivors. Although the teams did not succeed in finding anyone, they did manage to successfully navigate through buildings. They found it difficult to navigate over larger obstacles, had trouble with lack of traction and were under severe pressure to recover the robot as it was the only one present at the disaster site.

Risk of losing robot

The collapse of the Municipal Archive in Cologne in 2009 created a different scenario in that an entire building collapsed into a subway below[25]. This created a disaster area that was mostly below ground level, filled with water and with very small voids. Although two rescue robots were present at the site they were not utilised because the larger robot could not fit into the voids, and the smaller robot could not get to the voids as it lacked the mobility and ruggedness to travel there.

Size and terrain issues again

In March 2011 a huge earthquake and subsequent tsunami left four reactors at the Japanese power station of Fukushima Daiichi severely damaged. Here again, robots were used, and at the time of publication, the recovery work is ongoing. Because there were no victims left inside time was less of a pressurising factor; this enabled existing robots to be tailor-made for the task at hand[26]. The first robot to enter the building was the iRobot Packbot, a large, multi-functional track-driven platform. It allowed operators to determine that the radiation levels were too high for humans to enter; however since Packbot could not climb the stairs in the plant, its usefulness was limited. An existing and similar robot, QUINCE, was then reconfigured to carry out specific tasks within the building. Quince was able to climb stairs and take all necessary readings, although tether management was once again an issue.

Customised, task-specific robots

Necessity of rapid response

Research by the US Fire Administration[27] shows that the survival rate of entrapped victims in rescue scenarios decreases rapidly after the first day. The graph (Figure 2.3) shows the results of their research

Figure 2.3 Graph showing the survival rate of entrapped victims (recreated from[27])

and highlights the importance of being able to respond to a scenario and deploy robots quickly. After locating a victim, a skilled team can still take up to ten hours to extricate them if they are entombed[27].

2.3 EXISTING SYSTEMS

What is already available that might help solve the problem at hand?

This section details existing robots or robotic systems that have similar applications or similar specifications to the current project. Larger specialised robots, although undoubtedly of value in rescue scenarios, are not considered in great detail as their features are mostly outside of the scope of this project. As response robotics is still very much an emerging field, there is not yet a great range of different designs on the market; often, the same basic concepts are taken up and interpreted many times over by different manufacturers. As such, this section is by no means a representation of everything that is available, but merely some illuminating examples showing the best, or most prominent, small robots currently in the market. Broadly speaking, current small or "throwable" robots fall into two categories — two wheeled tail-draggers, and four-wheeled platforms (including those who use tracks or flippers). As such, representative designs are chosen that have been particularly successful, rather than detailing every individual attempt to realise similar concepts. In line with the aim of this specific project, the review focuses mainly on the mechanical construction and physical capabilities of the robot. The following sub-section then provides some criticisms and suggests small first-response robots as a clear direction for future work.

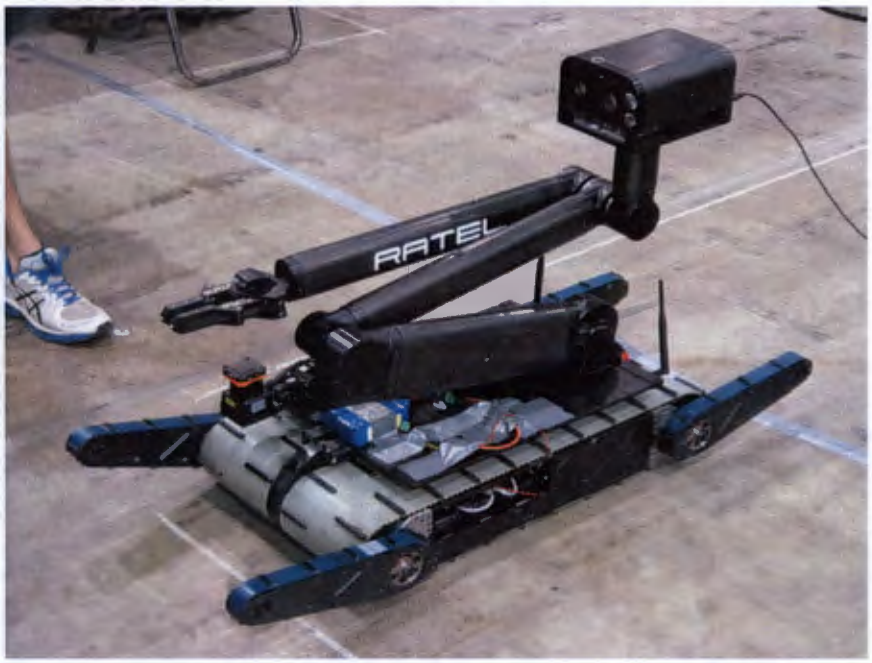

Figure 2.4
The UCT Ratel rescue robot. Photo credit: Julian Kent

2.3.1 *Large Robots and the UCT Ratel*

As previously mentioned, the UCT Robotics and Agents Research Lab (RARL) has experience in developing USAR-capable robotic systems. The RATEL UGV (shown in Figure 2.4) is a large, track-driven platform[28] equipped with a powerful robotic arm[29] and multi-functional sensor payload.

This work culminated in the Ratel competing in RoboCup Rescue 2012 in Mexico. Like many others in its class, it has to be transported in large cases and the robot alone requires at least two people to carry. Due to the complexity of the robotic arm and configurable track-flipper drivetrain, as well as the number of different sensors in the payload, two operators are required to drive the platform at all times. This robot is similar to a number of larger robots, such as Quince and Packbot, and is not discussed in further detail due to its unsuitability as a general purpose first response robot.

2.3.2 *Recon Robotics*

RECON ROBOTICS manufacture a range of several similar robots variously (and confusingly) referred to as the THROWBOT or RECON SCOUT range. They all follow the same basic principle of design; they are light, compact, two-wheeled tail-dragging, "throwable" inspection robots whose sole function is to provide video feedback from a single on-board camera. Some models include an automatic infra-red lighting system, enabling the robot to be used in total darkness. They are designed primarily for military and tactical inspection purposes in

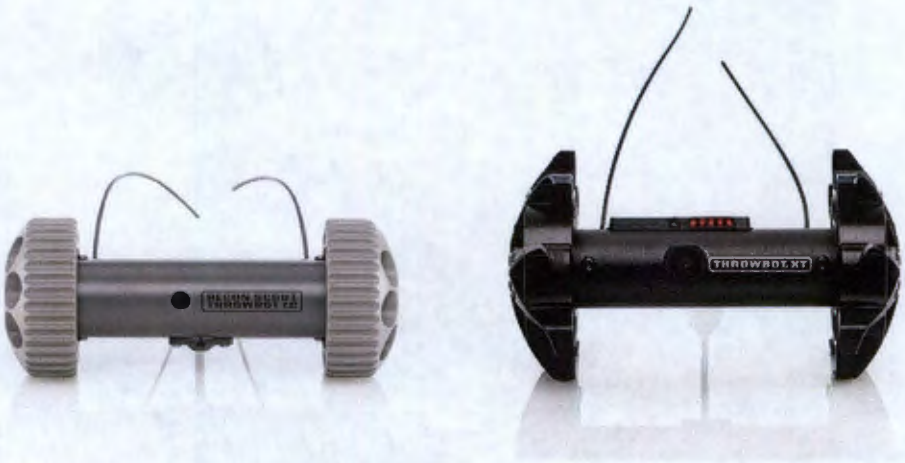

(a) The ThrowBot LE, designed to be "affordable" for police forces [30]

(b) The ThrowBot XT, with rugged wheels, audio feedback and IR vision [31]

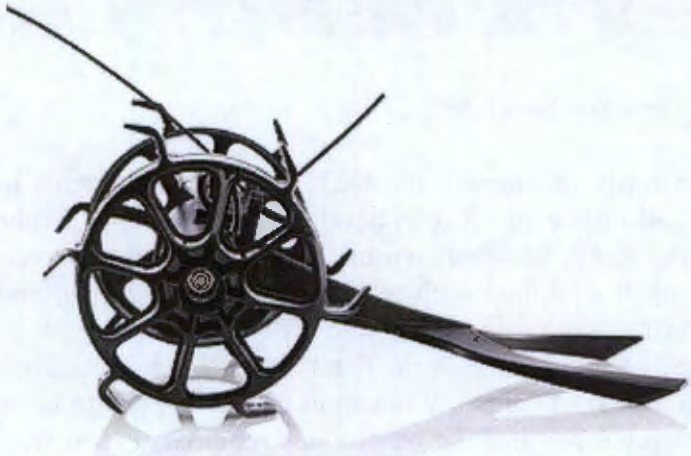

(c) The Scout XL, with even larger, obstacle-climbing, wheels. [32]

Figure 2.5 A range of different ThrowBots for different uses

stable environments, but their range has expanded to include robots modified to be better suited to rough terrain or search-and-rescue scenarios. A number of different robots from the range are shown in Figure 2.5.

The Recon system is successful for its simplicity. Boasting an "instantaneous" deployment time[30], it consists of a single wheeled robot which carries a single camera. A hand-held controller, consisting of a single video screen and a single directional joystick, is used to drive the robot around and view the video feed. The system is shown in Figure 2.6. The small hand-held package allows the robot to be controlled with a single hand, and the chunky joystick can be operated by a thumb, even when wearing gloves. This is critical to usability as soldiers and rescue workers frequently need their hands free to defend themselves or hold on to unsteady terrain.

Figure 2.6
The Recon Scout XT and OCU[31]

The specifications and capabilities of each different ThrowBot are generally not that dissimilar from the rest of the range[33] [30] [32] [34]. All can be safely dropped or thrown from great heights; this is a recommended method of deployment, as the robots are marketed as "throwable"[34]. All operate from the same control station and have the same basic mechanical design concept, and carry only a video camera (with or without IR illumination or additional audio feedback). Full pricing details of the entire range are not freely available, as some of the robots are considered "military technology" by the US government. However, with the civilian information available, prices for the available "kits" (including one robot, chargers, and one control station) range around US $13 000 with a single robot starting at US $7 500[35] [36].

As an example of the range that is particularly relevant to the topic under discussion, we examine in more detail the RECON SCOUT XL, the newest and most rugged addition to the range. Although some distributors[35] show a rescue-specific model, the "Recon Rescue", it appears to be a standard ThrowBot with a coat of fluorescent yellow paint and the ability to be deployed with a tether. It would be no better than the standard-issue ThrowBot at climbing obstacles or traversing challenging terrain, and is no longer featured on Recon Robotics' website.

Recon Scout XL

The Scout XL (shown in Figure 2.5c) is 300 mm long, 216 mm (wheel-to-wheel) wide and weighs 0.64 kg (excluding control unit). According to its specification sheet, it can survive a drop from up to 4.6 m; this resilience is partly achieved by the design of the wheels, which have flexible elements that deflect to absorb impact. In the Scout XL, these claw-shaped elements around the driving surface of the wheel are designed with a dual function of also providing grip on challenging surfaces such as "rocks, grass, sand and debris"[32]. It can also climb obstacles up to 102 mm high.

The Scout XL is equipped with a single camera, which captures video at 30 fps in a 60° field of view. Additionally, it is equipped with IR lighting which automatically turns on to illuminate areas of total darkness up to 7.62 m away. An included microphone enables the operator to hear what is happening in the surroundings of the robot but there is no feature to allow the operator to transmit sound back to a discovered survivor.

2.3.3 *iRobot 110 FirstLook*

The FirstLook is manufactured by iRobot, who are most famous for the invention of the Roomba robotic vacuum cleaner. The FirstLook (shown in Figure 2.7) is a small-to-medium-sized throwable inspection robot also designed for military and tactical use, but is more rugged and physically capable than the offerings from Recon Robotics. It measures 229 x 254 x 102 mm and moves around on tracks which are driven by four wheels with internal flexible suspension elements. Additionally, it features two flippers which rotate coaxially with, but independently from, the rear wheels, providing the FirstLook with a means of climbing up ledges, over obstacles, and autonomously righting itself after a fall.

Physically, the FirstLook is capable of surmounting a 178 mm ledge, easily lifting itself onto a pavement or over challenging obstacles. This is achieved by first reversing up to the obstacle, then rotating the flippers into the ground to rotate the body of the robot around and up onto the ledge. Smaller obstacles can be overcome by simply driving the robot towards them and using the flippers to lift the front of the robot up; this manoeuvre is also useful for raising the camera to look up at objects above its usual field of view. The two tracks are driven by wheels with curved spokes, designed to absorb impact when thrown or falling, and with these it can travel at up to 1.5 m/s. It is also capable of surviving a fall of up to 4.87 m. The main aerial is protected from damage as it is mounted on a highly flexible joint; it simply folds down in any direction and springs back into position when the

Figure 2.7
The iRobot FirstLook, flippers raised in anticipation[37]

robot rights itself. The iRobot also carries a rating of IP67 and thus is submersible up to 1 m depth.

The FirstLook is equipped with four built-in cameras (front, rear, and side facing) and has a "payload accessory port" which allows for other optional sensors such as "specialized cameras, thermal imagers, chem-bio sensors and charge deployment accessories"[37]. These, however, protrude from the top of the robot and are likely to impinge on its ability to survive a fall, throw or drop. It is controlled wirelessly with a game-style controller which includes a 5" LCD screen to relay video feeds to the operator. As a complete system the FirstLook can be transported in a large backpack which a single operator would have to remove in order to access the robot. Multiple robots can also be used to form an ad-hoc communication network, extending the useful range of a single robot by employing a second, intermediary robot to relay information back to the operator.

2.3.4 *Inuktun*

The INUKTUN VGTV (Variable Geometry Tracked Vehicle), now also known as the R212 DELTA EXTREME[38] was successfully used during the World Trade Centre collapse. It moves around on flexible tracks which allow it to traverse challenging terrains. One of its defining characteristics is also the ability to reconfigure its wheelbase, going from a wide, flat structure to a tall, narrow structure depending on the shape and terrain of the voids it must navigate; this is shown in Figure 2.8. The vehicle operates with a tether cable as long as 90 metres and can operate submerged to a depth of 10 meters. The standard system includes bi-directional audio, variable intensity lights, and a colour zoom camera. Options include a variety of sensors, a battery pack, Digital Video Recorder (DVR) and laser lines for on-screen

Figure 2.8 The Inuktun VGTV, in three stages of its variable shape[38].

sizing. Because the vehicle can change geometry, its dimensions can range from 280 x 430 x 150 mm to 280 x 280 x 340 mm[38].

Once again, pricing information is not readily available, but at the time of writing a second hand unit can be bought for approximately US $7 500.

Casper and Murphy[17] report that these robots could be set up within 1.5 minutes by experienced operators. They also mention a second Inuktun robot used at the WTC, named the MicroTracs. It had the same specifications, but appears to be smaller and has non-reconfigurable tracks which it uses to move around. This robot is no longer a part of Inuktun's product offering. Their current line does feature similar-sized miniature inspection robots, however these products are now oriented more towards use in pipe and duct inspection and are commonly fitted with curving or magnetic tracks for this purpose. Because of this feature, they would be unsuitable in a USAR scenario where challenging terrain — often incorporating scrap structural metal — is likely to be found.

2.4 CRITICISMS

Although large, multi-functional robots are still a crucial part of robotic USAR operations, they are often too large, too heavy, task-specialised and require specially trained operators. The research underscores the experiences of UCT's team that participated in the 2012 RoboCup Rescue competition and the subsequent IEEE/RAS Summer School, where a number of issues with the Ratel came to light, and rescue workers expressed the need for simple, lightweight, throwable robots that could simply provide visual feedback on the condition of structures and victims in a rescue scenario.

Although some of the small- and medium-sized robots reviewed here could potentially be seen as meeting this need, their cost — typically several thousand US Dollars apiece — limits their usability in actual rescue scenarios. This is a two-fold issue: for some rescue teams and organisations the initial cost is simply prohibitive, but for others who can afford perhaps one or even two robots, the financial risk of losing a robot is a limiting factor in deciding whether or not to deploy it. Additionally, the ThrowBot and FirstLook systems are both focused more towards tactical or military operations which typically

have less challenging terrain than those found in USAR scenarios, and would require additional sensors to render them truly USAR-capable.

2.5 CONCLUDING REMARKS

This section began with a history of robotics and an outline of the development of USAR with specific emphasis on the ways robots have been used, both successfully and unsuccessfully. Some key robots were highlighted for their feature offering, and from this review of the scenarios and robots a trend towards smaller general-purpose robots emerges. This is clarified in the final section which shows the shortcomings of the current offering. From these criticisms, the next chapter will develop some design goals, and ultimately a list of specifications towards which to design.

3

SPECIFICATIONS

3.1 INTRODUCTION

Drawing on the observations and criticisms made in the previous chapter, this chapter establishes the goals for which a new, small, inspection class robot could aim. These qualitative goals are then distilled into a list of quantitative specifications, and where test standards already exist for these specifications, they are noted. This chapter concludes with a table summarising the desired specifications for an initial prototype whose design process is detailed in the following chapters.

3.2 GOALS

It is clear from the preceding chapter that there is a clear, immediate need for smaller, general-purpose rescue robots. The challenges noted in the disaster sites and the shortcomings of existing robots reviewed serve to define this new category. The features that were particularly useful in — or notably absent from — specific robots and disasters are detailed below. The robot must be:

- low enough in cost that the operator's decisions must not be constrained by the risk of losing it
- low enough in cost that every local fire department, police station, or rescue service can own one
- carried in a backpack by a single rescuer
- easy to operate by sleep-deprived or stressed rescuers
- able to be deployed "instantaneously", i.e. little to no set-up time
- able to survive deployment by throwing or dropping
- rugged, and dust and waterproof
- able to navigate challenging terrain such as rubble
- able to operate in all orientations, or right itself reliably
- equipped with sufficient sensors to determine the existence of nearby human life, and possibly automatically identify these and highlight to operators

- able to carry a variety of differently-specialised sensor payloads for different scenarios
- able to operate without a tether, or have some automated tether control
- able to operate continuously for at least 20 minutes.

The next section elaborates on these goals and, where applicable and within scope, assigns them measurable properties.

3.3 DETAILED SPECIFICATIONS

This section assigns as many measurable quantities as possible to the goals outlined above, focusing only on those aspects which can be achieved within the scope of this project as defined in Section 1.4. As one of the aims of this project is to produce the platform as simply and cheaply as possible, some features (such as the ability to hold a straight line) are idealised goals and do not have a numerical specification. These will nevertheless be tested so that the platform can be compared to other similar products, and the viability of this attempt evaluated. Other features, such as the ergonomic and usability considerations, can only be assessed qualitatively; in this case the desired qualities are described rather than enumerated.

3.3.1 *Cost*

Based on anecdotal descriptions collected from rescue workers at conferences, it is desired that the cost of manufacturing the "expendable" part of the system — the combined robotic platform and sensor payload — should not exceed US $500.

3.3.2 *Size and Weight*

The robot must be small and light enough that the complete system can be carried and the robot deployed (potentially by throwing) by a single operator. Firefighters are capable of regularly carrying 30 kg of protective gear and equipment on their bodies[39] so the total system mass should be around, or ideally less than, this benchmark. The mass of the individual robot (including the battery and sensor payload outside of the scope of this dissertation) should be light enough to be throwable by any rescue worker. Data on what constitutes "throwability" is not readily available, however, a valuable starting benchmark is the athletics event of Hammer Throw. The women's standard hammer weighs 4 kg[40], but as this can only be thrown significant distances by elite athletes, the robot should certainly weigh less than this. The specification is thus set at a maximum of 3 kg.

In order for it to be carried easily on the operator's back it should not protrude significantly from the operator's own body. Again, a specification is arrived at by estimating that the robot should not exceed the size of a large backpack at around 350 x 250 x 500 mm (measurements from author's own survey). The robot should also be designed so as to be compatible with the carrying system designed by W.K. Fong in his concurrent M.Sc (Eng) project.

3.3.3 *Operation and Control*

As the controller and human interface are not part of this project, the specifications here merely pertain to the communication between the robot and the sensor payload and/or control station. As the wireless communications are managed by the sensor payload, one communication protocol between the motor control circuitry and the sensor payload must be specified such that the platform can be controlled. The communication protocol should have access to all of, and in no way restrict, the platform's physical abilities. This protocol will be some pre-agreed packet data structure transmitted via a simple serial data protocol. The motor control circuitry will receive speed and direction instructions for each motor, execute them and return local information such as motor temperatures and current consumption. This connection must be stable and in the event of a loss of communication, should self-repair.

The robot must move forward and backward without listing or veering off course, and perform sweeping turns evenly and in a controlled fashion when requested. It should also be able to turn upon its own axis to facilitate manoeuvring through tight spaces. As this project is partly an investigation into what can be achieved with the most minimal technology, these specifications are not set in advance, but will be considered as goals to maximise during the design process. Thereafter, they will be evaluated as a means of comparing the developed platform to other existing solutions.

3.3.4 *Other Ergonomic Considerations*

The robot must be designed so as to be deployed easily with an absolute minimum set-up time. Mechanisms must be provided such that the robot can be carried securely into the field, quickly removed from its case or container, and deployed without requiring any systems to be configured or checked. The robot should thus be gripped in one hand, and provided with mechanisms or structures to assist in its deployment (which could include throwing). Provision must also be made for charging the battery without having to disassemble or reconfigure the platform.

3.3.5 *Drop Survival*

The robot should be able to survive deployment by throwing into the upper level of a building, and then survive falling or leaping from that level to a lower level, should there be no alternative method of descent. As such the drop height of this robot is benchmarked at 3 m, approximately the height of a normal storey. This specification has to be developed with consideration for the drop survivability of any internal components; this is examined in more detail in Chapter 6.

3.3.6 *Surmounting Obstacles/Terrain*

The robot should be able to negotiate the challenging environments and terrain often found in USAR scenarios. The *ASTM-NIST-DHS Standard Test Methods for Response Robots* provide a number of quantitative tests involving ramps, 'stepfields' of varying uneven terrain, ledges, gaps and so forth[21]. Although an invaluable resource, these tests focus on larger, more capable robots and are designed to comprehensively evaluate a complete response robot system including its control, sensors, and so forth. As such, these tests will be attempted in future work focusing on the further development of the whole integrated system, and later tests could include trial deployment on actual or simulated disaster sites. To develop a simpler metric for the performance of the platform alone, which will guide later development of successive prototypes, it must be evaluated on its ability to ascend slopes, clear gaps, tumble over or traverse small obstacles and land safely, all in a controlled manner. After a fall or clearing an obstacle in an uncontrolled manner, the robot should either right itself or be able to operate in any orientation. As mentioned above, these features are not beholden to a pre-ordained specification but rather the focus is to establish a benchmark for what can be achieved in a low-cost environment.

3.3.7 *Ingress Protection*

The robot should be able to withstand dust, dirt and splashing with water as it performs tasks in disaster environments. Although a distinct advantage, making the robot truly submersible requires development cost and time out of the scope of this dissertation. The Ingress Protection Code *ANSI/IEC 60529-2004[41]* describes a range of levels of protection against dust and liquid. A suitable IP rating would be IP65 — total protection against dust, and able to withstand "jets of water", but not total immersion.

3.3.8 *Speed*

As the robot is intended to explore small and confined spaces, it need not move very fast. A modest walking speed of 0.75 m/s is deemed a sufficient maximum. It is imperative, however, that there is smooth control at lower speeds to enable the robot to "creep" evenly toward an object for inspection, or to assess a hazard more closely without endangering itself needlessly.

3.3.9 *Sensor Payload*

As the sensor payload does not fall under the scope of this dissertation, the sole aim of this section of work is to provide a "bay" or opening where sensor payloads, following some specification agreed upon with their designer, can be connected. This must ensure that payloads are afforded the same protection from harsh environmental factors as the platform's own internal works, and that they are securely fastened to the platform. The sensors that could be included in these payloads form the basis of the ruggedness and drop survivability specifications; the FLIR QUARK thermal camera is taken here as an example of a sensitive component and design must ensure that its absolute maximum safe impact and vibration loadings are not exceeded.

3.3.10 *Power*

As the battery and power electronics are not a part of this project, the only assessment that can be made here is that the mechanical design of the platform allows for a battery as specified by the designer of the battery sub-system. However, as the motors and motor control are within the scope of this project, these must be designed with appropriate limitations in mind. Accordingly, the motor control circuitry must accept a DC voltage within the range of common battery technologies and its current consumption must be within the bounds of what a small rechargeable battery is reasonably expected to supply. As such these are benchmarked at 12 V-20 V with a maximum (peak) current of 10 A.

3.4 SUMMARY TABLE

The table below summarises the specifications listed above, and links each specification to a test which will be carried out in Chapter 7. Specifications on a sub-system level such as the communication packet structure and some ergonomic considerations are mentioned above but not listed here; these will be evaluated as design goals in the respective chapters.

Specification	Goal	Test Method
Cost	US $500	Budget Check
Size	350 x 500 x 250 mm	Measure
Weight	3 kg	Scale
Communication	Stable	MTBM
Control	Respond to commands	Test controller
	Hold a line	Straight line
	Curved path	Successive radius turns
	On-axis pivot	Confined turn
Drop Survival	3 m	Drop test
	Self-righting	Drop test
Terrain	Slope climb	Successive slopes
	Gap Clearance	Successive gaps
	Obstacles (1 wheel)	Successive obstacles
	Obstacles (2 wheels)	Successive obstacles
	Tumbling	Obstacle field
	Tumbling	Ledge drop
	Any orientation	Inspection
Ingress Protection	IP65	
Forward Speed	1 m/s	Drag race
Sensors	Multiple payloads	Inspection
Power	12 V - 20 V, 10 A	Motor stall test

Table 3.1 Specifications

4

MECHANICAL AND INDUSTRIAL DESIGN

4.1 INTRODUCTION

This section describes the design and manufacture of the mechanical sub-systems and components in this project. It focuses particularly on the components whose development entailed simple applications of existing design and manufacturing techniques, or did not require new research and development work. These include the outer shell and chassis of the robot, the tail, seals, fasteners, and so forth. The energy absorbing wheels, whose development incurred significant experimental work, are mentioned here briefly but covered later in full detail in Chapter 6.

After an overview of the decisions leading to the proposed form factor of the platform, and an over-arching description of the design, each subsection covers a particular component, focussing on the design and mentioning manufacturing processes where relevant, as well as making observations on the quality of the manufactured parts. After each sub-system is treated, an overview of the assembly process is given, followed by concluding remarks on the design process. Recommendations for future work are made in a later section along with the recommendations relating to the rest of the project.

Note: Portions of the work described in this and the next two chapters have previously been published as "The Design of a Rugged, Low-Cost, Man-Packable Urban Search and Rescue Robotic System" in the Proceedings of the 2014 PRASA, RobMech and AfLaT International Joint Symposium [2].

4.2 CONCEPT DEVELOPMENT

4.2.1 *Form factor*

The form factor of the robot — simply, the general layout and structure of the robot — is dictated by the specifications laid out in Chapter 3 and an analysis of the similar existing products surveyed in Section 2.3. In order to protect the sensors no matter what combination of sensors was installed, it was necessary for the body of the robot to totally encompass the sensor payload. Sensors are thus afforded the same protection as the rest of the internal workings of the robot, and this restriction ensures all future sensors are afforded the same protection. If sensors are attached externally (such as with the iRobot FirstLook) they are exposed to environmental damage, especially if

the robot is dropped or thrown; additionally, they may affect the robot's ability to operate in any orientation. Figure 4.1a shows the first sketch from the author's notebooks suggesting what is essentially a sensor-carrying box on wheels.

The layout and number of wheels is motivated by the size, weight, and cost specifications. Although larger, track-driven robots such as the iRobot FirstLook claim greater mobility and object climbing than small, two-wheeled robots like the Recon Scout, they still are not capable of climbing stairs, a critical challenge in USAR environments. It was felt that the slight increase in mobility offered by tracks and flippers was not commensurate with the increase in weight, cost, and complexity. The successful adoption of the Recon Scout range by a large number of international tactical and rescue organisations suggests that the two-wheeled tail-dragging form factor has been found to be a viable solution. Operating on the minimum number of motors also reduces the cost and complexity of the electronics and control component of the design work.

In order for a two-wheeled vehicle to surmount obstacles, the wheels must exert a torque against the ground. If this torque is not balanced by some structure exerting an opposite torque that that holds the rear of the robot in position, the robot will simply rotate about the motor shaft with the wheels standing still. This functionality is provided by the tail, which doubles as a handle for carrying and can assist in deploying the robot into a disaster area by throwing.

4.2.2 *Design Overview*

For ease of manufacture, to aid scalability of production, and to reduce costs associated with high part counts, the body is designed such that the structural chassis, supports for fastening internal components, and an outer 'skin' are combined into a single integrated housing. As such, the bulk of the mechanical design is represented by the top, bottom and front pieces of this shell (shown as an exploded assembly in Figure 4.2).

The front panel is designed to support the sensors, cameras and other electronics that could be carried by this robotic platform and as such is removable and customisable to specific needs. Its shape and mounting features were specified, but its manufacture and customisation to specific sensor configurations fell under the scope of G Knox's concurrent M.Sc project, which focuses on the design of these payloads.

Two small aluminium heat-sinks are recessed into the shells to allow heat from internal electronics (RF transmitters and the motor controller circuitry) to dissipate to the environment. All the mounting surfaces incorporate a clearance for a rubber gasket, sealing the inner workings of the robot from water, dust, and other contaminants.

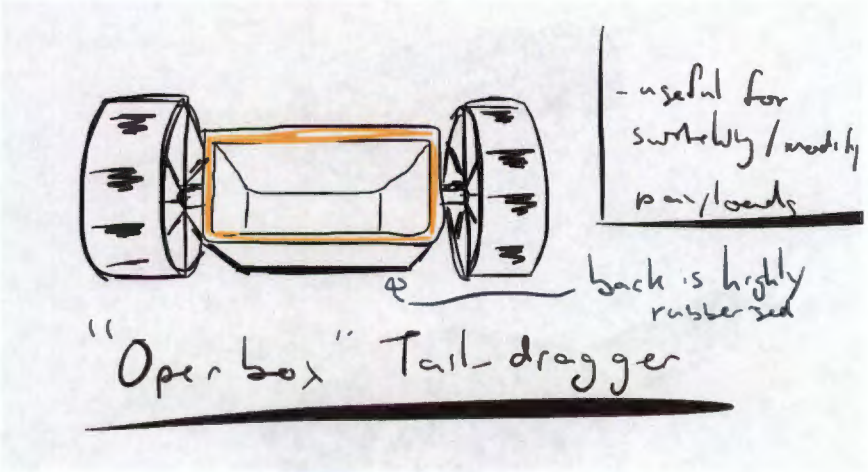

(a) The first "box on wheels" concept

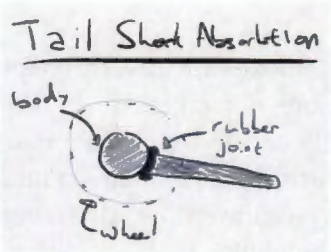

(b) Initial sketch of a flexible tail

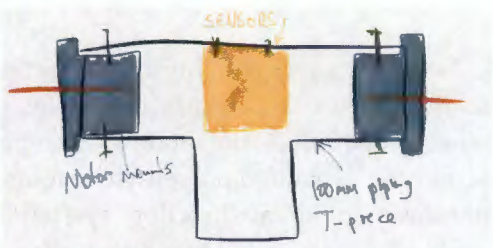

(c) Abandoned chassis concept using stock piping T-piece

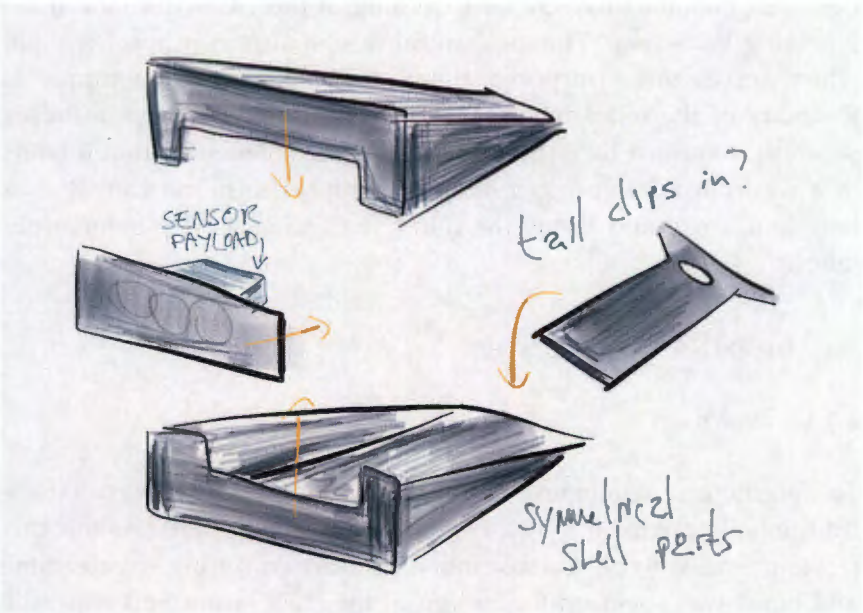

(d) Integrated shell/chassis concept

Figure 4.1 Concept sketch excerpts from the author's notebooks

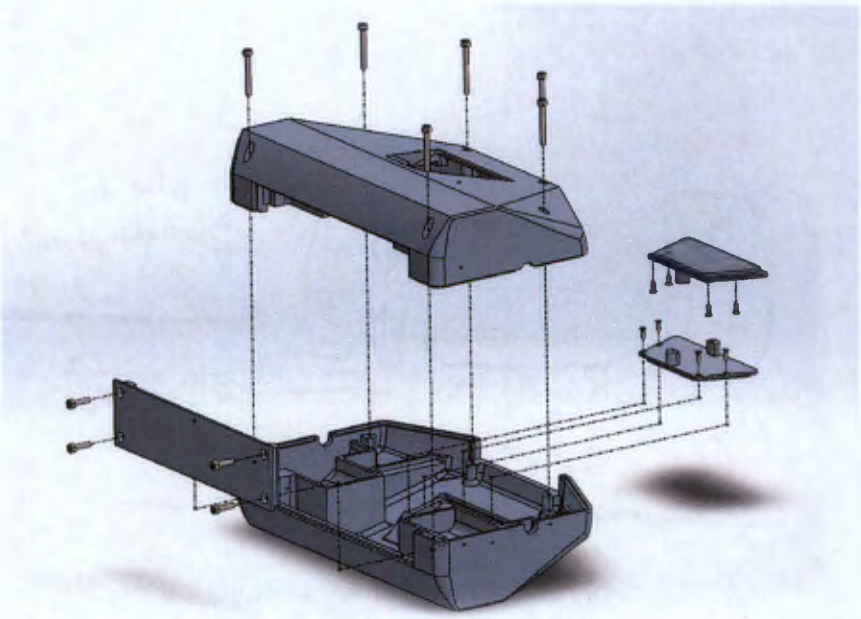

Figure 4.2 Exploded shell assembly (tail not shown)

Two DC motors with built-in reduction gearboxes are directly coupled to the wheels. To absorb any forces that are not taken up by the wheels themselves, the motors are completely encased in dense impact-absorbing expanded polyethylene foam, which allows a small amount of movement in any direction. The battery, communication and motor control modules are located at the rear of the platform.

Although it is envisaged that the final product can be mass produced by injection moulding, a first prototype of the mechanical parts has been manufactured by CNC milling at the UCT Mechanical Engineering Workshop. The mechanical design also incorporates a 'tail' which serves three purposes: firstly, to provide reaction torque to the body of the robot when it is attempting to surmount obstacles; secondly, to adjust the attitude of the falling robot such that it lands in a controlled fashion, face-first, on both wheels; and thirdly as a handle to carry and throw the robot, increasing its deployment distance.

4.3 HOUSING

4.3.1 *Design*

The plastic case combines several functions in a single part that are traditionally carried out by a system of connecting parts. As this project is intended to be scalable into a production setting, greater time and effort was spent on the design of the shell (a once-off expenditure) so that it could be spared in later manufacture and assembly stages. Accordingly, the structural chassis that holds components securely in their correct positions is combined with the outer shell that

Figure 4.3
One half of the robot's plastic shell

protects the components from environmental damage and contaminants, and there are no additional internal brackets or removable parts. The exception to this rule is the heatsinks, which must be made of a more thermally-conductive material.

The case is split along its centre into two symmetrical halves which clip together using a lip and groove and are fastened thus with six M3 allen-cap screws. A render of one half is shown in Figure 4.3.

The central trapezoidal hole with surrounding groove accommodates an aluminium heatsink which is fastened there using four M2 screws. In one half, this heatsink accommodates the motor control PCB, and the other cools a wireless video transmitter. The rectangular cut-out directly below this locates the charging connector, and as such is only present on one of the half-shells.

The battery and battery management system designed by G Knox is located above the heatsink as the aluminium plates also serve to protect the volatile lithium battery from puncture in the case of severe damage to the platform. It is encompassed by supports which protrude from the inside of both halves of the case and locate and secure the battery when the case is screwed shut.

A slot is cut out behind the battery, through which the tail protrudes, secured in place by two screws that pass through it and are fastened into the tapped holes in the case below. These, and all other fastening holes, are supported on circular bosses which protrude from the inside of the shell.

At the front of the case, a cut-away is made for the attachment of the sensor payload. As shown earlier in Figure 4.2, this part, ultimately with sensors attached to it, is inserted into the case assembly and can be removed to interchange sensor suites. A flat mounting flange is provided, with clearance for a seal and four more bolts that fasten the face to the shell at its corners. The final sensor payload can then extend in an inverted T-shape back into the robot, with sensors

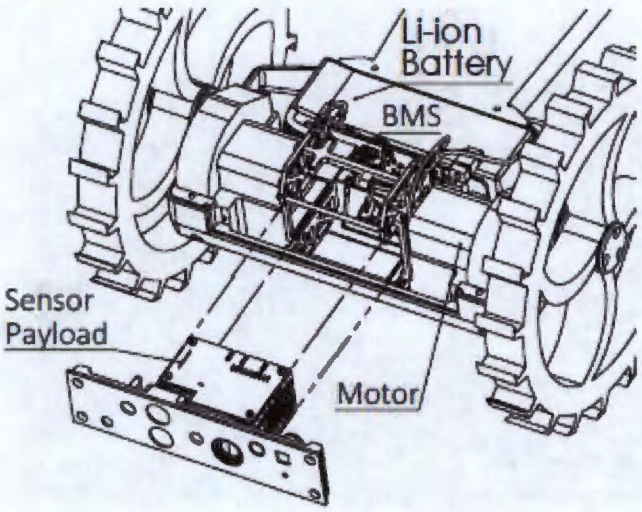

Figure 4.4 Wireframe of proposed sensor payload inserted into robot (Wheels depicted are an early prototype design) Image credit: G Knox

mounted to the front face and control circuitry extending back into the central space between the motors. Figure 4.4, reproduced with permission from G Knox's work, shows a proposed sensor payload inserting into the assembled lower shell.

Either side of the sensor payload cavity, two cavities are provided for the motors, which, covered in foam supports, are wholly encased in these cavities. Two of the bolts that fasten the two halves of the shell together are specifically located either side of the motor gearbox to prevent the motors' reaction torque from forcing the shell apart. The motor mounting is discussed in more detail in Section 4.4.

A render of the final assembly, with the top half of the shell removed, is shown in Figure 4.5 and indicates the relative positions of the sub-systems as they fit into the shell together. The right motor is shown inside its housing, whereas the left housing is hidden, to show the positioning of the motor within. One wheel is removed, and the other is an early prototype design for illustrative purposes only.

4.3.2 *Manufacturing*

Although the housing was designed ultimately to be injection moulded from some hard plastic, the massive costs associated with design and manufacturing a mould were not commensurate with the benefit this provided — particularly given the likelihood of serious revisions between the first prototype and any subsequent designs. As such, the prototype shells were CNC machined from solid blocks of HDPE in the UCT Mechanical Engineering workshops. HDPE was selected as it was readily available and thought to be easily machined; however this would not be recommended in future as it posed several shortcomings (detailed below throughout the manufacturing process).

Each half was machined in two stages; first the outer shape was cut from a solid block, then this block inverted and the inner geometries

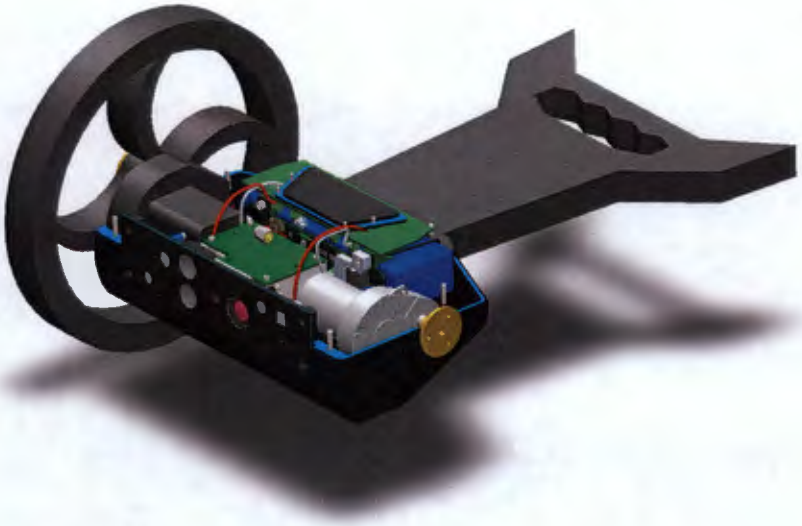

Figure 4.5 Render of the shell containing all interior sub-systems (Wheel depicted is an early prototype design)

(a) After first, rough cuts

(b) After second, finer machining

Figure 4.6 The shell during CNC milling

cut away. Each cutting process contained several passes of differing speed — fast, rough, low-resolution cuts at first to remove the bulk of the material, followed by slower, more accurate operations to bring the features to the correct dimensions and a smoother surface finish. Figure 4.6 shows the effects of this process.

During the machining of the inside of the shell, the part became progressively thinner and more flexible. To prevent it from vibrating or flexing during subsequent machining operations, wooden blocks were used to brace the empty spaces: these are shown in Figure 4.7.

To save machining time, some non-critical faces were left in the rough-cut state. These can be seen in the interior view of the finished part in Figure 4.8

During assembly it was discovered that the threaded holes in the HDPE material were not strong enough to hold the screws securely, with the threads stripping immediately when the bolts were (cautiously) fastened. Manufacturing inaccuracies lead to discrepancies between the two halves and the resulting misalignment caused the screws to become pinched. To mitigate this, the shell was re-worked

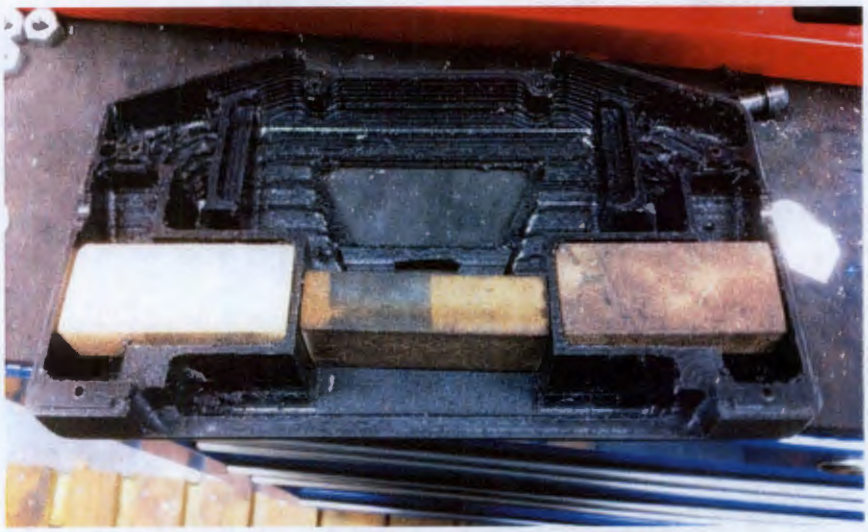

Figure 4.7
Use of braces during machining to support thin-walled structure

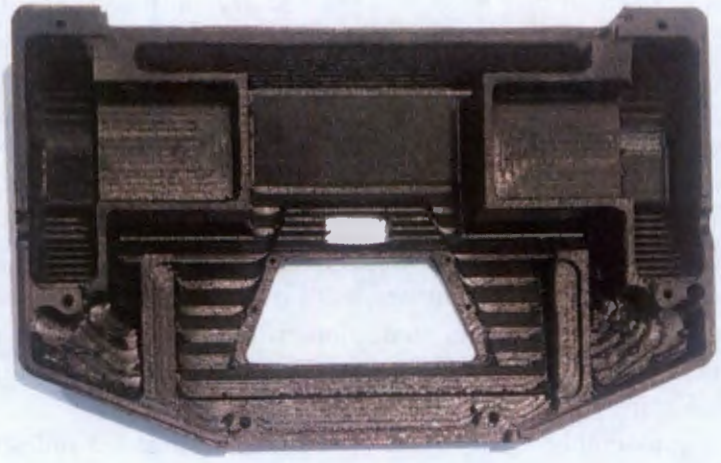

Figure 4.8
The finished part after CNC milling

Figure 4.9 Shell with brass thread insert

to incorporate brass thread inserts which were forced into the screw holes as shown in Figure 4.9.

Overall, although the manufactured shell was adequate to hold the sub-systems together and performed well in testing, a number of issues with the prototyping process are present that could be mitigated in a later, more accurate and better refined manufacturing method. 3D printing was investigated for this, but the costs were outside of the budget allocated to this iteration of the project.

4.4 MOTOR MOUNTS

4.4.1 *Design*

To provide a flexible and shock-absorbing coupling with the body, solid foam motor housings were designed that totally encompass each motor. The motors are shown in their housings in the SolidWorks rendering in Figure 4.10.

By designing to the exact shape of the motors and ensuring a snug fit between the outer of the housings and the corresponding cavity in the robot's case, the motors could be secured when the case was screwed shut. Although concerns have been raised about the foam trapping heat, it is not expected that, for the majority of the robot's operation, the motors will operate under heavy enough load conditions to significantly raise their temperature. High torques will tend not to be delivered continuously, but may be demanded in short bursts as the robot surmounts small obstacles. Should future testing find this to be an issue, conventional motor mounts could be used in conjunction with flexible shaft couplings. Alternatively, a thermally-conductive foam could be selected for this application.

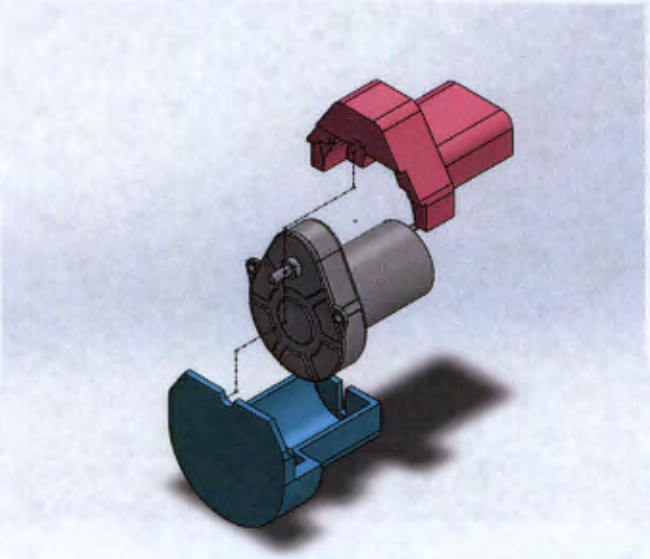

Figure 4.10 Exploded render of a motor and housing

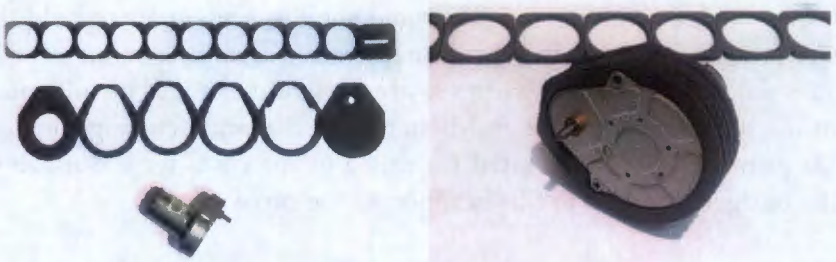

Figure 4.11 The motor mounts

(a) The flat pieces and motor laid out before assembly

(b) The motor mount being assembled onto the motor

4.4.2 *Manufacturing*

Each mount was to be manufactured as two separate shells, split along a line perpendicular to the split line in the housing to reduce the risk of water or dust ingress. Each half-shell would be made of individual laser cut sheets glued together in layers to form their final shape. However, when cutting thicker sheets of foam the divergence of the laser beam in the porous material tended to erratically increase the cut width. This made it almost impossible to gain sufficiently precise dimensions from a single cut. As the laser could cut thinner material in faster passes, causing less flaring of the cut, the motor mounts were cut from 3 mm SPX90 foam sheeting available. This, however, resulted in so many individual pieces that the resulting structure was too fragile and precarious to withstand ongoing development work. The housings were instead manufactured without a lateral split, and the motors "threaded" through the layers during assembly. This is shown in Figure 4.11.

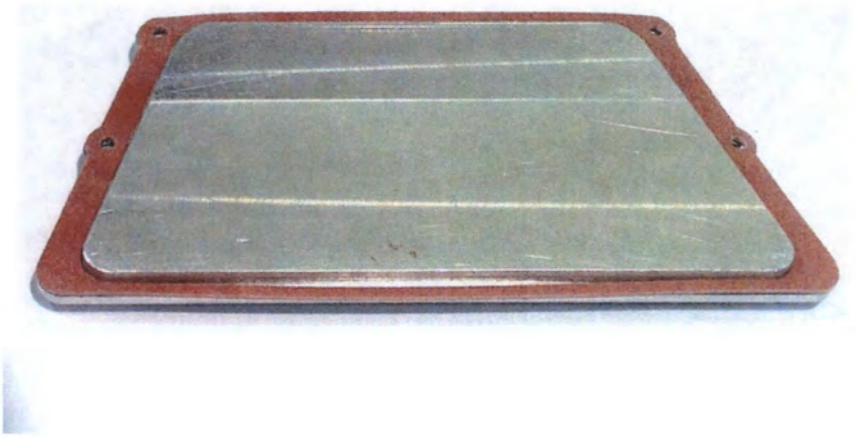

Figure 4.12
0.5 mm silicone seal in position on the heatsink

These mounts secured the motors adequately for testing the platform and integrations with other systems, but were nonetheless not ideal. Further development work in this area is recommended should the project be taken further.

4.5 SEALS

4.5.1 *Design*

To protect the internal components of the robot from damage by water or dust ingress, rubber gasket seals were designed. They are shown in Figure 4.5 in light blue, sitting inside the lip and groove attachment feature between the two halves of the case. They are clamped in place and compressed there by the bolts holding the case together.

4.5.2 *Manufacturing*

The seals were manufactured by laser cutting from 1.0 mm and 0.5 mm silicone sheets (depending on their intended location). This had remarkably good results as the thin sheet could be laser cut with a virtually zero-thickness kerf and the resulting seals were very accurate and seated well. Figure 4.12 shows a heatsink with its fitted gasket.

4.6 WHEELS

Although the design of the energy-absorbing foam wheels is covered in detail in Chapter 6, they are given a brief treatment here, focusing particularly on their manufacturing considerations which are not covered elsewhere.

(a) Laser cutting in progress (b) Re-focusing the laser beam

Figure 4.13 The laser cutting procedure

4.6.1 *Design*

At 200 mm diameter, the basic wheel shape was designed to provide 30 mm clearance between the wheel and the face of the robot when it falls face-first toward the ground. This dimension was derived from the analysis in Section 6.1.2 with an additional margin of safety added. They are attached to the robot by means of small two-part brass hubs which are coupled directly to the output shaft of the motors. Two set-screws hold the hub in position against the flat spot of the motor shaft, and three screws secure the wheel between the outer and inner hub.

4.6.2 *Manufacturing*

The SPX foams used (discussed in more detail in Section 6.3) were available in 10 mm sheet stock which could be easily machined by laser cutting; however, it was found that in order to obtain a clean surface finish and accurate outer dimensions, multiple passes of the laser with subsequent refocusing were required. This allowed the laser to cut approximately 3 mm into the foam on each pass with little dispersion of the cutting beam - this dispersion leads to wide kerf and poor surface finish. The correct speed and power settings for the laser cutter for each density of foam were obtained by iterative experimentation, after which successive cuts were made. Figure 4.13a shows a cut in progress, and Figure 4.13b shows thin scraps of material being used as a datum for refocusing the laser beam at successively lower levels for each pass of the cutter.

The resulting 10 mm thick profiles were cut eight at a time for each wheel prototype, then glued together using a spray-on contact adhesive to form two 40 mm wide wheels. This method rapidly produced high-quality wheels of significant complexity, but was limited to two-dimensional profiles only.

The brass hubs were turned from stock material in the UCT Mechanical Engineering workshop. This was achieved exactly to specification and the finished hubs are shown in Figure 4.14.

Figure 4.14
The machined brass hubs

4.7 TAIL

4.7.1 *Design*

The robot is equipped with a tail that serves a variety of purposes. First and foremost, it provides a reaction torque to propel the robot forwards when surmounting obstacles. Secondly, it is used as an aerodynamic "wing" whose drag forces, if the robot falls through the air, re-orient it such that the robot falls straight down with the tail behind it, similar to the flight of a dart or arrow. Thirdly, it has ergonomic cut-outs which provide a place for the operator to grip the robot during deployment, and assist in throwing the robot great distances into disaster areas.

The tail is designed to be manufactured by gluing two sheets of laser-cut SPX foam together. Antennae for transmitting sensor data, motor commands, and video stream are sandwiched between the two sheets, outside of the robot shell yet still protected from damage by the body of the tail. This has the additional advantage that the EMI associated with the antennae is somewhat removed from the electronics inside the robot, reducing the chance of unwanted interference.

As the robot rests on the tail during operation, the face that is in contact with the ground is a smoothly contoured surface that will slide over obstacles with ease. This profile is visible in Figure 4.15. This member of the tail is duplicated so as to provide a stable resting point for the robot. As the robot will rest on the wheels and tail whilst in operation, their relative dimensions are designed such that the robot's resting angle offers an optimal field of view to the primary camera in the sensor payload.

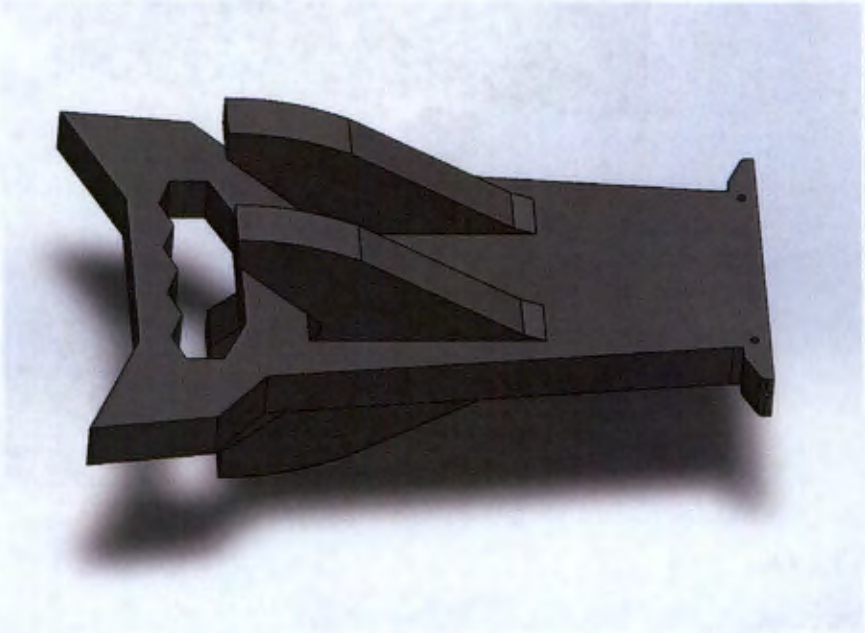

Figure 4.15 The robot's tail structure

4.7.2 *Manufacturing*

The tail was manufactured in the same manner as the wheels, i.e., from layered laser cut sheets of SPX90 foam glued together. The tail was also etched with a logo to identify the robot, shown on the assembled tail structure in Figure 4.16. As the sensor and communication sub-systems were not complete at the time of manufacture, it does not contain the proposed antennae and future work must incorporate them.

4.8 ASSEMBLY

The robot was assembled for testing according to the design, however, during this process a number of issues were highlighted. These are outlined below as they arise in a description of the assembly process.

The heatsink seals were placed onto the heatsinks and these inserted into their slots in the shell. Some filing of the plastic had to be done to accommodate the heatsinks correctly, but after this their fit was secure and four M2 screws were used each to secure them to the case.

The case seals were then fitted into their slots on the case (shown in Figure 4.17). It is recommended to increase the width of the sealing faces in future work, as they were not easily prevented from falling into the shell.

The PCB was mounted to its heatsink and its thermal conductivity ensured with a liberal application of heat conductive paste (Figure 4.18). Due to manufacturing flaws in the case, the charging connector could not be installed, however this was of no consequence as

Figure 4.18 Assembly of the control PCB and its heatsink

G Knox's final power management system was not ready for integration into the robot.

The motors in their foam mounts were inserted into their slots and their power cables soldered on. As noted in Section 4.4.2, the motor mounts were somewhat fragile so they were temporarily secured with tape. This stage of assembly is shown in Figure 4.19. As the motor housings were not manufactured to the correct specification, the temperature sensors could not be attached to the motors.

The battery, with its protection PCB attached, was then placed on its mounts and the tail fitted snugly behind it (depicted in Figure 4.20a and 4.20b respectively).

As noted in Section 4.3.2 the screw holes in the two halves of the shell were poorly aligned and the HDPE was not strong enough to support a thread. In order to expedite the testing process, the shell was fastened shut using tape which, although not aesthetically pleasing, was sufficiently structurally sound to support the robot during testing.

The final assembled platform is shown in Figure 4.21.

Figure 4.16
The assembled tail

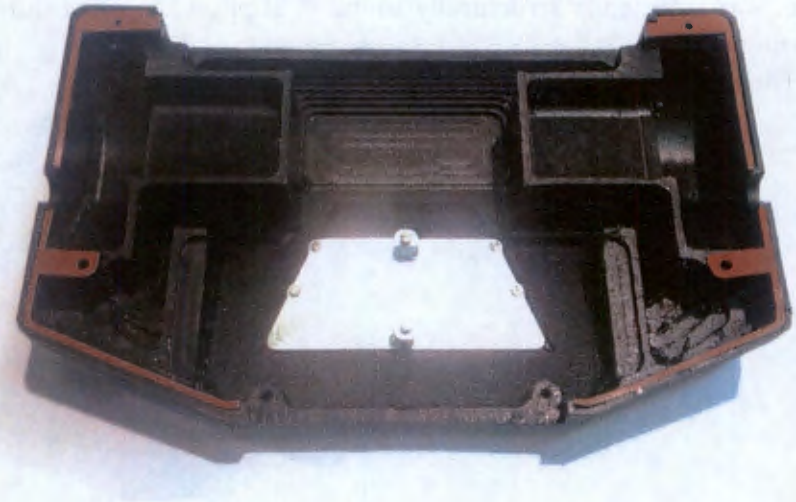

Figure 4.17
Heatsink attached and seals inserted

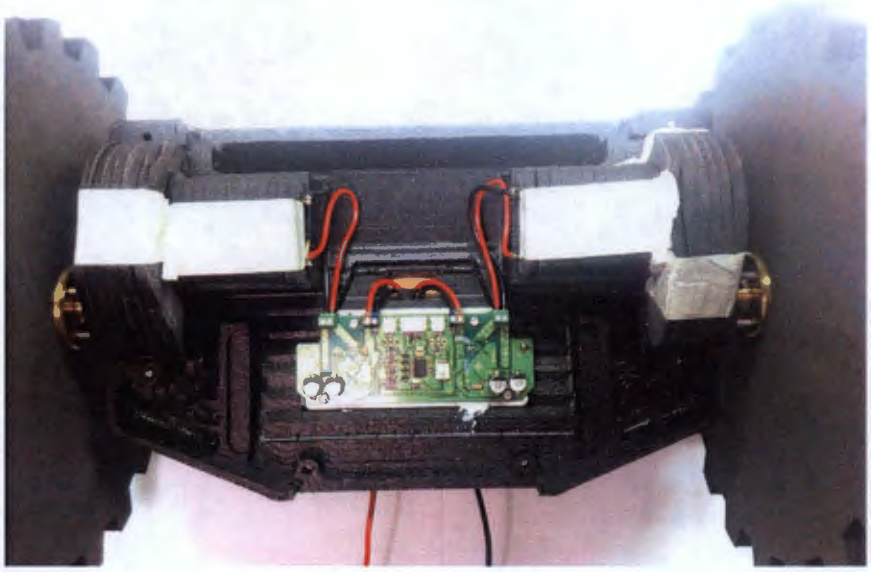

Figure 4.19 Motors secured and connected in shell

(a) The battery sub-system in position

(b) The tail secured against the battery

Figure 4.20 Assembly process showing battery and tail assembled

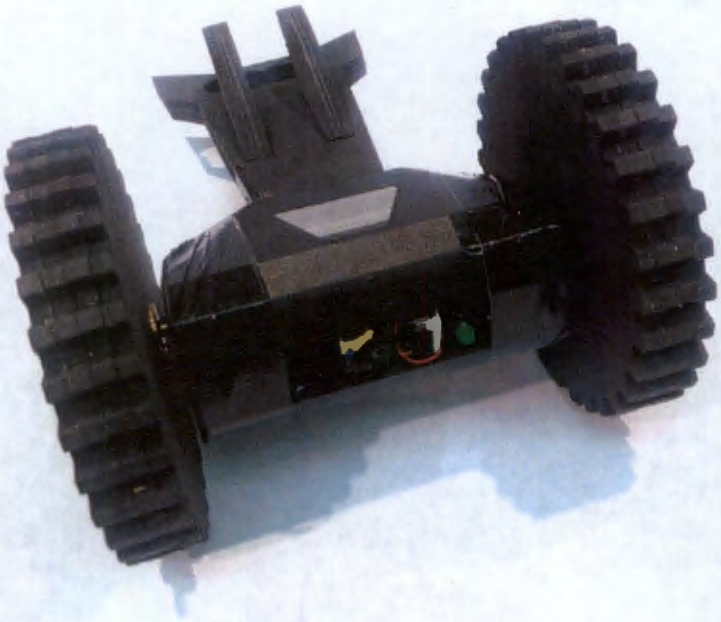

(a) Front view

(b) Rear view

Figure 4.21 The robotic platform as finally assembled (temporary testing controller visible within)

5

ELECTRICAL, ELECTRONIC AND SOFTWARE SYSTEMS

5.1 INTRODUCTION

This section details the design of the electrical, electronic and software sub-systems contained in the robotic platform. These are limited to only what is required to receive commands from an external "master" controller or base station, interpret these and transform them into appropriate control signals that power the motors. Additionally, data on the state of the system — the motor drivers' current consumption and motor temperatures — is captured and returned to the base station by the same communication protocol. Figure 5.1 shows the components used and their interconnections in one half of this simple sub-system — the other half, controlling a second motor, simply adds a second motor driver and feedback system, connected to the microcontroller in the same way as the first.

5.2 MOTORS

5.2.1 *Motor Specification*

A pair of motors with built-in reduction gearboxes was selected using the following criteria: torque, speed, input voltage, current consumption and, most importantly, price. These are elaborated on below.

5.2.1.1 *Torque*

A torque specification was achieved by considering the worst-case scenario; the robot must, using one motor only, lift its entire mass up a vertical ledge (assuming perfect traction). The highest ledge on which a wheeled robot can possibly find traction would be equal to the radius of the wheel, shown in Figure 5.2. The torque T experienced by the motors can be expressed as:

$$T = mgr$$

where m is the mass of the robot, r is the wheel radius and $g = 9.81^{m}/_{s^2}$, the gravitational acceleration. As the final dimensions of the robot could not have been known before the design was complete, the torque specification is based on the specified mass and dimensions from Chapter 7. Substituting $m = 3kg$ and $r = 125mm$ into the formula above yields a maximum torque of 3.68 Nm per motor.

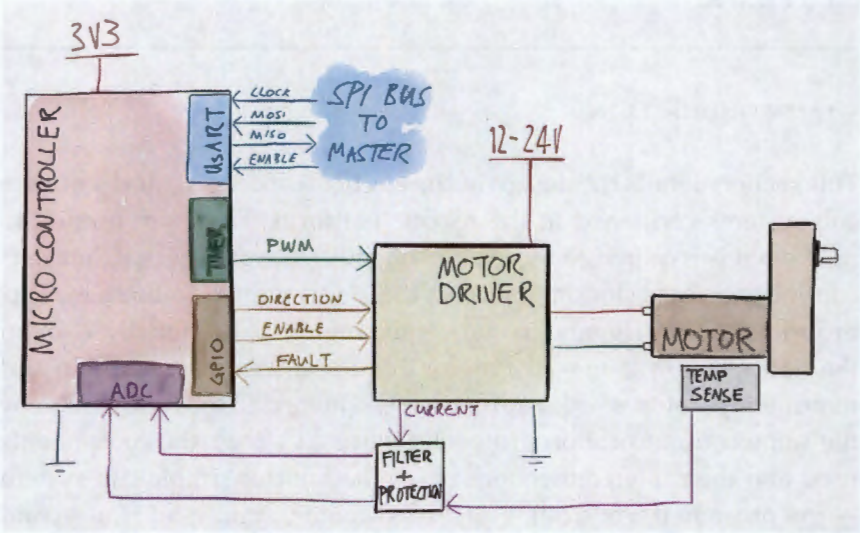

Figure 5.1 Block diagram showing electronic modules and connections

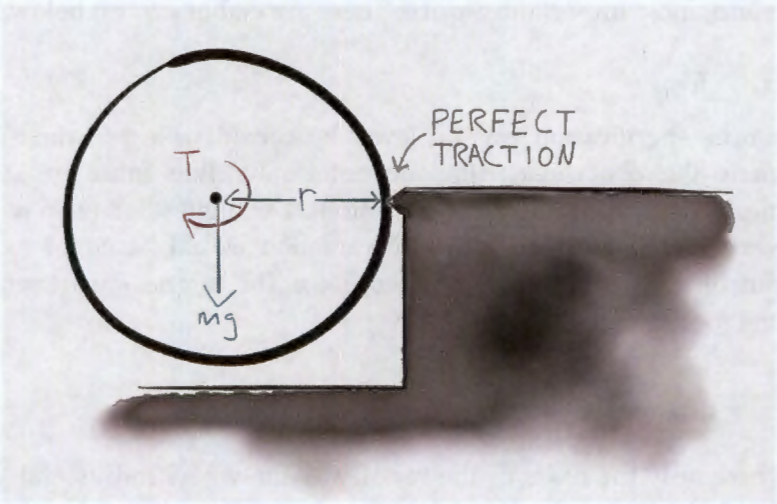

Figure 5.2 Diagram showing maximum torque requirement

5.2.1.2 *Speed*

The maximum speed for the robot, as specified in Chapter 7 is 0.75 m/s. The rotational velocity ω (in radian/second) of a wheel of radius r whose edge is travelling at v (m/s) is given by the formula:

$$\omega = \frac{v}{r}$$

Expressing this in terms of rotational speed s (in revolutions per minute) introduces a conversion factor:

$$s = \frac{60v}{2\pi r}$$

Substituting in $v = 0.75^{m}/_{s}$ and $r = 125mm$ (as above) yields a maximum motor speed of 57.3 rpm.

5.2.1.3 *Electrical Power and Control*

As specified in Chapter 7, the platform is to be powered by a rechargeable battery. The power management sub-system as designed by G Knox in his M.Sc contains a 3000 mAh four-cell Li-Ion battery and a range of voltage regulators to provide power to different components. The motors, however, must be connected directly to the battery as the inefficiency of voltage regulators at high currents would waste significant power. As such, the motors need to operate safely on a voltage between 16.8 V and 12 V: the battery voltage will decrease slowly during operation of the robot before being recharged. The current consumption of the motors and the current capacity of the battery were selected in consideration of each other: the final specification was that each motor's peak current draw should not exceed 5 A. This restriction on electrical power in turn restricts the mechanical power of the motors; consequently there was found to be no need to specify a maximum size for the motors as nearly all motors of this specification are sufficiently small for integration into a small inspection robot.

Due to the goal of design simplicity and cost reduction, it was decided to use a brushed DC motor rather than a more sophisticated brushless motor. Despite their better performance per size and increased efficiency, these motors are significantly more expensive and require more expensive and complex control circuitry and as such are not appropriate in a robot designed to be "disposably" cheap. Their increased reliability was also deemed unnecessary as the robot is not expected to be heavily or continuously used: during its entire lifetime the ratio of operating time to standby time is expected to be low.

Figure 5.3 The Crouzet 82 861 010 motor[43]

5.2.2 *Motor selection*

Maximum traction occurs when underlying terrain operates as a fulcrum, totally locked into the wheel tread.

An exhaustive survey of all known local suppliers quickly revealed that, within the limits of the other specifications, the torque specification was almost entirely unattainable. This was not deemed a serious disadvantage as it would be highly unlikely that the robot would ever attain perfect traction and much less so with only one wheel in contact with the ground surface. A number of suitable motors was found in the price range of US $300-500 each but this would have represented a significant incursion to the budget of US $500 total production cost per robot, so were deemed unsuitable.

The only remaining option from the suppliers surveyed was the CROUZET 82 869 006 which operates at a nominal 12 V drawing 3 W of power, delivering a top speed of 54 rpm and a maximum torque of 2 Nm[42]. This, however, was not stocked anywhere in the country and a special order would have been financially destructive and have taken more time than was available in the project plan. As such, to expedite the creation of the first prototype, the closest available motor from the same range was selected as a compromise. This was the CROUZET 82 861 010 (shown in Figure 5.3) which is identical except for a smaller gearbox that consequently can only provide 0.5 Nm torque. This was deemed to be sufficient to test the operating principles of the robot and serve as a proof-of-concept; later prototypes would, in any case, be more suited to refining the torque specification once the final weight of the platform was more accurately known. Future work will replace these with higher-performance motors if the first prototype is successful.

5.3 CONTROL AND COMMUNICATIONS

In order to control the motors, commands must be received from a master controller (in the base station, or possibly via the sensor payload), interpreted by a slave controller in the robot, then these conver-

Figure 5.4
The TI MSP430 Launchpad development board[3]

ted to control signals which drive the motors. Additionally, data on the current consumption and temperature of the system is gathered and returned to the master device. A full circuit diagram detailing the electronic sub-system is attached in Appendix D.

5.3.1 *Microcontroller*

The controller at the heart of the platform receives commands over SPI, interprets these commands and accordingly controls the behaviour of the motors. It also gathers data on the state of the motors and returns this to the device controlling it, which could be a controller within the sensor payload or a wireless communication module.

The microcontroller selected for this application was the TEXAS INSTRUMENTS MSP430G2553. The MSP430 family are 16-bit microcontrollers designed for their ultra-low power consumption (as low as 230 μA)[44]. The G series in particular is the low-cost range, costing less than US $1 per unit at volume. These factors, as well as their readily available LAUNCHPAD development boards strongly motivated their selection. The MSP430G2553 operates off a range of supply voltages from 1.8 V to 3.3 V and clocks up to 16 MHz with no need for an external oscillator[45]. It has two 16-bit timers necessary to generate PWM signals for motor control, a multi-channel 10-bit ADC with data transfer controller suitable for current feedback and other sensing, and supports a variety of serial data protocols. Figure 5.4 shows the Launchpad development board used to develop the circuitry.

5.3.2 *Motor drivers*

In order to control the motors at higher voltages and currents, motor driver ICs were used. These are single-chip solutions that contain

Figure 5.5 The Freescale MC33926 breakout board by Pololu[46]

an entire H-bridge control circuit; all that is required is to provide low voltage control inputs and the internal H-bridge amplifies these signals for driving the motors.

A pair of Freescale MC33926 throttle-control H-bridge chips was selected as suitable motor drivers as they were well within the electrical specifications of the motors, and readily available as a pair on a breakout board for rapid prototyping, shown in Figure 5.5.

They are capable of delivering up to 5 A at between 5 V and 28 V[47], significantly more than the motors were likely to consume but this provided a safe margin of tolerance, ideal when developing with new and unknown motors. This could be revised in future work. They are each powered directly from the battery and controlled by 3 V-tolerant control inputs connected to the MSP430 microcontroller. These control inputs provide a PWM signal — duty cycle proportional to requested motor power — and a binary direction signal which inverts the direction of rotation of the motors. Additionally, each IC can be enabled or disabled by toggling an "enable" pin which is also connected to a GPIO output on the MSP430. The outputs of the H-bridge ICs were connected to the motors directly. Another important feature of the MC33926, especially in critical scenarios encountered in USAR and tactical work, is that it has "soft" current limiting thermal protection; if the IC overheats, it gradually reduces the current supplied so that the motors can continue running at reduced power rather than shut off completely.

If a motor is turned by some external force (such as an untrained operator experimentally turning the robot's wheels) it will develop a voltage across its terminals. To protect the control circuitry from damage caused by this generated voltage flowing back into the system, a protection circuit was implemented. This circuit, shown in Figure 5.6, uses a MOSFET to isolate the ground planes. The gate of the MOSFET is connected via a pull-up resistor to the battery voltage line: when this line is high, the MOSFET opens and connects the main ground plane ("GND" in the diagram) to the motor driver's ground ("GND1"). This ensures that voltages generated by back-driving the motors do not reach the rest of the circuitry.

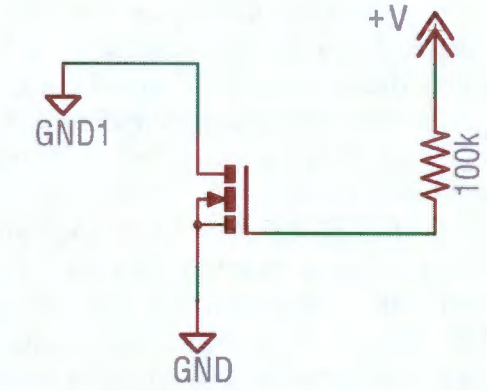

Figure 5.6 MOSFET protection circuit

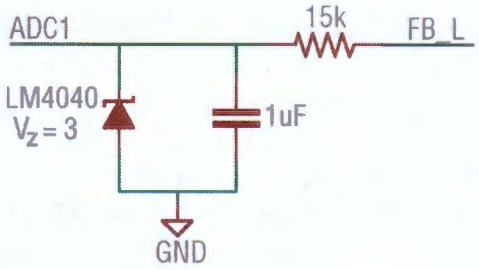

Figure 5.7 Diagram showing filter and safety diode

5.3.3 *Feedback, Control and Safety*

The motor drivers provide feedback on two pins: a "status fault" pin that indicates if an over-current event or overheating is occurring, and a current feedback pin which provides 0.24% of the high-side H-bridge current. To measure the current consumed by the motor driver, the current feedback pin is connected to ground through a 220 Ohm resistor to convert this current into a voltage that can be read by the ADC on the MSP430. This feedback, however, is of high enough temporal resolution that even with the PWM frequency at 20 kHz, the reference current fluctuates significantly with every pulse. To smooth this and obtain an average voltage representative of the average current being consumed at a given time, a low-pass RC filter was designed with a cutoff frequency of 10 Hz. To protect the ADC from transient bursts of very high (theoretically infinite) current as the motor starts and stops, a 3 V LM4040 voltage reference is used as a Zener diode to clamp the feedback line to 3 V, allowing a safety margin of 0.3 V when the MSP430 is powered from a 3.3 V line. This circuit is shown in Figure 5.7.

Two further ADC inputs were made available for temperature sensors that could monitor the motors to ensure they did not overheat, and the same circuit described above was used to smooth the data and protect the microcontroller inputs.

The status fault line has a pull-up resistor keeping it at a default of 3.3 V; in case of some error the MC33926 pulls the line down to

ground. This line is then connected to a GPIO input on the MSP430 such that, if a fault is detected, the software executes a command to safely disable that motor, and it ceases to draw current. It then then periodically attempts to recover control of the motor in case the cause of the fault has subsequently been removed. (described in more detail in Section 5.6.5)

No closed-loop control was implemented as the required sensors and processing power would significantly increase the production cost of this sub-system. Although this may be detrimental to the performance of the platform, there is also a need to benchmark what is technologically possible within severe financial and complexity limitations. Should the platform prove to be successful without these features it will serve as a valuable proof-of-concept.

5.3.4 *Temperature sensors*

To measure the temperature of the motors and ensure that they are operating within safe limits, two LM35 temperature sensors are used. These are powered by the 3.3 V supply and return a voltage signal proportional to their temperature. This is fed through a filter to remove noise caused by the motor EMF and a protection zener to ensure the voltage does not exceed unsafe levels before being passed to an ADC channel on the MSP430 for digitisation.

5.4 PROTOTYPING AND DEVELOPMENT

To expedite and streamline the design of the electronic sub-systems whilst minimising the risks associated with new and untested hardware, a strict iterative prototyping design process was followed. The microcontroller and motor drivers were thoroughly tested independently of each other on their respective breakout boards before they were connected. Specially made wires and jumpers were then used to connect the correct pins together and the entire system demonstrated to a minimum working proof-of-concept before custom PCBs were manufactured. This prototyping setup is shown in Figure 5.8.

Once the motors could be controlled and basic readings could be taken using this setup, a second-stage prototype PCB was designed. This board was manufactured externally and the components hand-populated and oven-soldered at RARL. The design of this PCB specifically allowed large gaps between components, many accessible test points, and jumpers connecting the various components such that they could be isolated for specific testing. This board established that IC footprints were correctly designed and the manufacturing and assembly processes were successful. The large spaces between components and many available test points also allowed for corrections to be made by reworking the board and changing or adding com-

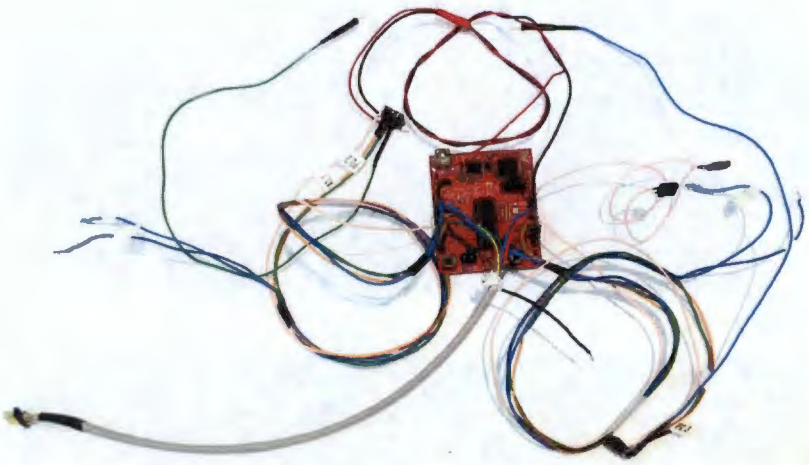

Figure 5.8
The TI MSP430 Launchpad with prototyping wires

Figure 5.9
The "beta version" PCB design, showing temporary connections to external microcontroller

ponents; Figure 5.9 shows this PCB, with additional through-hole resistors and wiring following a modification and a correction to the original design.

This intermediary "beta version" board also allowed for flexibility in the design process. After a major revision to the communication structure necessitated a re-allocation of the MSP430 pins, the microcontroller on the PCB could be disconnected at the jumpers and the ubiquitous Launchpad connected in its place using the prototyping wires seen at the top of Figure 5.9. This demonstrated and allowed for development of the new configuration without necessitating a new PCB manufacturing run.

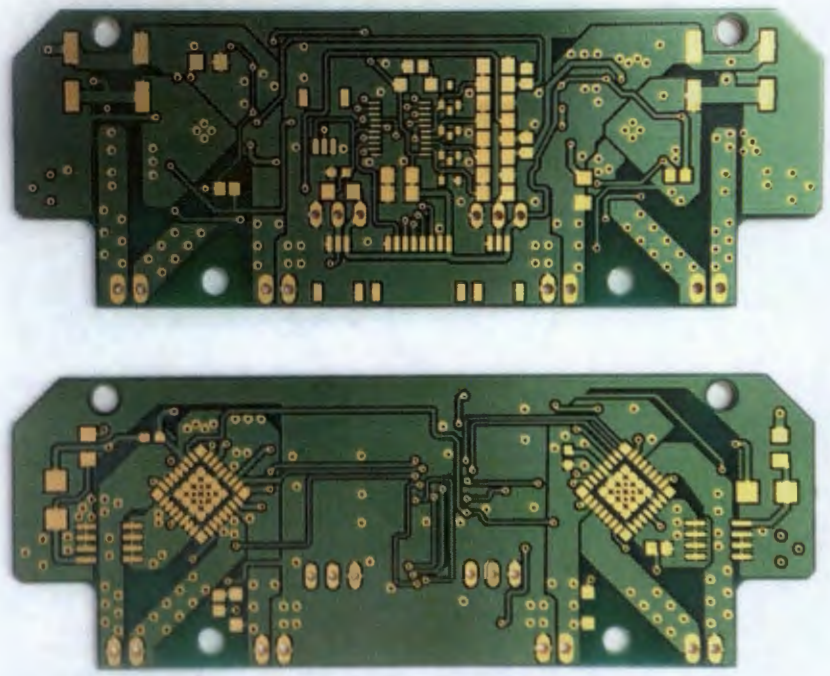

Figure 5.10 The final PCB (top and bottom views)

The following section elaborates more on the methodology of the PCB design and describes the final revision board that was used in the platform.

5.5 PCB DESIGN

The final PCB, shown in in Figure 5.10 was designed with a number of modifications from the prototype. The filter/protection circuit was added, the communication with the external master changed from UART to SPI (necessitating a reconfiguration of nearly all the MSP430 pins), and a number of minor errors corrected. Most importantly however, the PCB was dramatically reduced in size and given the correct shape to fit into the housing, and attachment points were designed with screw holes such that the PCB could be attached to its heatsink.

To dissipate heat into the aluminium heatsink, the motor driver ICs were located on the underside of the board. The design guidelines for the QFN package [48] specify that, to dissipate heat, vias are used to connect the central ground pad to a ground plane on the opposite side of the board. In order to electrically isolate the low-voltage microcontroller circuit and protect it from the noisy, higher-voltage motor drivers, the centre of the PCB on both sides was reserved for the low-voltage circuitry, whilst the two edges each contained a motor driver and its supporting components (see lower image in Figure 5.10). Furthermore, the microcontroller circuitry was concentrated on the upper side of the board (see upper image in Figure 5.10). This also allowed easier access to digital signals during testing and integration.

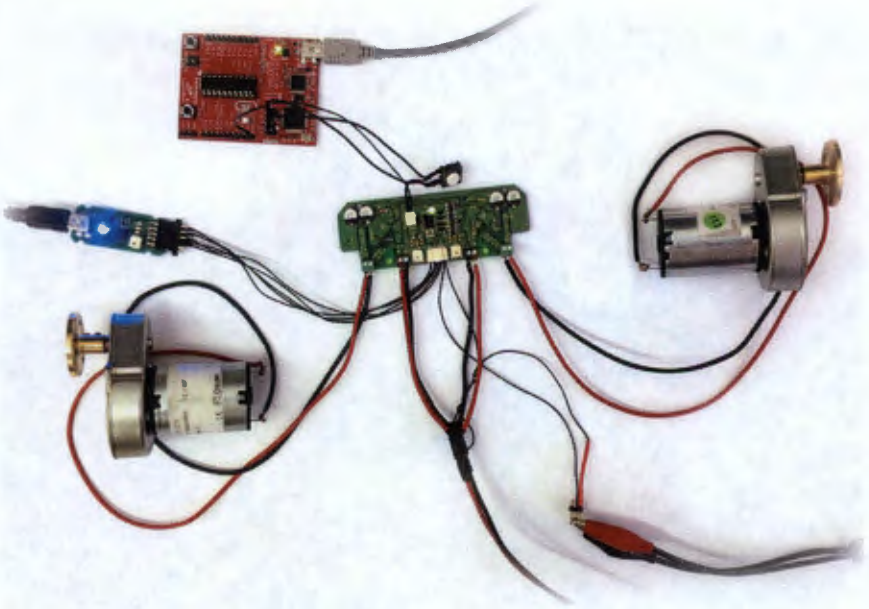

Figure 5.11 Electronics testing and software provisioning setup

5.5.1 *Testing and software provisioning*

Testing and loading of software was done by connecting the programmer on the Launchpad development board to the MSP430 on the assembled PCB using custom-made connectors. A USB-to-SPI converter was used to send commands to the microcontroller and the system tested using a simple GUI (described in more detail in 7.5.1) that interpreted commands from an Xbox controller and sent them out over USB to the USB-to-SPI converter. The motors were successfully driven and feedback from the current and temperature sensor recorded. This testing setup can be seen in Figure 5.11.

The fully assembled circuit board is shown in Figure 5.12 fastened to its heatsink inside the robot chassis.

5.6 SOFTWARE

The software written for this project implements a number of simple algorithms and runs in embedded mode on the MSP430 microcontroller. The software was written in C and loaded onto the microcontroller using the programming circuitry on the Launchpad development board. Various sub-systems co-operate to achieve the end goal of motor control, these are described in turn below. As the entire system relies on the receipt of commands from an external master controller, the communication protocol is discussed first.

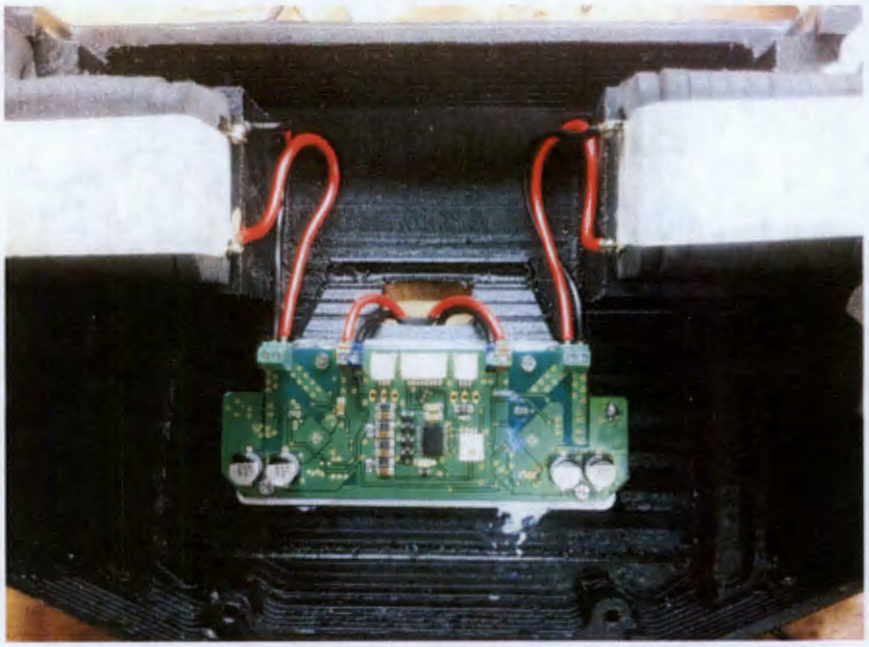

Figure 5.12 Assembled circuit board in robot chassis

5.6.1 *Communication protocol*

The MSP430 is configured to send and receive information over SPI, a full-duplex, clocked, 4-wire asynchronous communication protocol. Two arrays are initialised in memory; for data to be sent, and data that has been received. When the external master device pulls the MSP403's Chip Select line low, an interrupt is triggered and the master and slave devices exchange information simultaneously. Data is streamed out of the "transmit" array as a serial byte stream on the MISO line as the corresponding data is received serially on the MOSI and streamed into the "receive" array. This exchange of information is controlled by the master device and can be triggered at any time, during which other processes on the microcontroller are halted.

5.6.2 *Main Structure*

The main loop of the software follows producer-consumer architecture in that it simply manages the data generated or captured by other peripherals or functions. This entails loading the "transmit" array with the latest temperature and current consumption data and interpreting the data in the "receive" array, translating it into motor commands and setting the relevant GPIO pins and other peripherals to control the motors based on these commands.

5.6.3 *ADC and Data Transfer Controller*

The Analogue-to-Digital-Converter is configured to scan four channels (temperature and current draw for each motor) continuously, capturing the voltage on each of the four pins successively during the operation of the robot. To avoid using CPU time to store this data, the automatic Data Transfer Controller is configured to store the data at a specified memory address every time a ADC conversion completes. As the ADC scans successive channels, so the DTC stores the data in successive memory addresses until all channels are converted and the process repeats from the first channel and memory address again. The main loop accesses these memory addresses as it runs through its routine and the data is processed for return to the master. Thus the two processes can execute simultaneously and independently of each other.

5.6.4 *Timers*

Two timer modules are used in this software. The first creates a pulse-width-modulated square wave by raising and lowering the voltage on a pin at fixed intervals. The PWM frequency is set by writing to a register at the beginning of the code, and the duty cycle (switching intervals) is controlled by the value in the "Capture and Compare" register which is written to by the main loop. Control of individual motors is achieved using two separate channels of this module, each with their own Capture and Compare register.

The second timer channel is used to create a fixed-length delay which is used in the fault recovery described in the next section. This is activated by calling a function which sets the relevant timer control registers. The timer then runs until an interrupt is triggered, and in this interrupt the timer is disabled again. This allows the software to perform some task a known time after a previous task without using the CPU to mark the time. The CPU can thus continue to process data in the background until the timer period elapses.

5.6.5 *Fault detection and recovery*

In the event of a short-circuit, the MC33926 pulls the voltage on a Status Fault line to zero. This line remains low in its "fault condition" until the MC33926 is reset, whereupon the motor driver continues to operate, assuming the cause of the short circuit is removed. If the short circuit is not removed, another status fault is triggered. This status fault line is attached to a GPIO input on the MSP430 and this GPIO pin is configured to generate a software interrupt should the line go low. This interrupt immediately writes data to the "transmit" array, noting which of the motors is indicating a fault: this can ac-

cordingly alert the operator. The MC33926 enable line is set to zero, disabling the motor driver, and both motor speeds are set to zero. This leaves the robot in a safe state, not moving out of control, and as the motors are halted, excessive current draw from the short circuit is avoided. The delay timer is then activated, and the GPIO interrupt terminates. The CPU can now return to its main loop and continue to handle data to be sent or received.

After 0.6 milliseconds, the timer reaches its set value and another interrupt is triggered. This delay prevents the controller from getting stuck in an endless loop and allows the main loop to process data and maintain communication with the base station. The timer interrupt code then re-enables the motor drivers, and checks to see if either is still in a status fault state. If the short circuit condition has been removed, this "disable-wait-enable" reset routine will restore the motor driver to functionality. If either motor is still in a fault state, the cycle continues until the fault condition is removed.

This feature was tested by shorting across the output of the motor drivers. While the terminals were connected, the system drew only its quiescent current, and normal operation resumed immediately as the short was removed.

5.7 CONCLUDING REMARKS

This chapter has described the design, manufacture and development-related testing of the electronic sub-system in the robotic platform. This sub-system uses a small microcontroller and two motor controller ICs to control the movement of the two motors by accepting commands from an external "master" controller or base station and from these, generating appropriate control signals that power the motors. Safety mechanisms are included that successfully limit the current draw in the event of a short circuit, and temperature and current consumption data is returned to the base station controller. Additionally, embedded software was developed to integrate and control these components and manage communications with the base station controller. The combined system, integrating the mechanical and electrical sub-systems, will be tested in Chapter 7 after a description of the investigation into and development of energy-absorbing wheels to protect the systems from potentially damaging impacts during operation.

6

MECHANICAL DESIGN AND TESTING: WHEELS

6.1 INTRODUCTION

6.1.1 *Background*

A significant challenge in this project was the design of some structure or mechanism to absorb the impact incurred as the robot tumbles or falls during its operation, thereby protecting the chassis and delicate sensors within. When the robot collides with an object — or the ground below, in the case of a fall — it will rapidly decelerate to a halt over some distance determined by the structure and material of the contact surface. Ideally, as much of the energy associated with this deceleration should be absorbed in as short a time as possible. Furthermore it is desired that the motion be well damped; that is, that the kinetic energy is not rapidly returned, setting up oscillations (quite simply, bouncing of the robot) that could cause further damage. It is clear from these requirements that the design of some sort of suspension is required and this section sets out to explore the design options available to mitigate the effects of a collision.

In the interest of reducing part count, manufacturing cost and complexity, it was decided that this suspension should be incorporated into the structure of the robot's wheels. Preliminary investigations into the impact physics revealed that FEM and other numerical modelling would be laborious and out of the scope of this project, as a detailed material characterisation of the material would be required. In the interest of rapidly producing a testable prototype platform, a test-driven iterative rapid prototyping design approach was employed to develop impact-absorbing wheels suitable for this purpose. These provide traction and mobility as well as cushioning the relatively delicate internal components and sensors from otherwise damaging forces incurred when the robot falls or tumbles.

This section of work differs from the previous design chapters in that it relies on new research and testing as opposed to specification-driven design using well-understood components and existing methods. Accordingly, it can be treated as a sub-project within the main dissertation, and is presented with its own goals, background research, testing, results and conclusions, which ultimately feed back into the final design in order to meet the over-arching design goals outlined in Chapter 3.

6.1.2 *Collision Physics*

The worst-case collision that this robotic platform will have to survive is the case where the robot, whilst searching the upper storey of a building, is driven over a ledge or falls unexpectedly through the damaged floor to a lower storey. Benchmarking the height of a storey at 3 metres, Conservation of Energy can be used to estimate the final velocity of the robot before it makes contact with the ground. Assuming the initial kinetic energy of the robot is negligible compared to its gravitational potential energy, its potential energy before falling (state 1 in Figure 6.1) is equal to its final kinetic energy just before collision (state 2 in Figure 6.1) and as such:

Note: throughout this section, the gravitational constant $g = 9.81\text{m/s}^2$ is treated as a relative unit of acceleration

$$\frac{1}{2}mv^2 = mgh \tag{6.1}$$

Solving for the final velocity v estimates it at 7.7 m/s, significantly greater than the maximum specified velocity of the platform whilst it is being driven. As such, the 3 metre drop is used as the benchmark for worst-case loading within the robot's specifications, as the impact velocities are significantly greater than can be experienced whilst the robot is manoeuvring under its own power.

In any case, it is unlikely that the robot can be thrown higher than the first floor, limiting the height from which it can possibly fall.

This kinetic energy must be absorbed by some suspension element. By modelling the suspension as a simple linear spring, the kinetic energy before collision can be equated with with the total energy absorbed by the spring during collision. Thus it is possible to estimate the displacement δ_{max}which the suspension design must allow in order to absorb a specific collision energy. This develops the equation:

$$\frac{1}{2}mv^2 = mgH = \frac{1}{2}k{\delta_{\text{max}}}^2 \tag{6.2}$$

where m is the mass of the robot, H is the total falling height, and k is the elasticity constant of the spring.

Noting that by Hooke's Spring Law $\vec{F} = -k\vec{\delta}$ and Newton's Second Law $\vec{F} = m\vec{a}$:

$$k\delta_{\text{max}} = F_{\text{max}} = ma_{\text{max}}$$

Substituting the above into Equation 6.2, we see that

$$\delta_{\text{max}} = \frac{2H}{a_{\text{max}}} \tag{6.3}$$

where a_{max} is the maximum acceleration (measured in multiples of g, and denoted here with a capital G). Benchmarking the maximum safe collision deceleration felt inside the robot chassis at 250G (the conservative maximum rating of the FLIR Quark thermal camera[49]) results in a maximum suspension deflection of 24 mm for a drop height

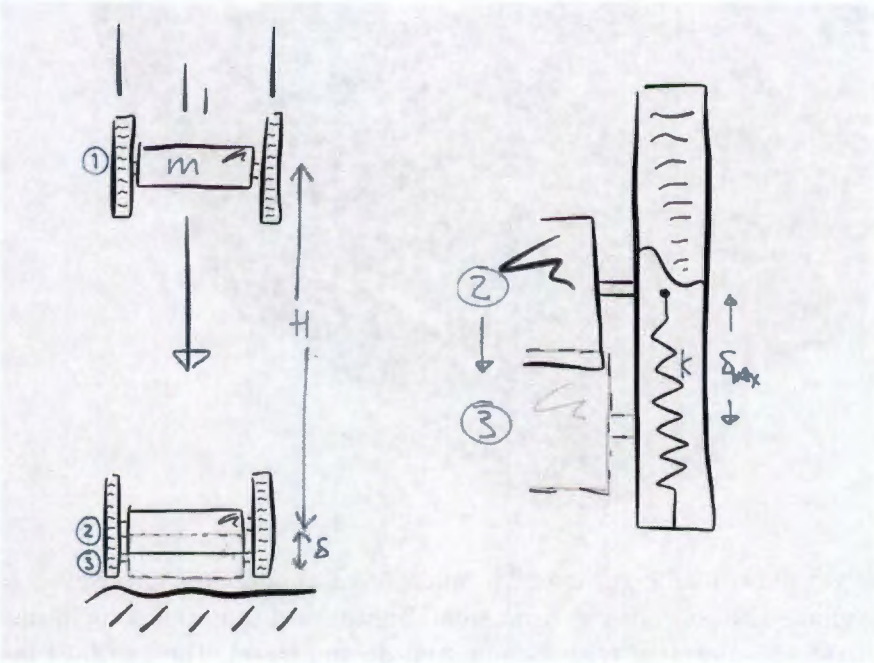

Figure 6.1 Robotic platform in falling situation

of 3 m (state 3 in Figure 6.1). This dimension was a chief consideration in designing the shape of the housing and the relative geometries of the shell and wheels.

This approach overlooks two critical areas: the non-linearity of any real suspension spring, and the effect of damping, which is present in every real dynamic spring-mass system (both of which may actually be desirable). Observing the full equation for a damped spring-mass system (Equation 6.4), it can be seen that including a damping term $b\vec{v}$ (where b is the damping coefficient) quickly makes the analysis non-trivial, as the velocity of the end of the spring at any point in the collision is entirely dependent on the design and material of the suspension. Furthermore the coefficients k and b are most likely non-linear; that is, they are functions of δ and v.

$$\vec{F} = -k\vec{\delta} - b\vec{v} \tag{6.4}$$

To make precise and meaningful inferences beyond this point, we would need to use numeric methods beyond the scope of this dissertation, as well as construct an accurate model of the chosen material, in itself a highly non-trivial task. The remainder of this chapter thus pursues a test-driven design methodology, and begins with an investigation of a range of existing designs.

6.2 REVIEW OF EXISTING DESIGNS

The majority of the existing body of research and development work on the topic of energy-absorbing wheels is concerned with shock

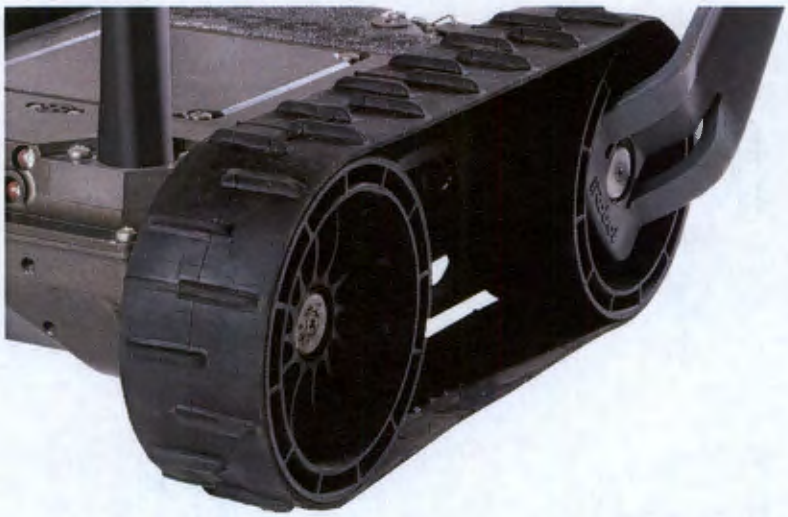

Figure 6.2 Close-up of the FirstLook wheel design [4]

absorption in the commercial automotive application: protecting a vehicle and its contents from small bumps and imperfections in the road or ground surface encountered during travel. The loadings incurred are typically of small deflection and high frequency. As such, these designs are only of tangential interest to the problem at hand: protecting the vehicle from low frequency, high deflection loadings incurred when the robot falls from heights orders of magnitude higher than its own size.

The academic and patent literature surveyed primarily concerns complex, multi-part mechanisms and so the attention is focused on designs visible in the public and commercial space, beginning with the designs used on existing 'throwable' robots and then moving slightly further afield.

6.2.1 *iRobot FirstLook 110*

As noted in Section 2.3.3, the iRobot FirstLook weighs 2.47 kg and can survive a fall of 4.87 m. How this is implemented is not exactly stated, but the close-up photograph shown in Figure 6.2 shows a wheel with many fine curved spokes which clearly provide some suspension. The wheel appears to be moulded from a relatively hard plastic but, as the internal design of the robot is not known, it could be that this is not the only suspension element. As with all the designs surveyed in this section, it is simply stated that the robot "survives"; no information is given on the impact felt by the sensors or internal components.

6.2.2 *Recon Scout ThrowBot*

The Recon Scout range is also "throwable" and drop-proof: weighing in at 0.64 kg, the Scout XL survives a 4.6 m drop. This is achieved by means of large, cast urethane wheels[50] which can be seen in

Figure 6.3 The Recon Scout and Scout XL, showing their wheels[5]

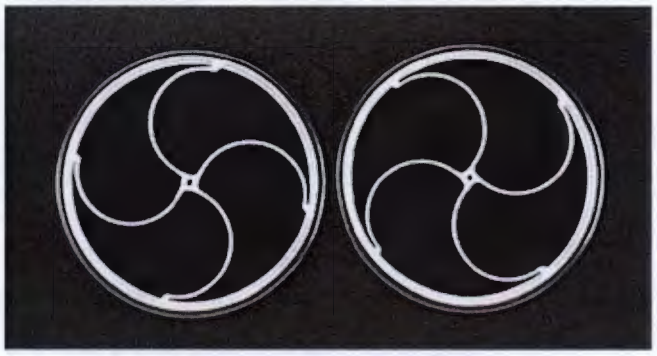

Figure 6.4 Hobby aeroplane wheels by GWS[6]

Figure 6.3 alongside the standard Scout. Given the size of the casing, it is assumed that these are the only suspension elements. The flexible urethane rubber is a chief contributor to their effectiveness; however they are also designed with struts and open holes that will flex upon loading of the wheel to absorb load. A supplier claims the Recon Scout can survive up to 1500G impact loading[51], but it is not specified whether this is a loading to the wheels or the body.

6.2.3 *Hobby RC Aircraft Wheels*

Another point of departure for this investigation is the landing gear for hobby model aircraft, which must be simple and ultra-lightweight, yet still protect delicate model aeroplanes from often less-than delicate piloting and terrain when landing. No concrete data was found on their specifications or effectiveness but Figure 6.4 serves as another good example of curved-spoke designs used in impact absorption.

6.2.4 *NASA — Mars Rover*

NASA's Curiosity rover, which landed on the Martian surface in August 2012, was possibly the most expensive, highly researched and well-publicised occurrence in history of a small vehicle dropping from a great height onto harsh terrain. However, details on the engineering that went into protecting the rover from this impact are hard

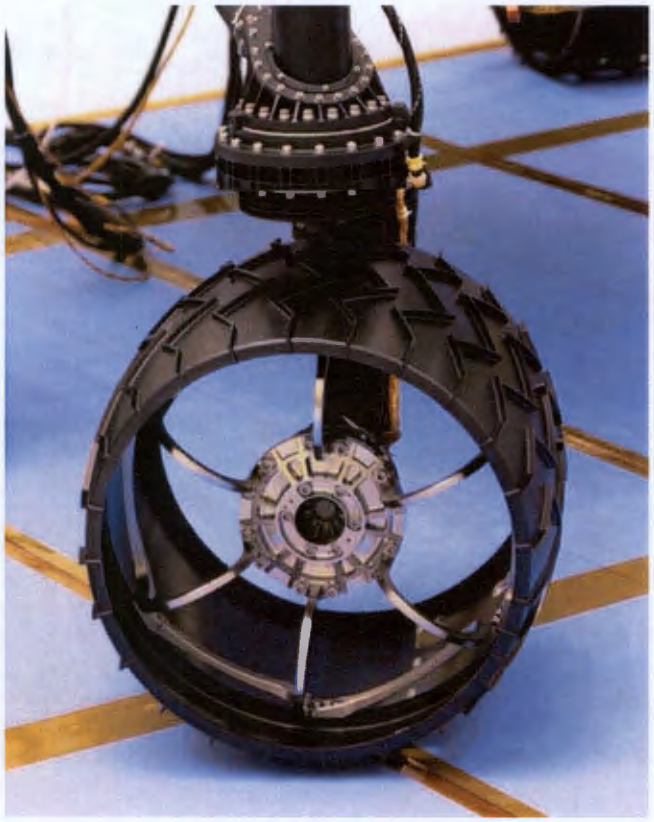

Figure 6.5 Close-up of the Curiosity Rover's wheel[7]

to come by. NASA does not allow non-US citizens access to its patents and research, and reports in the popular press are predictably scant on technical details. There is, however, a large body of photographs of the rover from which some details can be inferred. Figure 6.5 shows an outer rim attached to a central hub my means of spokes that curve in two directions: sharply outward and away from the hub before returning to curve more tightly towards the rim before their attachment point. There can be no doubt that the flexion of these thin curved spokes provides shock absorption to the rover, but to what extent cannot presently be discerned.

6.2.5 *Bicycle Wheels*

Another area that presents a number of innovative concepts for wheels with internal suspension is the bicycle parts industry. Many have attempted designs that incorporate shock absorption into the wheel structure, providing a way for riders to upgrade without changing the bicycle frame. The FLUENT wheel (based on a similar design called the ACROBAT, originally for wheelchairs) by Israeli company SOFTWHEEL uses three separate shock absorbers as spokes[52]. The LOOPWHEEL achieves similar results with three looped carbon springs[53], and the SHOCKWHEEL, invented by Chet Baigh, is a different realisation

(a) Bicycle featuring Fluent wheels[52]

(b) The Loopwheel[55]

(c) The Shockwheel[54]

Figure 6.6 Three different energy-absorbing bicycle wheels

of a similar design[54]. All three are shown in Figure 6.6 and could provide inspiration for future designs.

6.3 CONCEPT DESIGNS

As there was little direction to be found in the research, and only the broadest guidelines given by the modelling that was possible within the scope, an iterative design-and-test approach was taken. Two factors are known to influence the rigidity of a structure: its geometry and material properties. To simplify the investigation, a material was chosen that could be fixed throughout the testing, which would the focus on differing geometries.

The material selected is a proprietary expanded polyethylene foam manufactured by Sondor Performance Foams and sold in varying densities as "SPX<density>". For example: SPX90 corresponds to a

foam with a density of 90 kilograms per cubic meter. A variety of densities between 30 and 200 kg/m^{3}were used as testing progressed. The foam was supplied in 10 mm sheets such that two-dimensional geometries could be cut from it using the UCT laser cutter; these sheets could then be laid up to form thicker wheels, a process which is explained in more detail in Section 4.6. This material was selected for its manufacturability as well as its "memory" effect; when compressed it took some time to return to shape. This damping effect is desirable in suspension elements to limit the amount of oscillations experienced by the vehicle after impact. This decision was given confidence by the fact that the SPX foams are often used as an energy-absorbent packing material in specialised toolboxes for protecting delicate equipment from damage, with South African clients including Armscor.

Several concepts were devised with the intention of testing every geometry in standardised ways, characterising their response and combining design features, while refining them towards an ultimate design. These tests are described below. For the testing phase, all wheels were the same diameter and thickness (200 mm and 40 mm respectively) and were designed without traction; this was to be added later, by texturing the outer surface, once an optimum wheel was found.

As this was an iterative investigation relying on rapid prototyping, with design and testing happening concurrently, the following sub-sections simply introduce all of the concepts; a more detailed description of the design process is included with the results of the tests in Section 6.5.

6.3.1 *Straight Spokes*

Although neither the research nor modelling suggested that straight-spoked wheels would perform well in the tests, they were included as a benchmark to which other results could be compared. They were also used to compare the different foam densities and as such were made from both the SPX30 and SPX90 foam which were available at the time.

6.3.2 *Curved Spokes*

Following a very pervasive trend in the existing designs surveyed in Section 6.2, a curved-spoke design was attempted. The curved spoke was hypothesised to improve upon the straight spokes by providing a longer spring element that would gradually bend rather than buckling, as well as providing a more consistent response to impacts

(a) Straight-spoked wheel (b) Curved-spoke wheel (c) Composite wheel

(d) "Dreamcatcher" Mesh wheel (e) Solid wheel

Figure 6.7 Wheel concept designs

at different points around the rim. To establish a comparison to the straight-spoked wheel, these were designed with the same number of spokes, and the spokes and rim all the same thicknesses.

6.3.3 *Composite Wheel*

In an attempt to combine the high energy absorption of the softer SPX30 foam but add some damping and structural integrity, especially around the driving surface of the wheel where it would wear against rough terrain, a composite wheel was devised where the outer layer was comprised of the harder SPX90 foam. It was also hypothesised that, under increasingly large loadings the hoop stress in the outer rim would harden the structure to provide additional protection.

This design required a more complex manufacturing method; to prevent buckling at a join, the outer ring had to be a continuous piece of material. As the adhesive used bonds instantly on contact, it was necessary to invert the outer ring, apply glue, and then bond to the inner disc by aligning and re-inverting so the surfaces to be joined did not touch until they were perfectly in position.

6.3.4 *"Dreamcatcher" Mesh Wheel*

Manufacture by laser cutting has the powerful advantage over other 2-D methods that cutting complex and exact geometries, including internal hole features, is made trivially easy. To leverage this ability to make energy-absorbing wheels, a design was investigated whereby small holes were cut from a solid disc to make porous wheels. This was expected to have two advantages over the spoked designs; the response of the wheel to impacts at different points around its circumference would be more consistent, and there would be less chance of buckling. The material remaining forms a complex interconnected mesh of struts that can easily expand and contract evenly across the network to dissipate impact. The rounded edges of each hole provide resistance against stress concentrations forming at the "junctions" between struts.

To establish that certain struts or holes were not bending or stretching more than others, a rudimentary FEM analysis was conducted using the simulation tools in SolidWorks. Despite there being no model for the material used, it was nevertheless possible to gain a qualitative understanding of the weak points in the design by modelling it as another arbitrary material, and loading the structure until significant deformation occurred.

A modified version was also produced with smaller and fewer holes, to increase the stiffness.

6.3.5 *Solid Wheel*

As a benchmark of the hardest geometry a given material could provide, an entirely solid wheel was also tested.

6.4 EXPERIMENTAL DESIGN

In order to test the concept wheels, some new experimental techniques were devised. The objective of the experiment was to record, in a standardised and controlled manner, the response (peak acceleration and deflection) of each concept wheel design to a variety of drop loadings. Although unconstrained real-world tests were envisaged, it was necessary to at first constrain the falling to a single axis so that results could be reliably compared. This required the use of a drop test rig and a variety of sensors, whose implementation are described below. Not all concept designs were tested; some were abandoned without detailed testing due to more pressing issues with their design and/or manufacturability. These issues are detailed together with the quantitative results in Section 6.5 after a description of the experimental apparatus and method used.

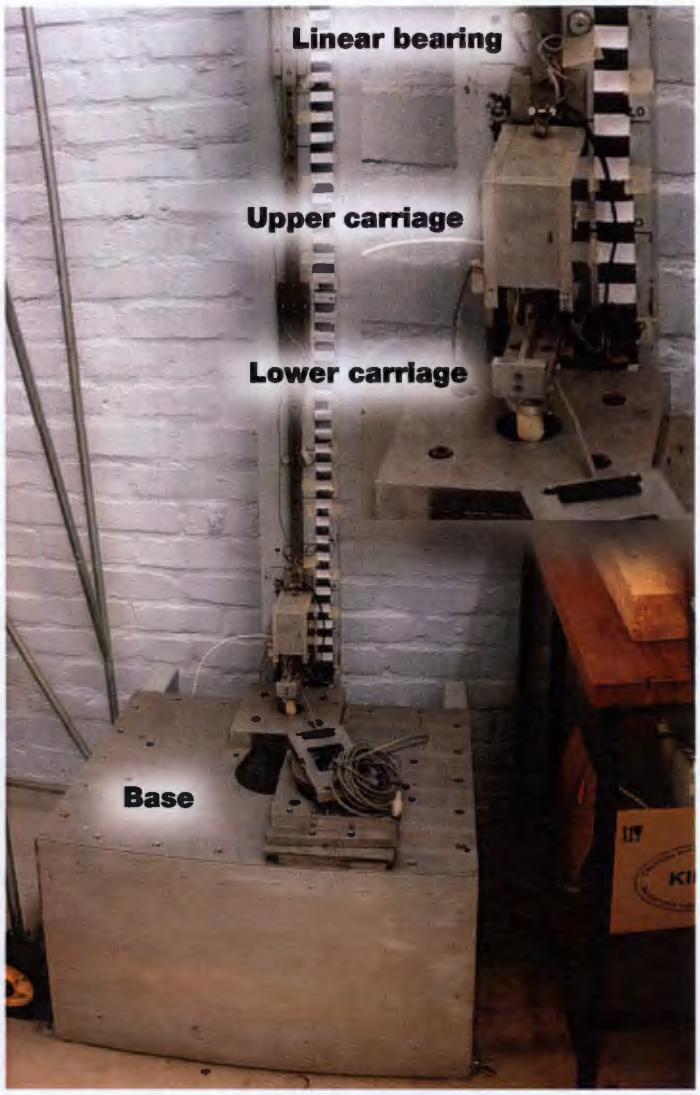

Figure 6.8 Photograph of lower section of drop tester apparatus before modifications. Inset: Detail of carriage assembly

6.4.1 *Drop Tester Apparatus*

An existing drop testing rig in the BISRU laboratories, shown in Figure 6.8, was re-purposed for these experiments. A vertical linear bearing in excess of 4 metres is used as the drop rail and a two-part carriage runs freely along it. The top part of the carriage is raised by a cable and pulley, and contains a solenoid-actuated clip. This clip connects to the bottom part of the carriage, which, by powering the solenoid, is released and falls to the platform below. This enabled the combined carriage to be winched up to the desired drop height and the lower part released remotely on command. This assembly is shown diagrammatically in Figure 6.9.

The existing instrumented tip was removed and the lower carriage equipped with a bolt-on attachment point for a stack of mass-pieces, the last of which was fitted with a threaded axle. Bolts through the entire stack fasten it together and a second set of bolts attach the stack to

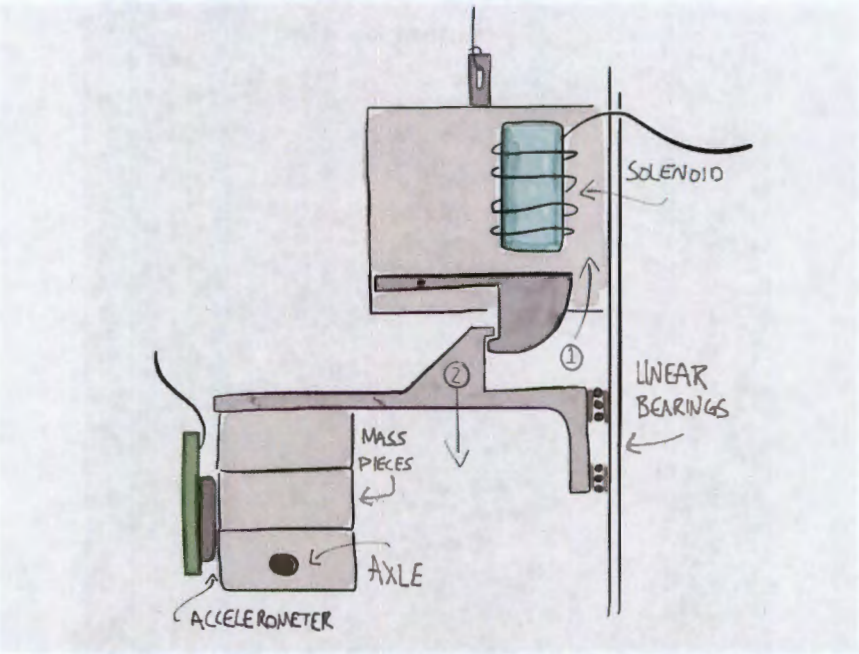

Figure 6.9 The two-part carriage assembly

the lower carriage. The entire lower carriage assembly was weighed and the mass pieces adjusted to 2.5 kg, the then-estimated weight of the finished robot. (As the sub-systems were all developed in parallel, it was impossible to accurately know the appropriate weight until after testing was completed.) This stack is fitted with an accelerometer which records the impact deceleration of the system when it hits the platform below, and the output of this accelerometer is captured by a computer with appropriate data capture hardware. Wheels, manufactured as described in Section 4.6, were threaded on to the axle and affixed with nuts and washers. The final apparatus setup is shown in Figure 6.10.

6.4.2 *High Speed Camera*

In order to accurately estimate the deflection of the wheels during impact, a Photron APX RS monochrome high-speed camera, shown in Figure 6.11 was used to film the drop tests.

Although originally only introduced to the experimental apparatus to confirm and validate the accelerometer data, the amount of noise present on the accelerometer signals made it preferable to measure displacement directly using the camera rather than to use numerical methods on the acceleration data. The camera was placed directly perpendicular to the front face of the mass-pieces so as to avoid any parallax or perspective errors in later processing. It was set to continuously capture at 10 000 fps and centre-triggered manually by pressing a button when the wheels were heard hitting the base. This resulted in a short video clip, centred on the moment of impact, which was

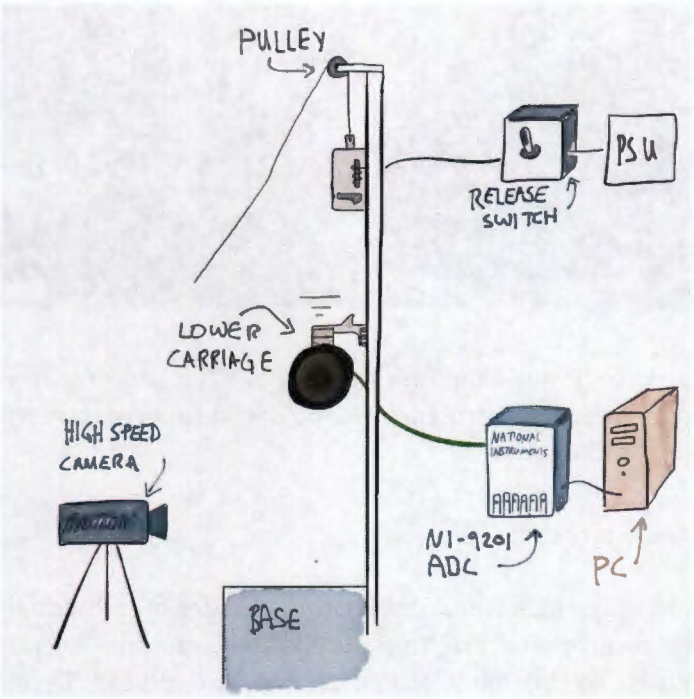

Figure 6.10 Diagram of complete drop tester apparatus

Figure 6.11 The Photron APX RS, focused on the carriage assembly, with LED video light for additional illumination

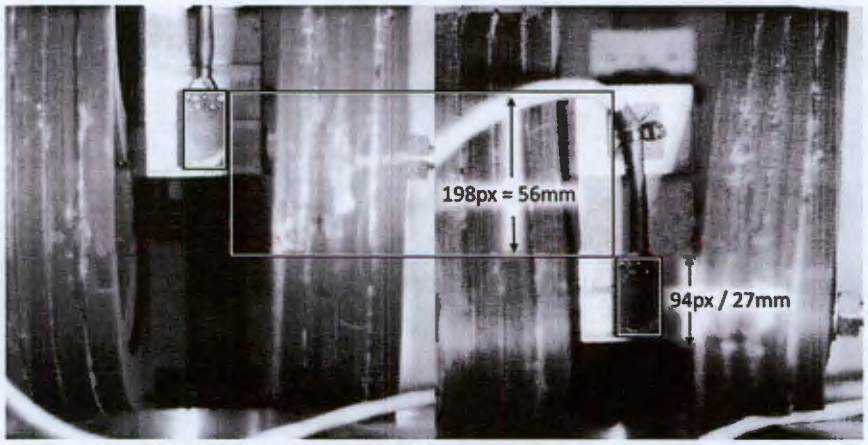

Figure 6.12 The manual image processing method, measuring a displacement of 56 mm.

trimmed to only show the first "bounce" — full compression and relaxation of the wheel structure — and saved to a computer for later processing and analysis.

6.4.3 *Image processing*

The saved video files were converted to a folder of individual frames and their contrast and brightness enhanced using free software tools Aoao Video to Picture Converter and XnConvert. By manually searching through the folder of files, the images showing the moment of first contact between the wheels and the base, and the moment of maximum deflection could be found. These were loaded alongside each other into the free image editing software Paint.net and a rectangle manually drawn around the accelerometer PCB in each frame. The dimensions of these rectangles (in pixels) were noted and compared to the known size of the PCB; this was used to create a calibration factor (in pixels/mm) for that particular experiment. To correct for any lens distortion, only the vertical axis was considered, and the average between the two frames was taken. A line could then be drawn from the top of the PCB in the first image to the top of the PCB in the other, and this line's length, using the calibration factor, gave an estimate of the final deflection of the wheel structure.

The results for an example test are depicted in Figure 6.12.

These measured maximum deflections could be substituted into Equation 6.3 to predict the maximum acceleration experienced by the dropped mass. This provided a measure of checking the accuracy of the measurements. Although the simple spring model is definitely not a faithful representation of reality, a consistent discrepancy between the measured and calculated acceleration would show that the error is non-random and purely systematic. This could also be useful in future work to create numerical models of the responses of the designed wheels.

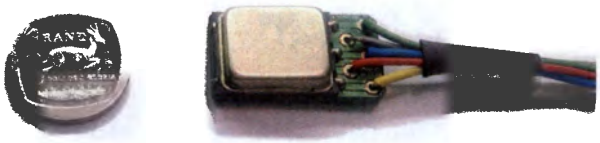

Figure 6.13 The 834-M1 accelerometer, mounted to PCB. (R1 coin shown for scale).

6.4.4 *Accelerometer*

The mass-pieces were fitted with a Measurement Specialities 834M1-2000 tri-axial Piezo accelerometer [56]. This was chosen for its high bandwidth (2-6000 Hz) and high acceleration amplitude (up to ±2000G). A severely limiting factor in the selection of a suitable accelerometer was price. Most others in this range of sensitivities were quoted in the order of thousands of USD, and hence entirely unaffordable, whereas this sensor is modestly priced at just over US $100. As the range of accelerations to be measured was not well-known before the experiments began, it was necessary to set the specifications so high; future work could re-consider this. A tri-axial accelerometer was also chosen as it allowed for the possibility of doing unconstrained real-world drop tests where the robot could tumble through space freely; the resultant total acceleration could then be found by combining the acceleration vectors from each axes.

The accelerometer is connected to power and the data capture hardware via a custom PCB (shown in Figure 6.13) and it is permanently bonded by its metal case to the metal mass-pieces using strain gauge cement. The wires that connect to the PCB are bound in a grounded braided-shield cable so as to limit the effect of electro-magnetic noise on the low-amplitude signals.

6.4.5 *Accelerometer Power and Data Capture*

The 834M1 requires an excitation voltage of 3.3 V. Its outputs are biased at half of the supply voltage; that is to say that when one of the axes is reading zero acceleration, its output is 1.65 V. The output then swings above or below this bias voltage as it reads positive or negative accelerations along that axis. As the output sensitivity of the accelerometer is only 0.62 mV/g, it was necessary to ensure that the voltage supplied to the accelerometer was as consistent and noise-free as possible. This was achieved by placing a 3.3 V LM4040 voltage reference circuit on the accelerometer's supply; this reference was then fed with 4 V from the most noise-immune bench power supply available to ensure that the accelerometer received a consistent voltage. This behaviour is shown in Figure 6.14, an oscilloscope trace captured during testing, which shows the LM4040 being fed with a 400

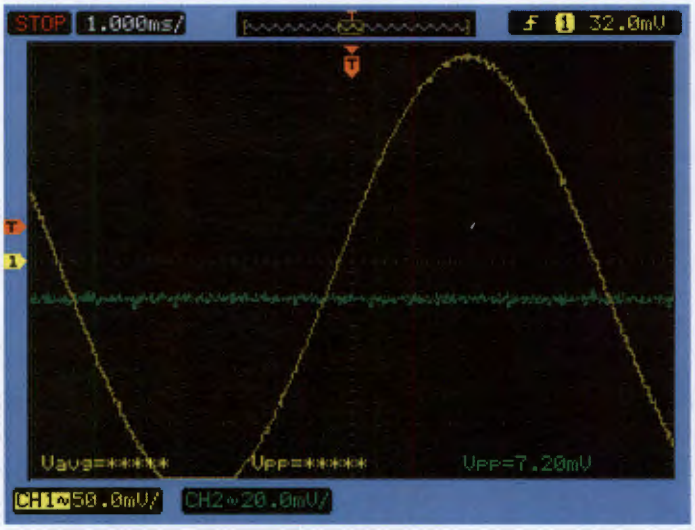

Figure 6.14
An oscilloscope trace showing a simulated sine-wave noise input (yellow) and clean output (green) of the LM4040.

mV peak-to-peak sine wave (simulating a noisy power supply) and its output remaining remarkably stable (both signals are DC-blocked so appear relative to 0 V).

Note that although it is generally not recommended to use a voltage reference to provide power, the 834M1 draws less than 22 μA of current, which is well within the safe operating conditions of the LM4040.

The data capture is done by a National Instruments 9201 12-bit multi-channel ADC operating at 48 kHz per channel, plugged into a cDAQ-9171 USB carrier, which is connected to a computer and accessed using simple software written in LabVIEW. The voltage supply and three outputs are all captured relative to the accelerometer's supply ground and saved as a .CSV file for processing and review in SciLab, an open-source numerical software package similar to MATLAB. The full testing workstation, with both laptops, all power supplies and the capture hardware is shown in Figure 6.15.

6.4.6 *Accelerometer Signal Processing*

Due to the electrically noisy environment (mostly due to air conditioning and overhead fluorescent lighting), the high sensitivity of the sensor, and the fact that the majority of the test results were of such low magnitude that they approached the noise floor of the device, it was necessary to apply extensive signal conditioning to make the captured data usable. The final implementation included a 10-pole low-pass Butterworth filter with a cutoff frequency of 500 Hz, followed by a 80-point rolling average. The Butterworth filter was designed by using the built-in function in SciLab and increasing the number of poles until an almost-vertical cutoff was obtained. The processing overhead associated with this number of poles was found to be insignificant. Although this processing left the data still appearing somewhat noisy

Figure 6.15
The full test bench and data capture setup (high speed camera out of view).

it was sufficient to extract the important information. The topmost graph in Figure 6.16 shows the test data before and after filtering overlaid on top of each other.

6.4.7 *Signal Processing Validation*

By integrating both the processed and raw data and comparing the results, the signal processing methods were tested to ensure that only noise was removed by the filter and that the data was not damaged. Random electronic noise distributed above and below the genuine signal causes miniscule peaks and troughs in the waveform; in the numerical integration these peaks and troughs form positive and negative contributions to the total integral, which, if the noise is truly random and the sample size sufficiently large, will cancel each other out. Therefore, a noisy signal will have the same integral as its clean counterpart.

Although the first and second integrals of the captured acceleration history are not necessarily very accurate measurements of velocity and distance, they can be compared with another measurement to further confirm the validity of the integrated data. In this case, the total displacement of the lower carriage/wheel assembly during impact was known from the high speed camera footage (described in Section 6.4.2) and this was compared to the value of the double integral at the time point corresponding to maximum deceleration.

The point of maximum deceleration is the point at which the wheel's velocity passes from negative to positive through zero, and hence is also the point of maximum deflection.

The first and second integrals of the clean and noisy data were acceptably close to each other, which confirms that the high-frequency components stripped out by the signal processing were not part of the

genuine acceleration signal. Figure 6.16 shows the raw accelerometer data in blue and the filtered data in red, followed by their successive integrals, with the difference between the raw and filtered integral as a green line.

6.4.8 *Accelerometer calibration and validation*

As the sensor was new and not well-understood in the research facilities available, an investigation was undertaken to determine the validity of the manufacturer's claims and gain a deeper understanding into the capabilities of the device. As such, the sensor was attached to the end of a single instrumented Hopkinson Pressure Bar and the bar subjected to varying pulses with a gas gun. (A diagram of this apparatus is reproduced in Figure 6.17 and a detailed description of its operation found in Appendix B) These pulses were chosen so as to be representative of the order of magnitude of the accelerations that the robot was predicted to undergo during final testing.

After the first reflection in the bar, ringing effects and increasing dispersion corrupt the data

The accelerometer readings were found to be acceptably close to the readings from the Hopkinson bar; the waveforms of the first pulse were of consistent shape and form, and the variation in maximum acceleration no greater than the noise on the signals themselves. An example of the readings from one such test is shown in Figure 6.18. It is expected that, as the accelerometer is at the free end of the bar, it experiences twice the velocity — and hence twice the acceleration — as the strain gauge in the middle of the bar. This phenomenon is explained in more detail in Section A.3. Note also that in Figure 6.18 the two traces are superimposed to demonstrate their similarity; in actuality they are separated by a phase shift (the time for the pulse to travel from the middle to the end of the bar) but this is to the detriment of the legibility of the graph.

6.5 CONCEPT TESTING AND DEVELOPMENT

This section presents and discusses the development of the iterative design process and the results of each wheel concept. A tabulated summary of all the viable test data is attached in Appendix B and all the raw data is included on the accompanying DVD.

6.5.1 *Straight Spokes — SPX30*

These wheels were not tested on the drop tester as it was immediately obvious that they were not rigid enough even to support the mass of the robot without collapsing, and testing would have caused damage to the drop test apparatus. Furthermore, after some manipulation the material was prone to tearing, which is shown in Figure 6.19. This discovery led to this material not being used in any further tests as

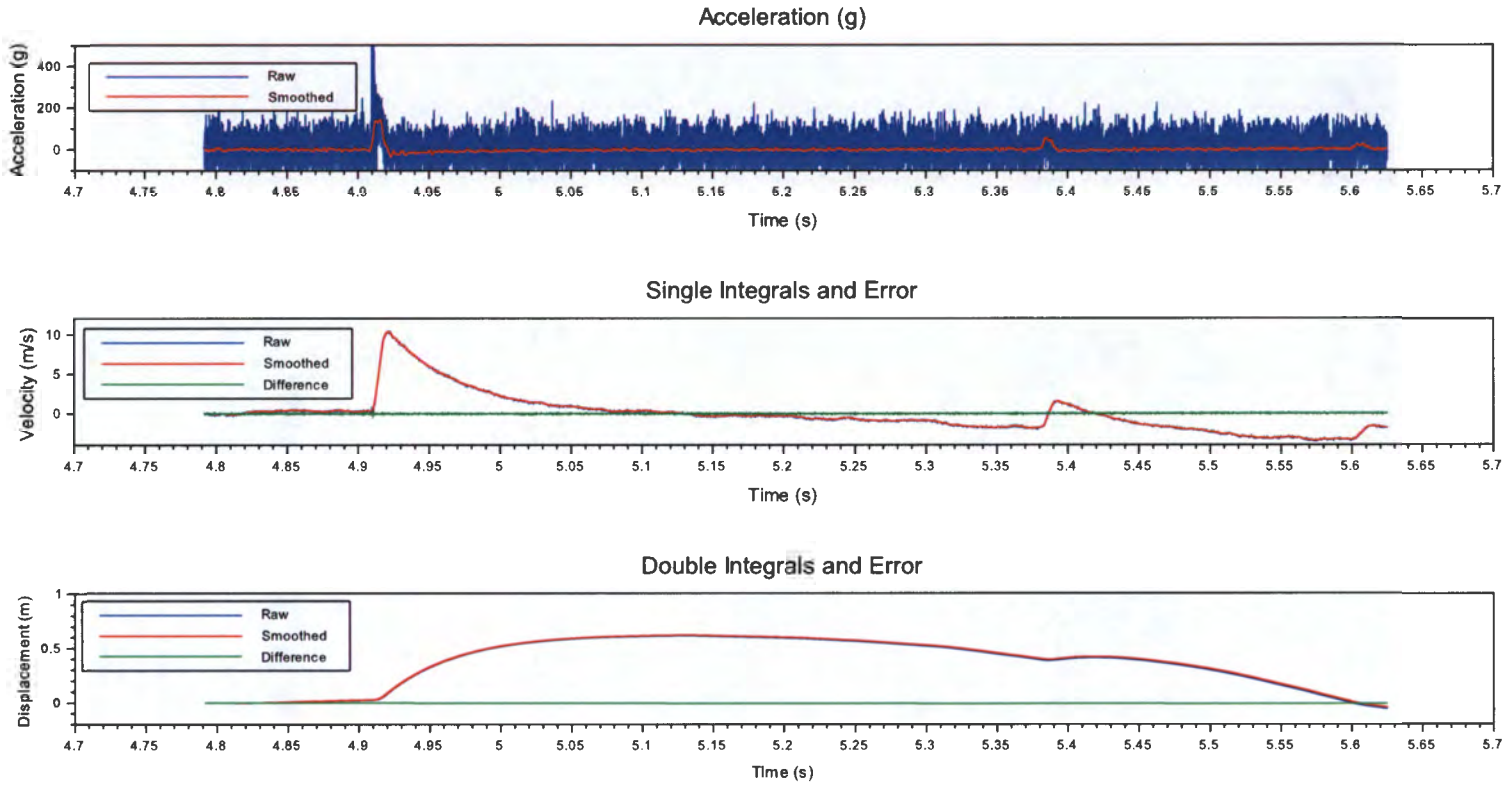

Figure 6.16
Test data before and after filtering

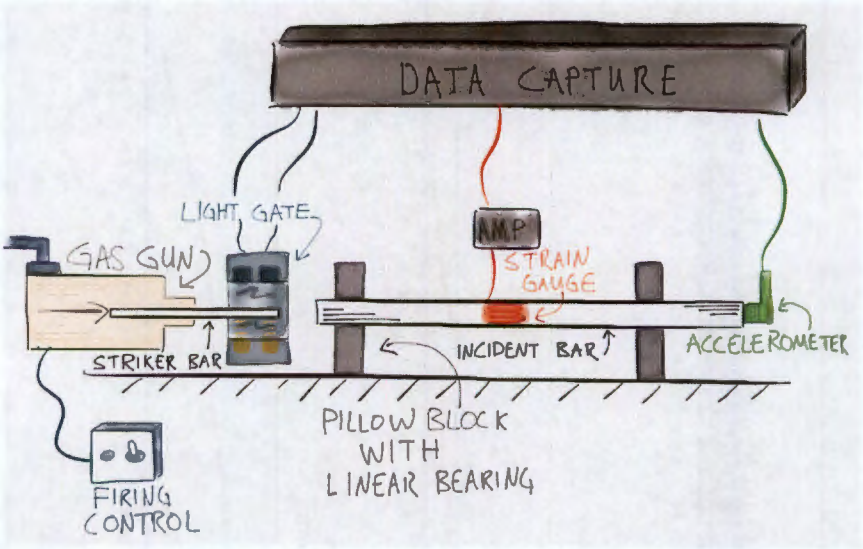

Figure 6.17 The Hopkinson Bar Apparatus

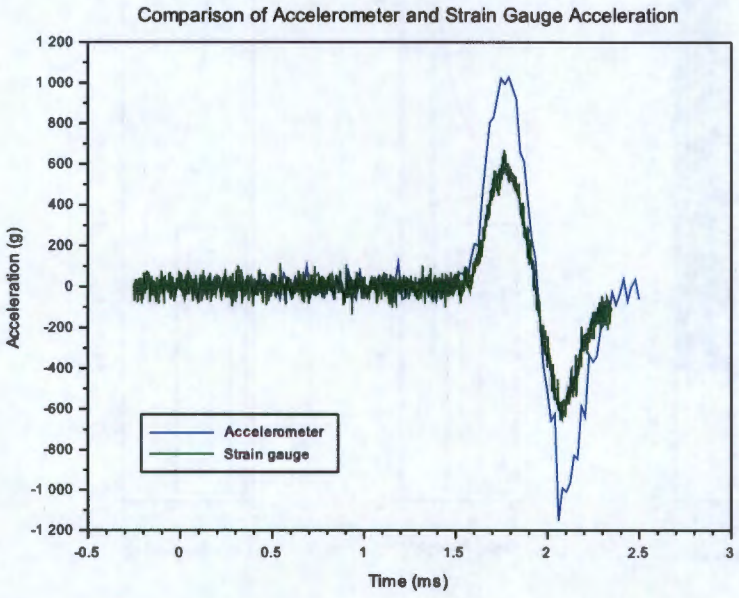

Figure 6.18 Acceleration experienced by the strain gauge and accelerometer, data traces time-shifted to overlap.

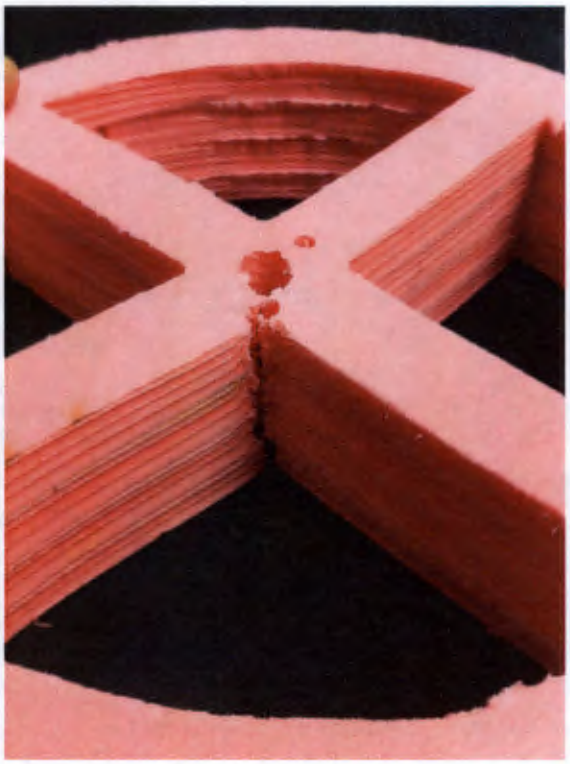

Figure 6.19 The Straight-Spoked SPX30 wheels, showing tearing

the risk of tearing the fastening or traction surfaces would severely limit the functionality of the robot. The exception to this rule is the compound wheels, which sought to address these specific concerns by adding a harder material on critical surfaces.

6.5.2 *Straight Spokes — SPX90*

The straight spoked design was attempted again with a harder, denser foam, i.e. the 90 kg/m^3 SPX90. Upon dropping from 3 m along the axis of the spoke, the spoke buckled, and when dropped between the spokes the drop test apparatus "bottomed out" with the wheels compressing so far that the mass pieces collided with the base. As such this test data is not included. Further manipulation qualitatively confirmed that the response of the wheels when compressed along the axis of the spokes was notably different to the response when compressed between spokes, with the rim also displaying a tendency to buckle under sufficient load. After some time resting under the load of the drop tester carriage, these wheels were also observed to plastically deform, shown in Figure 6.20.

Many of these results could have been mitigated to some extent with more spokes, thicker members, harder foam (or any combination thereof) but this was not attempted immediately as it was felt that already-existing prototypes would be more effective in this regard.

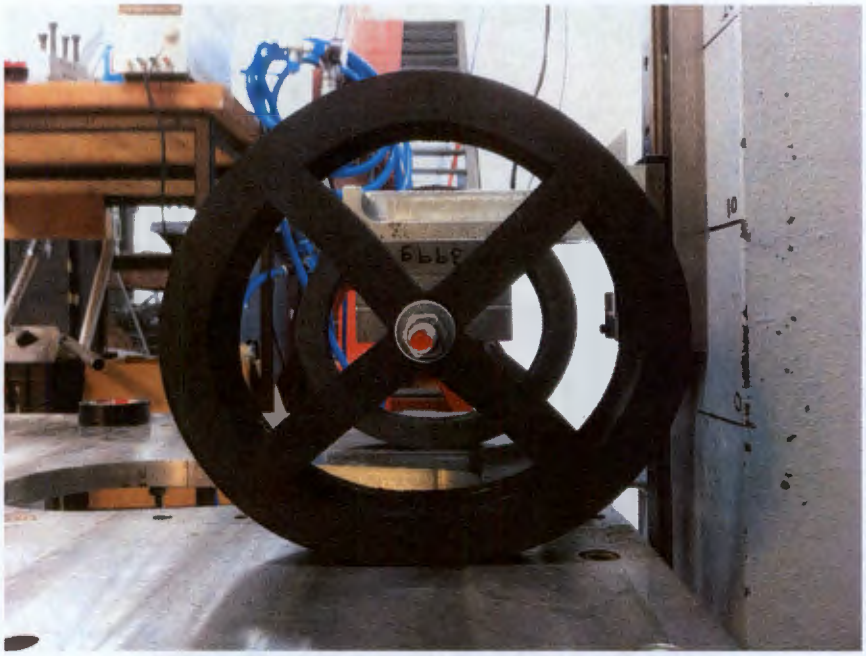

Figure 6.20 Deformed straight-spoke wheels on the drop tester

6.5.3 *Curved Spokes — SPX90*

The curved spoke wheel, made from the same density foam as the straight spoked wheel, did in fact perform notably better. The curved spokes somewhat increased the uniformity of the response around the rim of the wheel, reduced buckling of the rim and — although this was not expected — provided greater resistance to impact than the straight spokes. These wheels, when dropped from 2.7 m, allowed only an 80G acceleration to be imparted to the drop mass; however this was at a displacement of 54 mm, more than allowed by the design of the platform.

6.5.4 *Composite Wheel*

The composite wheels, as expected, provided a totally consistent response to loading irrespective of their rotation. When dropped from 3 m they allowed only 70G to be transmitted to the drop mass, but still offered an improvement over the displacement, at 43 mm. This suggested that this concept might warrant further investigation — for example, changing the density of the foams, or thickening the outer layer to decrease their deflection under loading. However, a number of secondary issues were noted. Their assembly process is complex and challenging, foam is wasted in making the outer rim as a continuous part, and overheads would be incurred by stocking two different foams. These led to this concept being deemed unsuitable for the challenge at hand.

Figure 6.21 Original dreamcatcher (L) with harder version (R)

6.5.5 *"Dreamcatcher" Mesh wheel — SPX90*

The dreamcatcher wheel addressed many of the concerns of the composite wheel. Despite a massive increase in the complexity of the geometry, the overall manufacturing time and complexity was significantly decreased, with no apparent disadvantages compared to previous designs. In a 3 m drop they performed comparably, allowing 75G impact deceleration to be felt by the sensor, with an average displacement of 36 mm; this was much closer to the safe limits of the design of the casing, but still not sufficient for a safe landing.

Of all the concepts covered, this was felt to be a rich starting point for further study, due to its ease of prototyping and the extent of variation that could be introduced by altering the size, position, and number of holes. Due to time and funding constraints, a full study into a range of different meshes could not undertaken; this and an attempt to model their behaviour numerically would be a valuable topic for further work. Within the constraints of the project, a slightly harder mesh (Shown next to the original wheel in Figure 6.21) with fewer and smaller holes was designed, and as an upper-limit benchmark, an entirely solid wheel was manufactured. The harder dreamcatcher wheels were to be tested after this — however, due to the results of that test, they ultimately were not tested.

6.5.6 *Solid Wheels*

Entirely solid wheels made of SPX90 foam, when dropped from 3 m, allowed 90G to be felt by the drop mass and although Equation 6.3 predicts that this would correspond to a decreased deflection, this was not markedly dissimilar from the SPX90 dreamcatchers at an average of 38 mm. Accordingly, as it was still required to reduce this displacement, solid wheels of SPX200 were tested. These absorbed sufficient energy to allow readings of, on average, 150G at the accelerometer. The high speed camera was regrettably not available for

Although not an immediately useful result, this does prove that different geometry affects the spring model.

these tests, but estimates using Equation 6.3 and factoring in the measured systematic error (see Section 6.4.3) of previous predicted displacements estimate the deflection to be in the order of 25 mm to 30 mm; an improvement but still not sufficient for safe operation within the constraints of the design of the robot's casing. This disproved the hypothesis implicitly present in the design: 30 mm would not be sufficient clearance to protect the case from a 3 m drop with the chosen materials.

6.6 FINAL DESIGN

Although the investigation undertaken was in no way complete or exhaustive, a pragmatic view was taken that, considering the ultimate design goal of the project, and given time and budget restrictions it was necessary to expeciate the commissioning of an initial prototype that could be tested. Based on the preceding investigations, a final design was devised. Having established that stiffer geometries and harder materials could not solve the problem at the chosen dimensions, the wheel diameter was increased by 40 mm to 240 mm. This would provide an additional 20 mm clearance between the wheel rim and the shell of the robot to provide a greater margin of safety for the event of the suspension "bottoming out" and the robot case striking the ground when the robot is dropped or thrown. As all the results thus far suggested a regime of impact decelerations well below the specific 250G safe maximum, this final wheel was manufactured from the hardest foam tested, the SPX200. So that these test results would give the best possible prediction of the robot's actual performance, these wheels were made "robot ready" and given a textured surface to improve traction. These are shown in Figure 6.22.

6.7 RESULTS

The proposed final wheels were tested in the same manner as before, but additionally subjected to a number of drops of varying height so as to characterise them more exhaustively. The results for both peak acceleration and maximum deflection over a range of heights are shown in Figures 6.23 and 6.24 respectively.

The peak acceleration felt at a 3 m drop is 150G, still well below the safe maximum of 250G, and the deflection this causes is 35 mm. Given that the new safe maximum deflection is 50 mm, this gives a good margin of safety.

As with all the tests, there are not sufficient repeated tests to use traditional statistical measures of assessing uncertainty and confidence. However, as there were a larger number of tests done with the same wheel, it became possible to estimate and characterise the scale and nature of the discrepancy between the measured displacements and

Figure 6.22
The final wheel design

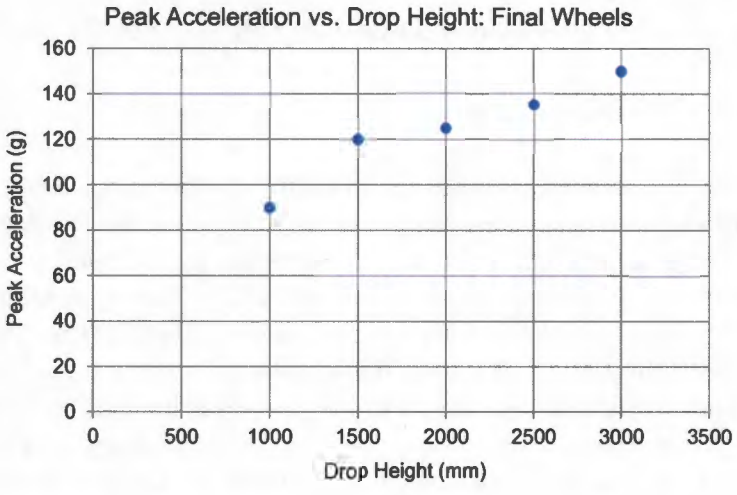

Figure 6.23
Graph showing peak acceleration at varying drop height

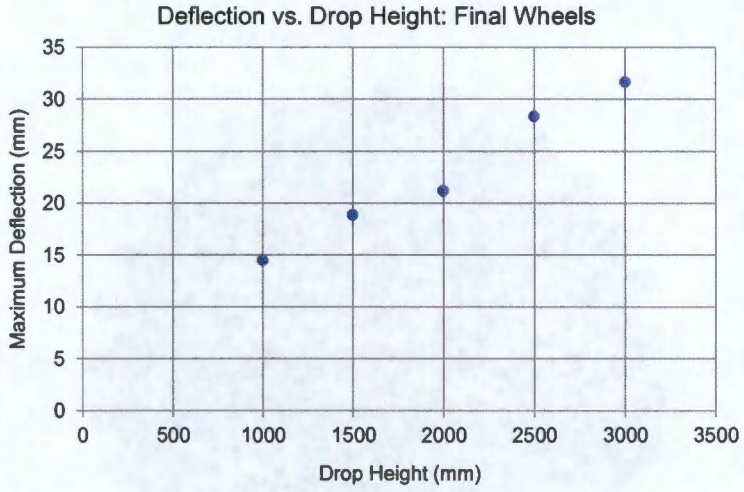

Figure 6.24 Graph showing peak deflection at varying drop height

those predicted by Equation 6.3. Using MS EXCEL, a straight line relationship could be found between the measured and estimated data, with a R-squared value just over 0.95 (shown in Figure 6.25). This high degree of conformity to a linear relationship shows that random error is low and any discrepancy can confidently be attributed to systematic error in the measuring apparatus or spring model. This gives a degree of confidence in the test results; although they may not be absolutely exact, they are consistent and repeatable.

After this test data was gathered, a final 3 m drop was attempted and this caused a failure in the axle attachment point of the wheel. The resultant tearing is shown in Figure 6.26. Recommendations based on this and other observations are made in Chapter 8.

6.8 CONCLUDING REMARKS

This chapter detailed the research, iterative development, design, and testing of new energy-absorbing wheels for use on the robotic platform being designed. In so doing, experimental apparatuses and methods were described, and the data gathered using these was described and its impact on the iterative design process shown. The chapter ends with the testing of a final wheel selected from the prototypes and some comments on the merits of the experimental techniques used. These results form part of the body of work from which conclusions and recommendations will be drawn in Chapter 8, after a description of the testing carried out on the whole assembled platform.

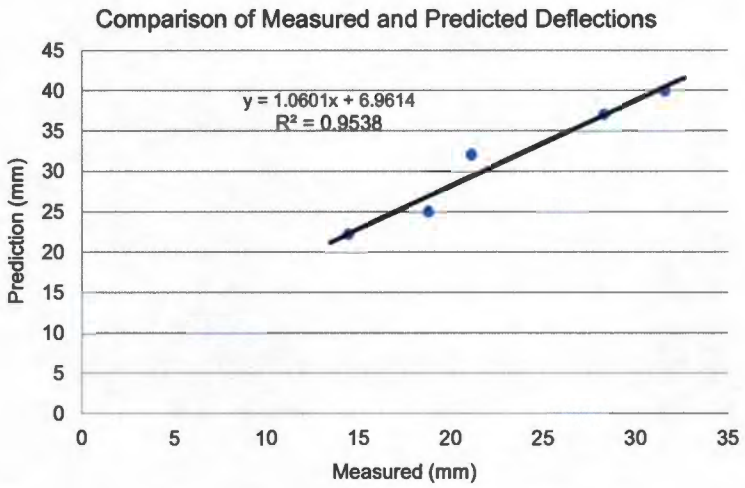

Figure 6.25 Graph showing correlation between measured and predicted deflection

Figure 6.26 240 mm Solid SPX200 wheel after tearing failure

7

TESTING AND RESULTS

7.1 INTRODUCTION

This chapter details the testing of the complete prototype platform and quantifies its successes or areas for improvement in a number of categories.

Some tests required the platform to be powered and have communications with the operator. As the power and communication subsystems designed by G. Knox in the course of his M.Sc were not fully complete at the time of publication, these tests were achieved either by partially integrating the work-in-progress systems or building a temporary sub-system that would provide the same function. As these sub-systems do not fall within the scope of this project, they are discussed only where their use could conceivably have had an impact (beneficial or limiting) on the performance of the platform.

Where tests describe a "human operator", this was, in all cases, the author. Development of a natural user interface, and analysis of the Human-Machine Interaction with a wider sample group is highly recommended, but not within the scope of this project.

Only after some tests had been completed was it observed that the motor gearboxes, which were known to be sub-standard, were showing signs of slipping. This failure is documented in detail in Section 7.19, but is mentioned here as it significantly impaired the robot's performance. New motors with a higher torque rating could not be purchased within the time and budgetary constraints of the project, as integrating these motors would have required a re-design of the entire housing; this is recommended as the first priority of future work. As such, some proposed tests were not completed, and the results of some tests were compromised. This is noted where relevant.

7.2 COST

7.2.1 *Description*

This specification was evaluated by keeping a record of the costs incurred in manufacturing the first prototype. Although significantly more money was spent in development work leading up to the prototype, this budget reflects only the stand-alone cost of a single prototype as manufactured. Should the design go to production, it is expected that some costs, such as plastics manufacture, may increase. Equally, some components could be bought for reduced prices at

Figure 7.1 The robot stored in the transportation harness

greater volume. However, it provides a useful initial estimate of the viability of the project.

7.2.2 *Results*

The total cost of manufacturing a single prototype was R3353 (approximately US $287 at time of writing). An itemized breakdown of this can be found in Appendix E.

7.3 SIZE

7.3.1 *Description*

This specification was tested by confirming the dimensions of the finished prototype with a tape measure. Additionally, the robot was fitted into the transportation harness designed by W.K. Fong.

7.3.2 *Results*

The robot measured 240 mm x 330 mm x 440 mm and fitted successfully into the transportation harness as shown in Figure 7.1.

7.4 WEIGHT

7.4.1 *Description*

The platform was weighed using a digital scale. To obtain the most realistic indication of final weight, this included the aluminium sensor payload face, battery and power management system, prototype communication hardware and the testing controller developed by G Knox.

7.4.2 *Results*

The mass of the robot was found to be 2.4 kg by weighing the assembled platform on a digital scale.

7.5 CONTROL AND COMMUNICATION

7.5.1 *Description*

In order to test that the controller board was able to receive commands from an external master device and control the motors, a work-in-progress prototype of G Knox's sensor payload central controller and wireless hardware was adapted to receive communications from a computer and pass them to the motor control PCB. A simple GUI was written in LabVIEW to interface with a Logitech Xbox-style controller, convert joystick positions to motor commands, and send these to the wireless transmitter. Figure 7.2, the testing interface, shows the joystick input, converting these inputs into motor power and direction indicators, and the serial string transmitted to the robot. Additionally, the data received from the robot is displayed and, where relevant, displayed as indicators.

The returned data string is analysed and, if the format and layout is correct, this is reported on the GUI. During all other tests, this status was logged to a file once a second. From this, it was possible to determine the reliability of the communications link. This logging feature was left on during all testing so as to gain an understanding of the robot's behaviour during "normal" operation. It must be noted that all results measured below were unavoidably affected by the testing systems; any less-than-ideal performance of GUI software, wireless link, or Xbox controller may be reducing the measured performance.

7.5.2 *Results*

It was possible to control the movement of the robot with an Xbox controller. If the joystick was pushed forward and abruptly released, the robot displayed a tendency to flip forward as the motors decel-

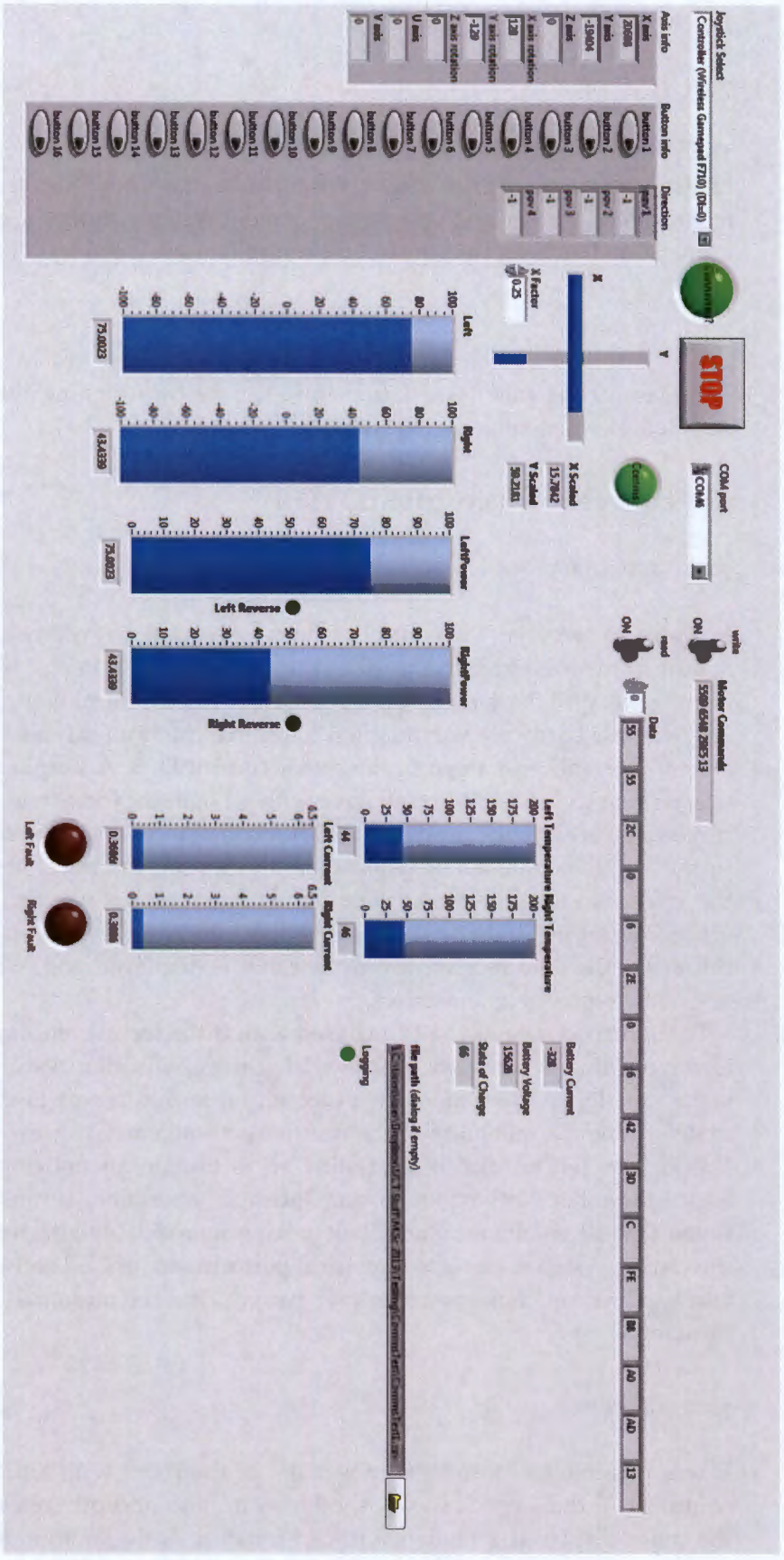

Figure 7.2
A screenshot of the test GUI developed in LabVIEW

erated - shown in Figure 7.3. This is, in part, due to the centre of gravity being too far forward. However, if the control was released gently, and the robot allowed to come to a gentle halt, it could do so without flipping over. This suggested that control software could be implemented that would ramp down the deceleration gradually; however this was not attempted. Beside being out of the scope of the project, the most urgent future work is a re-design of the robot shell, which would change the centre of gravity and could make this control code redundant.

The longest period measured with no break in communication was 22 minutes before the robot was turned off. If we define a "self healing" connection as able to restore communication within 5 minutes without assistance or reset, the longest period measured was 35 minutes and 19 seconds long, during which communication integrity was lost and successfully regained 45 times.

7.6 STRAIGHT LINE

7.6.1 *Description*

Although no goal of "straightness" was specified, it was nevertheless desired to establish the performance of the platform and determine if better motor control should be recommended. The tests were carried out by setting both motors forward at 100% and 50% power and placing the robot on a level floor, on which a 250 mm grid was marked. The tests were filmed from directly overhead and the video footage analysed (by overlaying straight lines and counting grid markers) to determine the straightness of the robot's path. Ideally this test would have been carried out over specified distances and the deviation reported in millimetres away from target over a certain distance, as well as noting any angular deviation; however this could not be completed as the motor failure made the robot's performance totally unreliable.

7.6.2 *Results*

During these tests it was noted that the robot had a tendency to veer suddenly to the right as it was accelerating up to speed, but then remain on a relatively straight trajectory thereafter. A typical attempt is shown in Figure 7.4, a composite image made by overlaying successive frames of video. The robot immediately veered off course by 40°, but then held a line that appears straight to the eye. The straightness of this line however cannot be measured with the current tools as it is not possible to determine the position where the curved path ended and the straight section began.

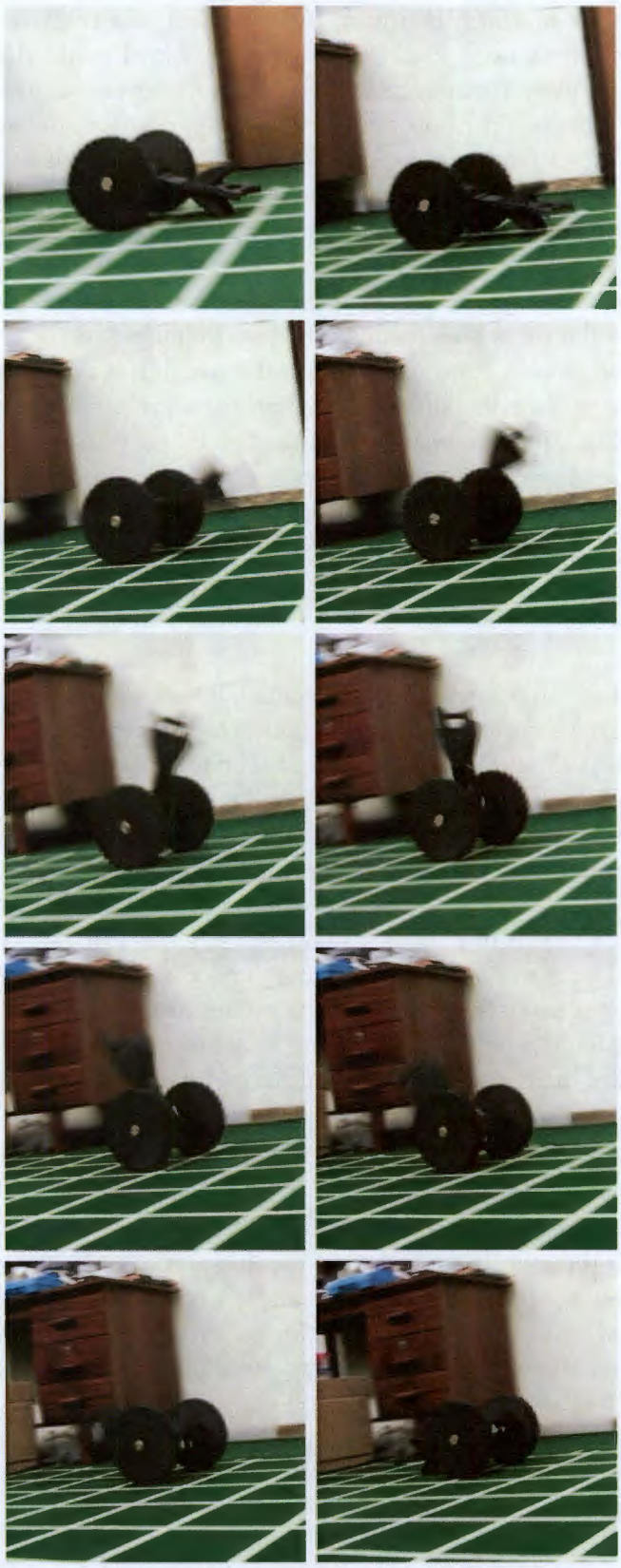

Figure 7.3 Frame-by-frame video capture of robot flipping during deceleration (reads left-to-right, top down)

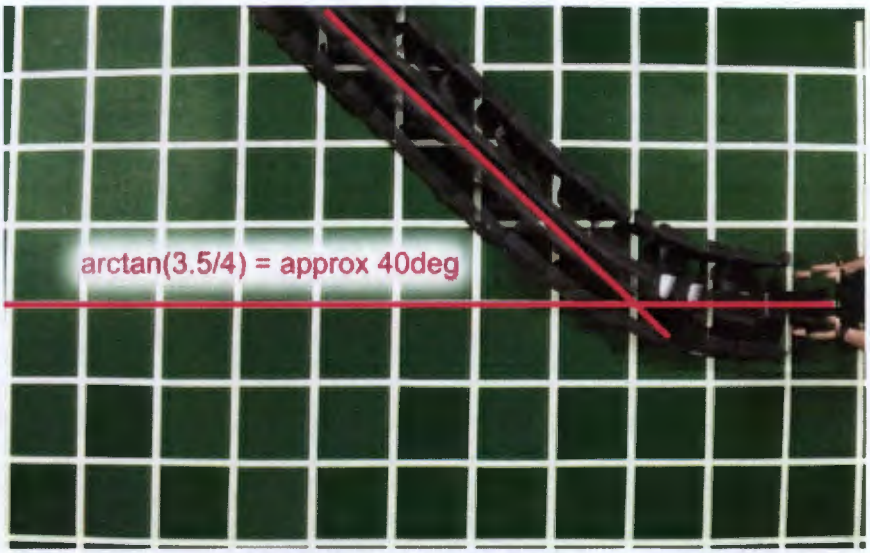

Figure 7.4 Composite layered frame-by-frame capture of straight line test

7.7 ON-AXIS PIVOT

7.7.1 *Description*

In order for the robot to operate in confined spaces, is it essential that the robot be able to turn on the spot. This was tested in two ways: first by using the Xbox controller and then by using the GUI to manually fix the wheels at the same speed but in opposite directions. This was done on the grid-marked floor and filmed from directly overhead so as to measure the radius of the turning circle. To eliminate human error or bias, the test using the directly-set speeds is taken as the achieved specification.

7.7.2 *Results*

As expected, the directly-programmed wheel speeds produced a tighter and more controlled turn. The robot was able to turn on its axis without leaving a 650 mm square box - this is is shown in Figure 7.5.

7.8 CURVED PATH

7.8.1 *Description*

As well as travelling in a straight line and pivoting on its own axis, it is desired that the robot be able to combine these movements and execute a sweeping turn. As before, this was performed both by operating the robot with the Xbox controller and by locking the wheels to pre-set speeds. In the human-controlled version of the test, a corner is defined using obstacles through which the robot must pass; in the

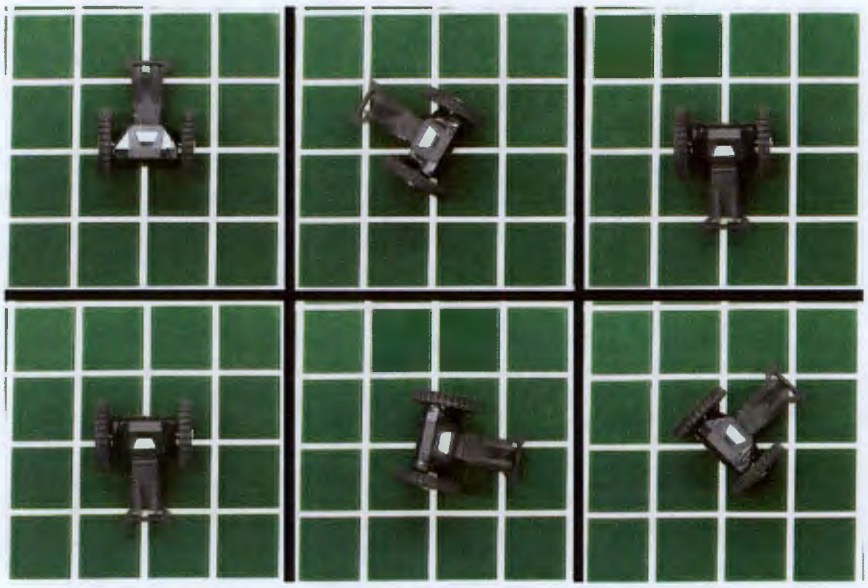

Figure 7.5 The robot performing a turn on its own axis

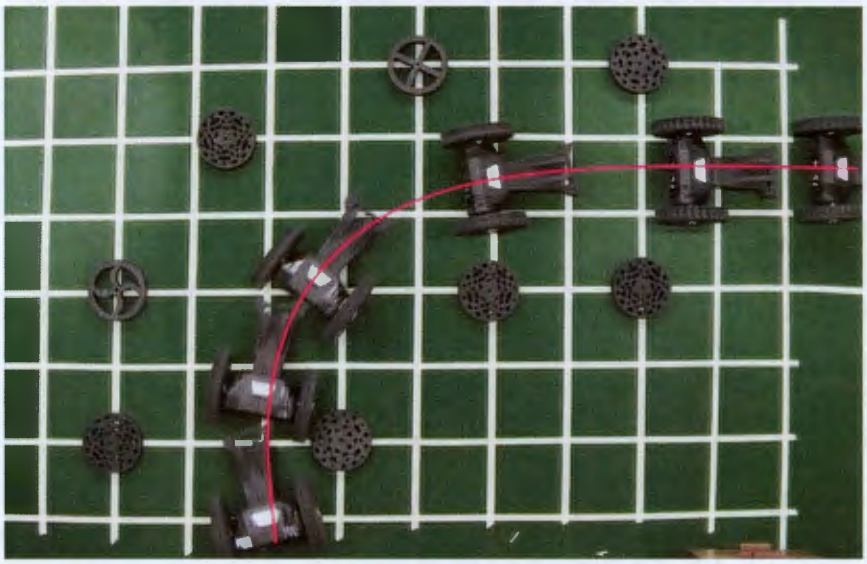

Figure 7.6 The robot performing an operator-controlled turn through obstacles

fixed-speed case the robot is allowed to describe a continuous circular path on the grid-marked floor which is measured using the overhead video camera.

7.8.2 *Results*

Figure 7.6 shows the robot, controlled by a human operator, performing a sweeping turn through a series of obstacles that define a smooth corner. This serves merely to illustrate that such movement can be achieved using the test GUI and controller; future work could consider the optimal controller response and usability thereof.

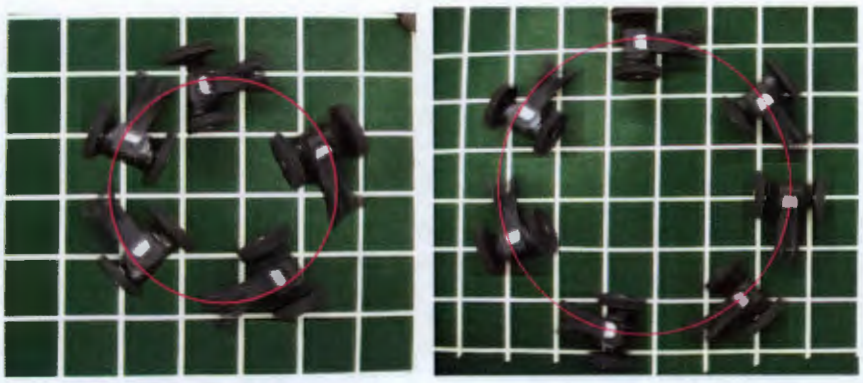

(a) 50-80 small turn (b) 100-80 wide turn

Figure 7.7 The robot performing two pre-programmed sweeping turns

Figure 7.7 shows the robot performing two pre-set turns: the first with one wheel at 80% and the other at 50% power, and the second, wider turn with one wheel at 100% and the other at 80%.

7.9 DROP SURVIVAL

7.9.1 *Description*

Although the original intent was for the robot to be subjected to real-world drop tests — i.e. driving it off a 3 m ledge onto concrete — there was significant risk of this irreparably damaging some components: the platform was still needed for the two other concurrent projects which interface with it. As such this test was not attempted and the drop survivability is estimated from the extensive wheel testing in Chapter 6 and other results in this chapter.

7.9.2 *Results*

The final wheels tested in Section 6.6 displayed good energy absorption, with peak accelerations well below the 250G limit set by the proposed thermal camera. Graphs showing its peak acceleration and deflection over a range of different drop heights are repeated here as Figures 7.8 and 7.9.

This test data was gathered in highly idealised conditions, and as such may differ from real-world performance. A description of some of the limitations of the test data is given below, but as it is not possible to fully quantify these inaccuracies, this specification is based entirely on the wheel testing but taking into consideration the reduced mass of the robot. As such it can be confidently stated that the designed wheels are sufficient to protect the robot and sensors (to the 250G specification) from drops up to at least 3 m.

The limitations of this are as follows: as noted, the real platform weighs 2.4 kg, slightly less than the 2.5 kg experimental mass. This

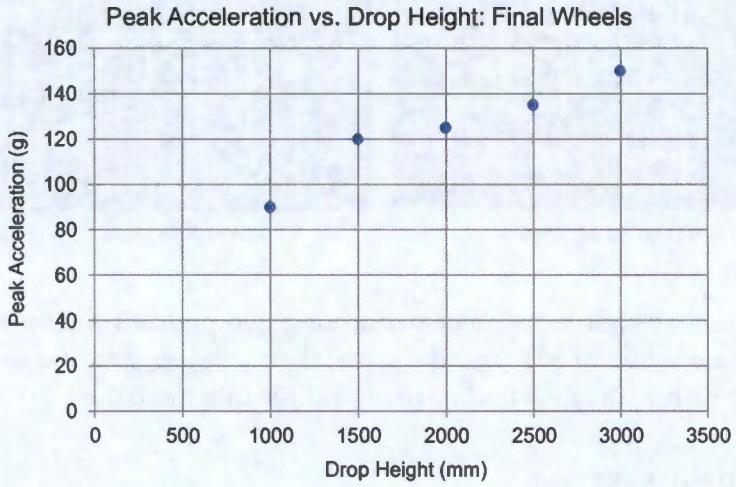

Figure 7.8 Graph showing peak acceleration at varying drop height

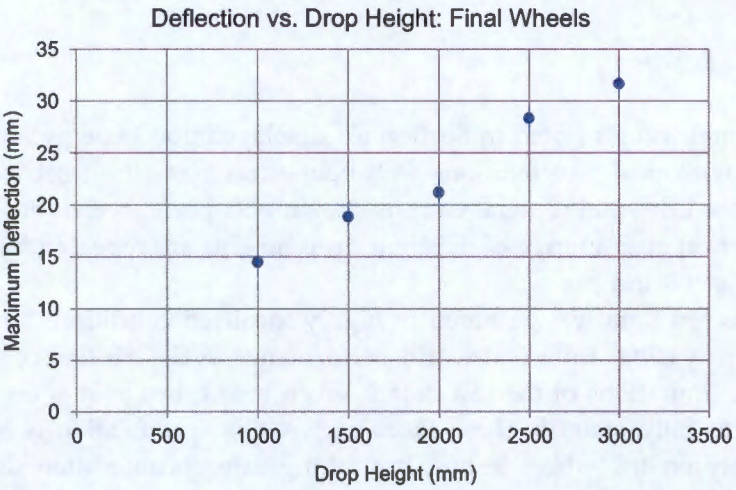

Figure 7.9 Graph showing peak deflection at varying drop height

could lower the peak accelerations and decrease wheel deflection when dropped from the same height.

Secondly, the experimental apparatus only allowed for controlled falling onto both wheels, whereas a real-world drop could load one wheel more than the other. This could decrease the maximum height from which the robot can safely be dropped, but extent of the effect this might have is not known and further testing is required.

Thirdly, as noted previously, the motors in the prototype were not at the desired specification and accordingly their shafts were more susceptible to damage. The tumbling test in Section 7.14 showed that even a modest drop of 400 mm was sufficient to cause damage to these shafts if the robot landed on the outer face of the wheel.

7.10 SELF-RIGHTING

7.10.1 *Description*

In an attempt to ensure that the robot landed evenly on both wheels, its tail was shaped to provide some aerodynamic effect, like that of a dart. This was evaluated by dropping the robot from the specified height of 3 m and filming its descent using the "slo-mo" video setting on an iPhone 6. This allows the effect of the tail, if any, to be evaluated by examining the position of the robot as it rotates in successive frames of video. Two directions of rotation were tested: pitching (nose over tail rotation) and yaw (one wheel over the other) which necessitated drops from two different starting positions. To prevent potential damage, the robot landed on a large cushion.

Upon landing, it is desired that the robot can operate in any orientation to which it might fall. In order for the controls to adapt to operation in either direction, additional sensors (in G Knox's sensor payload) were required; the testing here is merely to show that, mechanically, the robot is capable of operating in either direction.

7.10.2 *Results*

The results of the pitching and yawing drop tests are presented in Figures 7.10 and 7.11 respectively as overlaid composite images showing the robot's trajectory and orientation in successive video frames.

The attempt to aerodynamically create pitching motion is markedly more successful than the yawing motion. Due to the design of the tail, in the pitching scenario, more of the tail's surface area is presented to the oncoming air mass, increasing the drag forces necessary to right the robot. Additionally, the yaw direction of rotation is resisted by a greater moment of inertia, as the mass of the motors and other internal components are now rotating perpendicular to the axis of rotation.

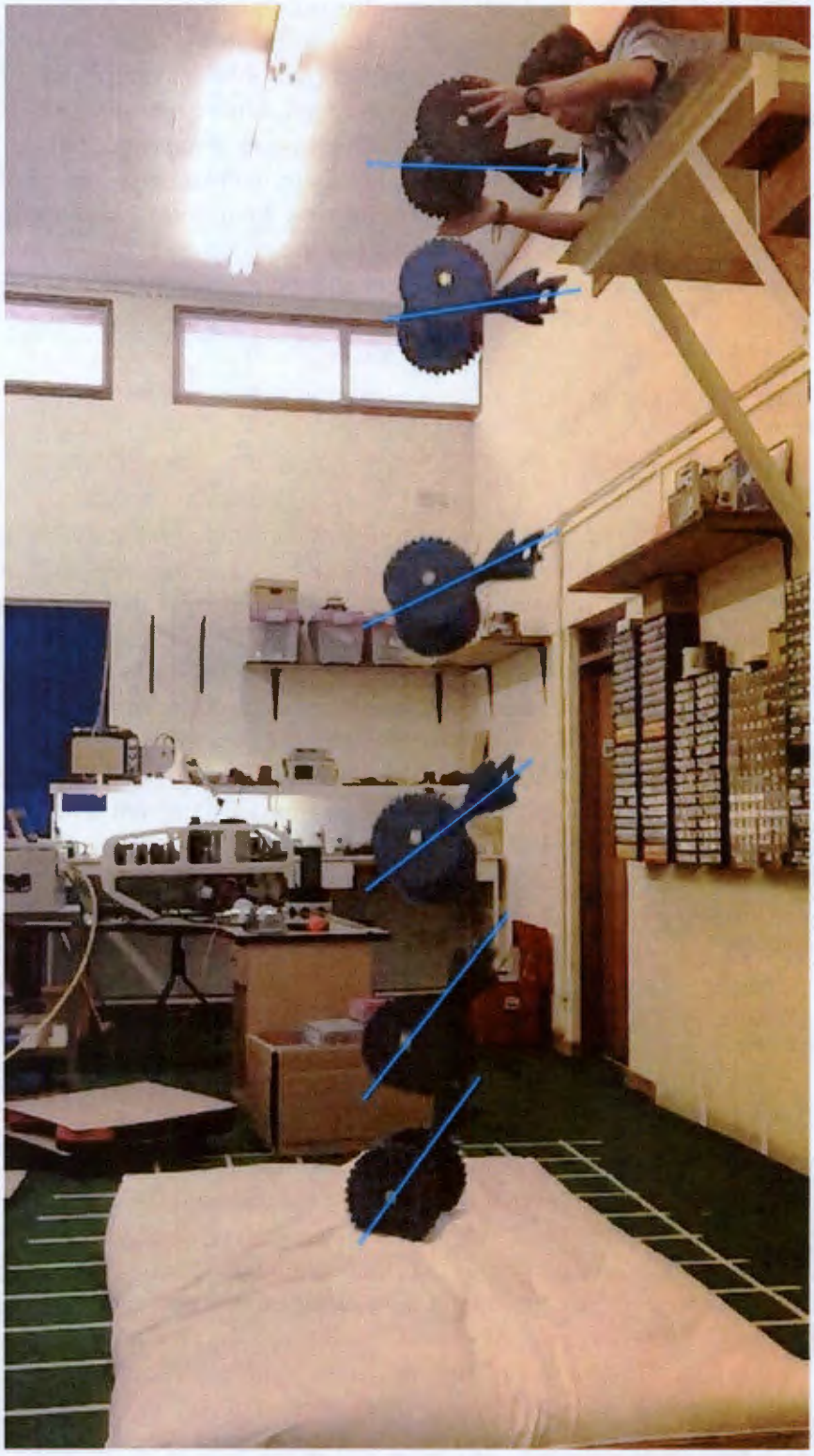

Figure 7.10 Composite image showing pitching effect of tail in drop test

Figure 7.11 Composite image showing yawing effect of tail in drop test

Figure 7.12 Composite image showing robot in both orientations

The robot successfully operates in either direction due to its symmetrical design. Figure 7.12 shows this in a composite image showing the robot with each side facing up.

7.11 SLOPE CLIMB

7.11.1 *Description*

In order to assess the robots ability to surmount obstacles and ascend ledges or slopes, it is driven up a series of plywood slopes of increasing gradient. Plywood is used by the *DHS-NIST-ASTM Standard Test Methods* as it has a coefficient of friction similar to that of dusty concrete[21]. The robot is placed at the foot of a slope and driven straight up. The gradient is increased until the robot can no longer ascend the slope.

7.11.2 *Results*

Due to failure of the motors, the robot only managed to ascend a 4 degree slope. During earlier, sadly undocumented operation, it was felt that the poor friction of the wheels would be a limiting factor before the torque delivery of the motors, however by the time the slope tests were carried out the motors' performance had significantly degraded and this was not the case.

Given that the motors supplied were of substantially lower torque rating than specified, it is informative to estimate their performance had they not failed before this test. The torque on the motor is given by multiplying the perpendicular components of applied force and distance from the application of force to the axis of rotation. As a benchmark of the motor's expected performance with the current motors, a theoretical maximum slope is calculated. Assuming both wheels are in contact with the slope, the following equation describes the torque T on a single motor for a given slope angle θ:

$$T = r\frac{mg}{2}sin\theta$$

where r is the radius of the wheels and m the mass of the robot. Substituting in a radius of 120 mm, mass of 3 kg and a torque of 0.5 Nm and solving for θ gives a maximum slope angle of 20.7 degrees. Although no specification exists regarding the angle a robot must be able to climb to be deemed USAR-capable, it is clear that twenty degrees is not sufficient.

7.12 GAP CLEARANCE

7.12.1 *Description*

To assess the robot's ability to traverse challenging terrain, a controlled gap clearance test was conducted. The robot was driven from one raised plywood platform to another, with the two platforms separated by a small gap. The gap was increased in increments until the robot became trapped in the gap. The test also accounts for static and dynamic clearance: smaller gaps could be surmounted even if the robot came to a standstill in the middle of the gap, whereas larger gaps required the robot to have some forward momentum. These are duly noted as separate specifications. This specification was also likely affected by the poor performance of the motors but is noted here as a low benchmark that could be improved upon.

7.12.2 *Results*

Figure 7.13 shows the robot in the process of clearing a 150 mm gap, the largest that it could achieve with damaged motors with some forward momentum. From a standing start, the robot was then able to clear gaps up to 70 mm before getting irrecoverably stuck.

7.13 OBSTACLES

7.13.1 *Description*

To further test the reliability of the robot in tasks requiring the traversal of challenging terrain, the robot should be demonstrated surmounting obstacles of increasing size, using both or only one of the wheels. Thereafter, a simulated "rubble field" could be created by filling an area with random loose objects that could be scrambled over, tumbled down, or collided with. It was expected that these tests would be strongly affected by the performance of the motors, and when they were attempted the robot lacked sufficient torque to surmount a 5 mm block placed in front of one wheel.

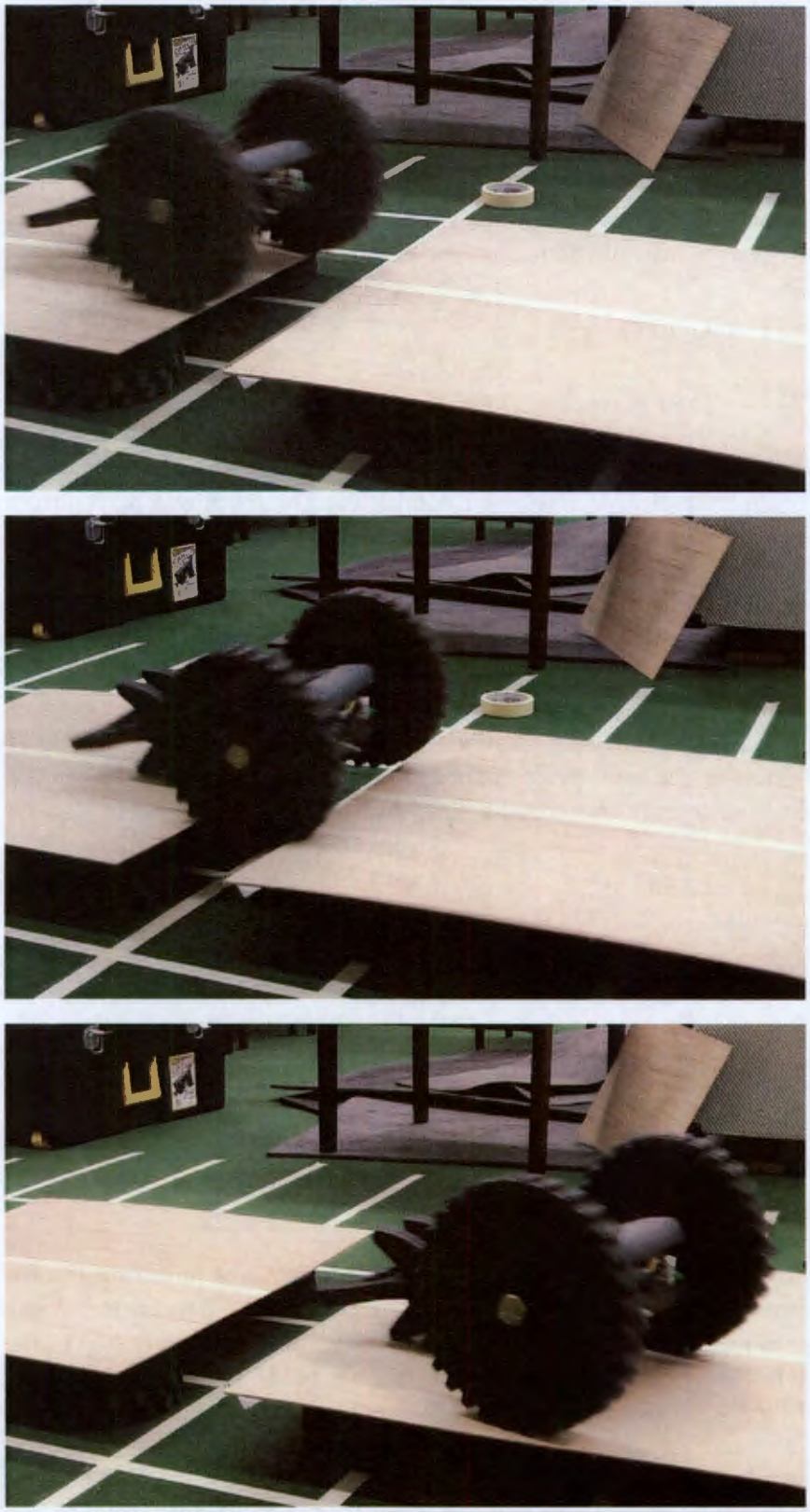

Figure 7.13
Robot clearing a 150 mm gap

7.13.2 *Results*

Tests not run due to failure of motors.

7.14 TUMBLING

7.14.1 *Description*

The tumbling and self-righting capabilities of the robot were tested by using the GUI controller to drive off a ledge at an angle so that one wheel fell before the other. The robot then fell to another surface approximately 300 mm lower, was driven off that ledge to the ground (approx 400 mm) and an attempt was then made to continue driving the robot along the ground. This test was devised to be repeated with different angles and speeds, and a second test was devised whereby the robot would travel on a straight surface littered with a variety of randomly-sized and -shaped obstacles. However, as this took place after significant damage had already been done to the gearbox, and in itself caused more damage, only one ledge drop was attempted.

7.14.2 *Results*

The robot fell at an angle over the first ledge, righted itself and was driven over the edge to the ground, where it fell flat onto the face of one wheel. In so doing, the output shaft of the corresponding gearbox was bent, hampering the robot's abilities even further. This series of events is shown in Figure 7.14.

During this test the robot landed on the outer face of on of the wheels (the second-last position in the sequence shown in Figure 7.14). The robot then fell back, applying a significant bending torque to the motor shaft. The extent of this damage, shown externally in Figure 7.15 is described in more detail in Section 7.19 but is mentioned here as it can be considered a serious limitation of the robot's ability to perform tumbling tasks safely with the current motors.

7.15 FORWARD SPEED

7.15.1 *Description*

The robot was placed on the grid-marked floor with both motors set to full power. A camera perpendicularly above the floor filmed the robot crossing the gridlines and by analysing the video frame-by-frame, the number of frames (at 25 per second) to cross each gridline will infer the robot's speed. If the robot did not travel directly along the gridlines, the deviation across the whole image was measured, and trigonometric ratios were used to correct the distance. The

Figure 7.14 Composite image showing robot tumbling from one surface to another

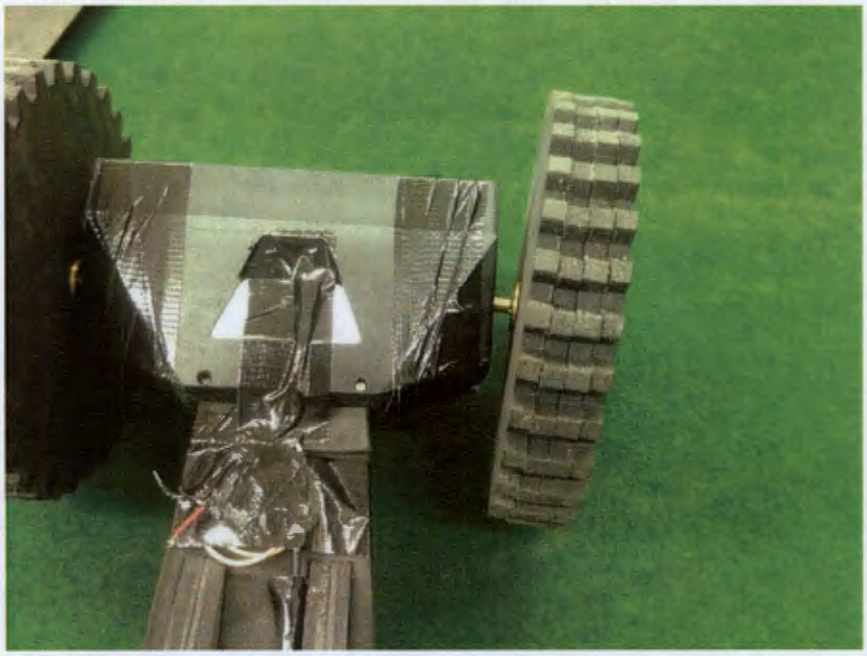

Figure 7.15 Robot showing bent right-side shaft after falling

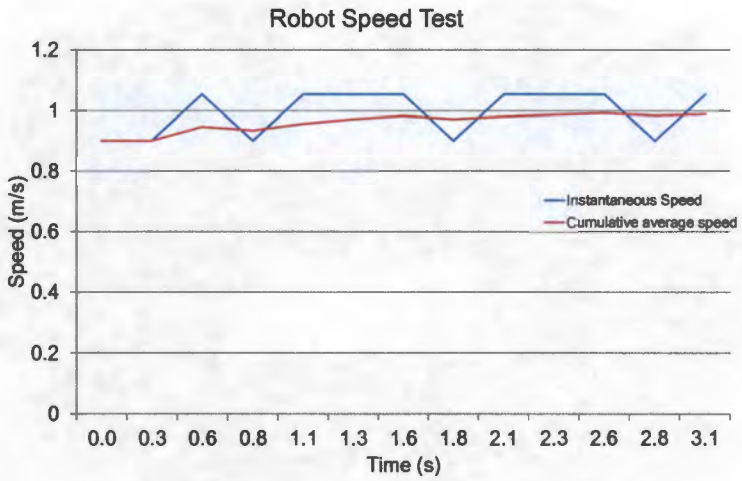

Figure 7.16 Graph showing results of speed test

frame counts and distances are analysed using MS Excel and a graph of speed drawn. To ensure that the platform was running at its top speed, a long run-up distance was allowed, and the speed was monitored throughout the test. This specification is also reduced by the failure of the motors but recorded here nonetheless as a benchmark for future work.

7.15.2 *Results*

Figure 7.16 shows the speed of the robot across the 3.25 m test grid as it crossed each 250 mm gridline. The instantaneous speed varies slightly so a cumulative average is also shown. This shows that the robot was still accelerating to top speed during the test but it displays asymptotic behaviour as it tends towards an average of 1 m/s. This is more than originally specified, and can be attributed to the increase in wheel size.

7.16 SENSORS

7.16.1 *Description*

The platform is inspected to ascertain compatibility with a range of custom sensor payloads. As these were not yet fully manufactured at the time of testing, this specification is inferred from design and test fitting of prototype parts.

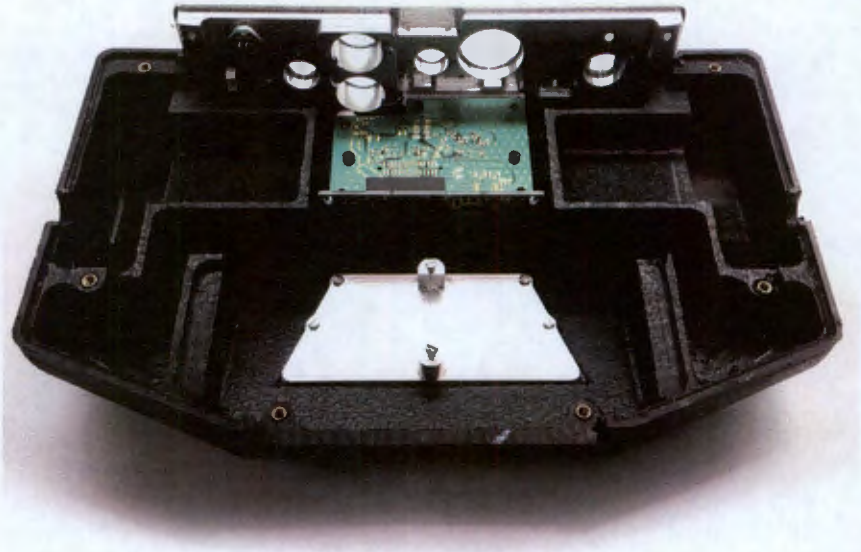

Figure 7.17 Test fit showing the housing fitting with the sensor payload face

7.16.2 *Results*

Figure 7.17 shows one half of the robot shell fitted with the manufactured aluminium face which supports the sensor payload circuitry. Un-populated PCBs are also shown in their correct position. Although a specific payload configuration is shown, any grouping of sensors which fits into the available space could be used.

Manufacturing inaccuracies in the HDPE caused the face to fit somewhat poorly — a few millimetres misalignment — but these inaccuracies have subsequently been resolved by manual post-machining rework. Future work will assess the mechanism by which these subsystems connect and interface and make any improvements necessary.

7.17 INGRESS PROTECTION

7.17.1 *Description*

Although many companies offer formal testing to determine the achieved IP rating of a new device, it is easy to more cheaply and simply estimate IP rating by subjecting the device to dusty and wet environments. Dust ingress could have been tested by driving the robot through a container of flour or similar powder, and water protection by showering the assembled robot with water, drying the exterior, and then dismantling and inspecting the interior for any ingrained drops. However, due to inaccuracies in manufacturing the plastic housing, and difficulties in obtaining a waterproof power connector, this test was

not attempted and the prototype is deemed to have failed in this specification.

7.17.2 *Results*

Test not run due to sub-optimal manufacturing of plastic parts.

7.18 POWER

7.18.1 *Description*

To determine the safety of the designed motor control board, the motors would be stalled at full power and the current draw of the motor control sub-system recorded. Due to the slipping of the gearboxes it was however not possible to produce this result. Additionally a test to deduce the effectiveness of the heatsinks was stipulated, but this test was also not possible.

7.18.2 *Results*

This test was not run due to motor failure. Informally, the highest current observed on the feedback GUI (returned by the battery management system which was calibrated against a bench multimeter) was around 2.5 A during a previous stall. This benchmarks the current draw safely below the maximum 10 A that can be supplied by the battery and well below the 5 A that can be supplied per motor driver, but this specification does not by any means stand up to scrutiny or due rigour.

7.19 MOTOR FAILURE

During testing it was observed that the motors, despite drawing power and making the expected sound, were not rotating the wheels if obstacles or slopes (see Sections 7.13 and 7.11) were placed in the robot's path. This, as well as the robot's irregular right-turn whilst gaining traction in the straight line tests (see Section 7.6) led to the hypothesis that a gear inside the gearboxes was slipping on its shaft.

Further damage was caused during the tumbling tests (Section 7.14) when the robot landed on the outer face of the wheel and visibly bent the output shaft of one of the motors.

Figure 7.18 Disassembled gearbox

7.19.1 *Investigation*

After all other tests were complete, the worst-damaged motor was removed from the robot and its gearbox disassembled. This is shown in Figure 7.18.

The final gear on the output shaft was found to be made of plastic and is presumed to have, at one point, been press fitted onto the metal output shaft where it was prevented from rotation by splines in the shaft. However these splines (visible as small striations on the shaft) lacked sufficient grip and the gear could be rotated freely around the shaft.

The shaft was also severely bent - this is shown, with the brass hub still attached, in Figure7.19.

7.19.2 *Failure mode analysis*

Although it is not known what exactly caused the gear to strip its shaft, the "maximum slope" analysis undertaken in Section 7.11 gives an indication of how poor the performance of a 0.5 Nm motor is expected to be in this application. Given that the robot was extensively driven in an informal manner during the fine-tuning of the control GUI before testing commenced, it is highly likely that a collision with some obstacle could have caused the gearboxes to fail.

7.20 CONCLUDING REMARKS

This section details the tests done upon the completed platform subsystem. Although many results of this first prototype are promising, the testing is inconclusive in many areas due to the damage incurred to the platform during testing. This could have been mitigated with

Figure 7.19
Bent output shaft

better experimental planning and risk assessment of each test, such that more low-risk tests could have been conducted before the platform's performance was permanently impaired.

The next section draws conclusions from this testing data and upon these conclusions, recommendations for future work are made.

8

CONCLUSIONS AND RECOMMENDATIONS

8.1 INTRODUCTION

The previous chapters detailed the design and development work that took place, as well as the testing thereof. The successes and failures of these tests, as well as critical analyses of the designs, allow for conclusions to be drawn. These, along with the experiences and observations of the author during the design and development stages, form the basis of recommendations for future work. These are detailed below, categorised by the section of development work that they apply to.

8.2 MECHANICAL DESIGN

A number of issues were present in the mechanical sub-systems. Some can be attributed to sub-standard manufacture, but others are flaws in the design that were only revealed during development and testing. These are described below.

8.2.1 *Platform Centre of Gravity*

As demonstrated in the control tests (Section 7.5.2), the centre of gravity of the platform was too far forward and this contributed to the instability of the platform when it was driven. This could be improved by redesigning the housing such that the motors are behind the axle rather than ahead of it. This would distribute weight more to the rear of the robot and assist in holding the tail down during manoeuvring the platform. An added benefit of this would be increased suspension clearance in front of the robot: without the motors ahead of the axle, the front face could move closer to the axle. If new motors are selected, it could be advantageous to avoid those with off-centre shafts such as the existing selection.

8.2.2 *Suspension Clearance*

The development of prototype wheels for this platform described in Section 6.5 revealed that it was not possible to design a wheel that would meet the drop height specification using the chosen materials and specified dimensions. The solid (and therefore hardest possible) 200 mm wheels were unable to safely absorb the impact of the robot within the 30 mm clearance designed between the front of the

shell and the rim of the wheel. In this project, this challenge was overcome by increasing the size of the wheels, but this came at the cost of increasing the torque requirements of the motor, the cost and mass of each wheel and increasing the overall bulkiness of the design. It is proposed that the clearance be increased by re-arranging internal components such that the front face is further from the wheel contact surface. If the tail of the robot is successful in directing the front face down during a fall, this is the only critical clearance dimension. Further increase of the density of the wheel material is not recommended as it is preferred to meet this specification by increasing the allowable deflection rather than increasing the loading transferred to the robot's internal workings.

8.2.3 *Tail*

The test in Section 7.10 demonstrated that it is possible to use the aerodynamic properties of the tail to rotate the robot into a favourable position for impact. However, although this was successful in one direction of rotation, the tail could not sufficiently control the rotation in the other axis. As such it is recommended that the upright tail fins be closer to the end of the tail and increased in size to provide a greater turning moment with the aerodynamic forces.

Concerns have been raised regarding the handle feature in the tail hooking onto debris during operation. Further testing should examine the validity of these concerns and, if appropriate, re-design the handle to avoid its catching on protrusions in the ground surface. Reinforcement of the handle may also be necessary; this will become clear with real-world drop- and throw-testing.

Additionally, the location of the battery in the housing only allowed for a small, thin tab of foam to protrude into the case. To strengthen the connection between the tail and the robot body, it is recommended that this be redesigned to increase strength, perhaps also with studs protruding from the case that lock into holes cut into the tail.

8.2.4 *Wheels - Side Impact*

There were several issues present in the wheel design and testing, which are discussed fully in Section 8.4. One issue, however, pertains to the "industrial design" aspect of the wheels though: their ability to withstand impacts from the side. As Sections 7.10 and 7.14 demonstrated there is a risk of this happening and the present design does not offer sufficient protection.

Using moulded wheels like those of the Recon Scout range could allow for a similar three-dimensional design; adding material to the outer face of the wheels would provide impact resistance in this direction and could also be shaped to provide a pivot that would allow the

robot to roll or tumble back onto two wheels. This would, however, significantly increase the width of the robot and affect the integration with W.K. Fong's transportation harness. Further work in this area combining industrial design conceptualisation and prototyping, along with more detailed testing, is strongly advised.

8.2.5 *IP rating*

No degree of water- or dust-proofing was obtained due to issues in manufacturing of the plastic shell. Furthermore, if these had been corrected, the charging connector specified by G Knox and W.K. Fong would still have presented problems as it was not waterproofed. Future work must either develop a plug or cover to seal the charging connector while the robot is in operation, or specify an existing waterproof connector.

As noted in Section 4.8, the width of the sealing faces was not sufficient to safely locate the seal during assembly. It is recommended that these features be re-designed in accordance with some standards or guidelines for successful seal design.

8.2.6 *Motors*

Due to supplier issues, incorrect motors were used, which lacked sufficient torque to lift the robot over obstacles and challenging terrain (as noted in Sections 7.11 and 7.13). During testing the gearboxes failed completely as a result of pushing them beyond their rated capability. Tumbling tests (Section 7.14) also revealed the susceptibility of the motor shafts to bending.

However, these motors did serve well to demonstrate the functioning of other sub-systems, and the tests that were attempted, although not yet conclusive, suggest a robot such as this could be successfully operated using simple brushed DC motors without odometry and complex control systems.

It is recommended that future work replace the motors with a higher-torque alternative, and that their shafts be suitably supported to resist bending damage. One such alternative motor is the MFA Como Drills 940D, shown with an epicyclic reduction gearbox in Figure 8.1[8]. Integration of this motor would necessitate a re-design of the entire shell as it is significantly longer and of a different layout and mounting type.

8.2.7 *Housing*

Although the CNC-machined HDPE housing was successful in providing a platform for testing the integration of various sub-systems, it had significant drawbacks. The UCT workshop was unable to manu-

Figure 8.1 The MFA Como Drills 940D motor[8]

facture to specification and a number of features were left in a sub-optimal condition. Due to the limitations of the CNC milling process, some features were left solid (adding significant mass to the shell), which ideally would have been hollowed out. HDPE also lacks the hardness to hold a screw thread or secure the brass thread inserts. Future work might consider coarser-threaded or self-tapping screws to alleviate this issue. Even so the the shell could not have been screwed shut due to alignment issues between the two halves of the shell.

It is recommended that future work consider alternative manufacturing methods and materials, including design for injection moulding with a harder plastic.This would allow the shell to be thinner overall and add the complex geometries required to hollow out structures for further mass reduction. If this is not possible and milling is attempted again, Nylon is suggested as a more machinable material, however its threadability should be tested as fastening the case shut is critical in demonstrating the viability of the prototype.

The charging port's location, near the aluminium heatsink on top of the robot, is not ideal as it is likely that during plugging or unplugging the connector may short against the aluminium, causing damage to the charger. Although the proposed anodising treatment would decrease the conductivity of the aluminium, it is still advised that the connector be moved should the anodised layer have imperfections or become scratched away. Re-locating it closer to the rear of the robot could also allow it to be re-purposed as a tether connection point in subsequent development.

8.3 ELECTRICAL

Electrical and electronic systems were designed and developed, and appropriate software written to control and integrate their components as well as manage communications with the base station. These were successful in controlling the robot when used with the appropriate wireless hardware and a test GUI.

Although the electrical sub-systems appear to have performed well, they were not tested to their limits due to the failure of the motors, and the concurrent sub-systems developed by G. Knox and W.K. Fong not being ready for integration. The interested reader is referred to

their integration test results for more details in this regard as they may highlight issues with work done under the scope of this project.

8.3.1 *Motor Drivers*

Although the performance and ease of use of the Freescale MC33926 motor drivers could not be faulted in this application, they do represent a significant portion of the cost of the electronic sub-system. Future work could look into alternative ICs that provide the same functionality at a reduced cost. A significant cost saving could be achieved by lowering the specification when new motors are selected; it is unlikely that a 5 A continuous current supply will be necessary.

8.3.2 *Control*

Given the correct components and some simple software, the robot's movement would easily be controlled. However, issues with the stability of the platform during deceleration are noted in Section 7.5.2. Although much could be achieved by re-locating the centre of gravity, it is recommended that future work investigate the integration of a small, affordable IMU onto the controller board in order to correct the motor power and maintain stability. Additionally, this could be used to maintain correct heading, as advertised on the Recon Scout robots[5], correcting the robot's direction of travel in case of wheel slippage or motor inconsistencies. This may require upgrading of the microcontroller to allow communication with the IMU — the ST Microelectronics STM32Fo range provide specifications comparable to (or improved upon) the MSP430 range at similarly affordable prices.

If this is not possible, an open-loop controller could be implemented in the existing microcontroller software to provide a gentle "ramp-down" even when the control joystick is suddenly released to zero.

A natural, intuitive user interface with video and sensor feedback would be required to control the robot in real-world scenarios: this is within the scope of W.K. Fong's concurrent M.Sc and is currently under development.

8.4 WHEEL DESIGN AND DEVELOPMENT

A method for designing and testing impact-absorbing wheels has been demonstrated in the preceding sections. Its results were adequate to aid the design of a wheel that would protect the robot from deployment by throwing or falls incurred during its operation, although issues were present that limited its application. Specific issues for future consideration, as well as further research into wheel designs, are highlighted below.

8.4.1 *Testing equipment*

The 834M1 accelerometer was able to record accelerations in the range required. However, as it was selected before the precise regime of accelerations the experiments would incur was known, it was somewhat over-specified and future work could select an accelerometer with a maximum in the order of 500G. This would likely have a positive result on the signal-to-noise ratio of the data gathered, as the low-magnitude accelerations captured in these tests were close to the noise threshold of the device.

The high-speed camera provided a suitable method for estimating the deflection of the wheels; however this could be improved with image-processing software that cold track the position of a feature in successive frames of video. This would allow for the velocity and acceleration to be inferred, as well as plotting all three quantities as they vary against time during the impact.

8.4.2 *Further tests*

The wheel concepts were tested extensively in one orientation only. At present it is not known how these concepts would perform when subjected to loading in other directions. Future work could consider the testing, and if necessary, design to mitigate the effects of, side impact. The tumbling test in Section 7.14 revealed that such impacts are likely to occur and as such must be better understood.

8.4.3 *Further research*

Although the iterative design-and-test approach has been shown to be capable of producing results, further development would benefit significantly from more advanced modelling. An investigation into possible alternative materials is proposed, and this material should ideally be fully characterised so that FEM modelling can be used to simulate and optimise wheel performance more rapidly, although this would certainly be a non-trivial exercise. Due to its ease of manufacture and promising (albeit limited) results, the "dreamcatcher" concept is proposed as a starting point for such an investigation.

8.5 FINAL SUMMARY AND OVERVIEW

As robots are often used in situations where it is too dangerous or unpleasant to send a human worker, these robots often operate in conditions that threaten their safety. The financial implications of damaging or losing a robot often constrain the decisions of their operators and lead to reduced usage of existing robots. Furthermore, the high cost of existing robotic systems reduces the extent of their usage, particu-

larly in emerging economies. As such, there is a demonstrable need for low-cost, rugged robotic systems.

In this dissertation, the development of the Scarab, a rugged, low-cost inspection-class robotic platform, is described. Designed to withstand deployment into Urban Search and Rescue environments, its potential applications also include security and tactical work, building inspection, nuclear leak surveillance, or any inspection task where it is too dangerous or confined to send human workers.

Its applications are further extended by its ability to accept a range of different sensor payload configurations. This also serves to decrease the risk associated with losing or damaging the robot in challenging terrain; if a scenario is particularly dangerous the platform can be fitted with the bare minimum of sensors for the task and consequently incur a minimized risk.

To protect the robot from damage incurred during falls or deployment by throwing, large, energy-absorbing foam wheels were designed. To aid this, an iterative design-and-test method was developed, including significant experimental work and data analysis.

To control the movement of the platform, geared motors are controlled using a custom electronics PCB including a microcontroller which runs control software and manages communication with the base station. Although the two concurrent M.Sc projects were not at a sufficiently advanced state to integrate into the combined system, the progress thus far predicts success in that regard.

As this project is a first prototype, significant weight is carried by the recommendations for future work. These are based on testing of the platform and sub-systems within it and will form the basis of the next step in the development of this project.

APPENDICES

A

HOPKINSON BAR CHARACTERISATION

The experimental apparatus known today as the Hopkinson Bar was proposed by Bertram Hopkinson in a 1914 paper published by the Royal Society [58]. Originally devised as a method for measuring the pressure induced during detonations or projectile impact, it has found use in a variety of other applications. In the following appendix, it is set up to validate and, if necessary, calibrate the readings from a piezo accelerometer. In order to achieve this, the bar must be calibrated, which requires an understanding of the physics involved. This is covered after a description of the apparatus, and followed by documentation of the procedure undertaken to calibrate it.

Kolsky's work[57], 35 years after Hopkinson's publication, lead to the development of the Split-Hopkinson Pressure Bar commonly used in materials testing today.

A.1 APPARATUS AND METHOD

The apparatus used in the experiment is shown in Figure A.1. A single 'incident' bar, supported at intervals along its length, is equipped with a pair of diametrically opposed strain gauges half-way down its length. These are oriented axially on the bar and connected in a Wheatstone bridge so as to correct for bending effects. The signal from the Wheatstone bridge is passed through an INA110 strain gauge amplifier circuit with 1000x gain.

The bar is struck at one end with a second, smaller 'striker' bar, which is fired from a gas gun. This striker bar passes through a light gate that measures the speed at which it impacts the incident bar. At the other end of the bar, the piezo accelerometer is directly affixed using strain gauge cement. The readings from the light gate, strain gauge, and accelerometer are recorded using data capture hardware and the signals fed into a computer for processing and analysis.

The stress history recorded by the strain gauge is mathematically manipulated into a velocity history, the first derivative of which is compared to the acceleration history captured by the accelerometer.

A.2 LOADING OF UNIFORM BARS

(This and the following sections draw heavily on the work of T. J. Cloete and D. Bonorchis [59], which in turn is based on M.F. Spotts[60])

Consider a long bar of cross-sectional area A, length l, and density ρ. If a sudden compressive stress σ is applied to one end, it causes a stress wave to run down the length of the bar at the speed of sound in the bar material, c. At some time t, the length of the compressed section is ct and the velocity v of any particle in this section is the longitudinal deformation δ divided by t.

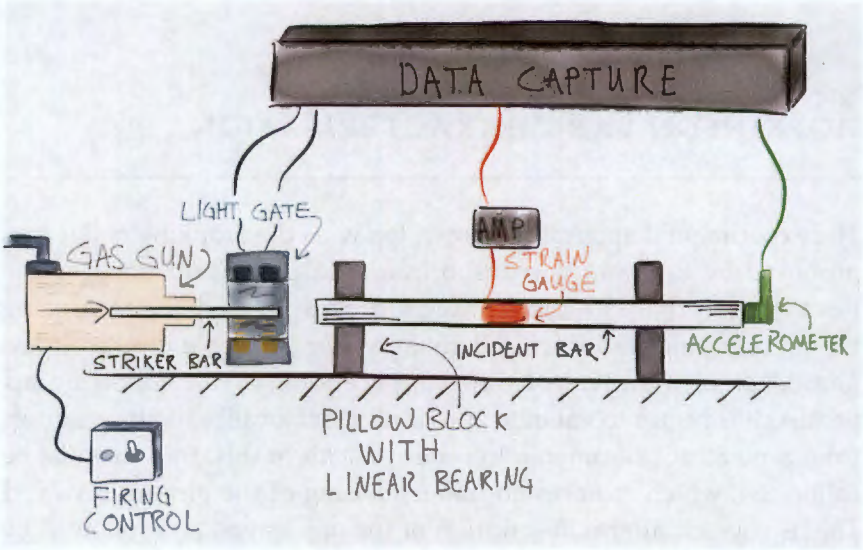

Figure A.1
The Hopkinson Bar Apparatus

Given that deflection is equal to strain multiplied by original length ($\delta = \epsilon l$) we can rewrite:

$$v = \frac{\delta}{t} = \frac{\epsilon l}{t} = \epsilon c$$

Strain can be expressed as stress divided by the Young's modulus of the bar material E, thus:

$$v = \epsilon c = \frac{\sigma c}{E} \tag{A.1}$$

At time t, the mass of the compressed section is given by ρAct and consequently its momentum (mv) can be expressed as $\rho Actv$. This momentum must be equal to the transferred impulse Ft where the force F is equal to the compressive stress multiplied by the cross-sectional bar area ($F = \sigma A$). Consequently:

$$\rho Actv = \sigma At$$

and hence we arrive at Equation A.2

$$\sigma = \rho cv \tag{A.2}$$

The density is calculated simply by weighing and measuring the bar, and dividing the mass by the volume. The speed of sound in the bar can be determined by noting the time taken for a stress wave to cross the strain gauge, reflect off the free end of the bar, and return to the strain gauge. The distance from the strain gauge to the free end of the bar is divided by half this time to obtain the wavespeed c.

The Young's modulus of the bar can be found by equating particle velocities from Equation A.1 and A.2 and re-arranging:

$$E = \rho c^2 \tag{A.3}$$

Same-material bars are chosen in order to simplify the calculations.

If this impact loading is caused by the bar being struck axially by another bar of the same material, the resultant stress in each bar can be found. If the bars are of different diameters, it is assumed that the contact is made over the entire face area of the smaller bar. Additionally, the bars must remain in contact during the entire impact event - therefore their velocities are equal. In addition, because the incident bar is initially at rest, its velocity v_b is equal to the change in velocity Δv_b. Given this, the particle velocity v_s in the striker must be equal to the original striker speed v_0 less the change in speed Δv_s incurred during the impact with the incident bar.

Note: These are all scalar quantities.

$$v_s = v_b = \Delta v_b = v_0 - \Delta v_s \tag{A.4}$$

The impact produces compression waves in both bars, running in opposite directions away from the contact face. From Equation A.2, the change in particle velocities in each bar are

$$\Delta v_s = \frac{\sigma_s}{c\rho}$$

to the left and

$$\Delta v_b = \frac{\sigma_b}{c\rho}$$

to the right.

Substituting these into Equation A.4 and re-arranging to be in terms of v_0:

$$v_0 = \frac{\sigma_b + \sigma_s}{c\rho} \tag{A.5}$$

The two faces must also be in force equilibrium, therefore:

$$\sigma_s A_s = \sigma_b A_b$$

As such, by writing Equation A.5 with σ_s as a function of σ_b and the ratio of bar areas, the following can be derived:

$$\sigma_b = \frac{A_s}{A_s + A_b} c\rho v_0 \tag{A.6}$$

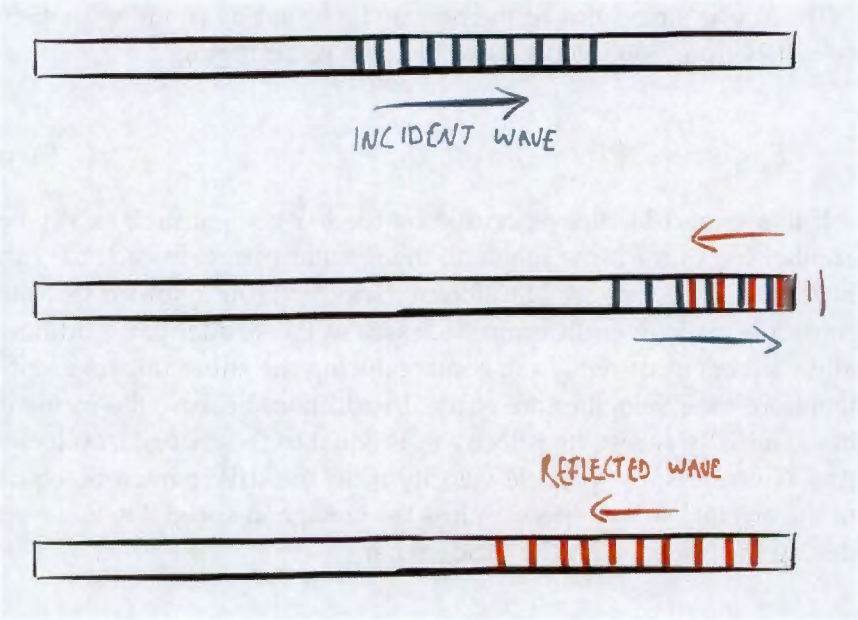

Figure A.2 Stress wave reflection in the free end of a Hopkinson Bar

A.3 FREE-END REFLECTION

In order to meaningfully compare the readings from the strain gauge in the middle of the bar and the accelerometer at the free end of the bar, the behaviour of this free end must be understood.

If the far end of the bar is not axially in contact with anything, it can have no axial forces acting upon it, and hence the stress on its end face must be zero. As the front of the stress wave approaches the free end, it is immediately reflected as a tensile wave, folding back on itself and running towards the struck end of the bar, as shown in Figure A.2.

This behaviour is not easy to directly visualise but can be modelled as follows: consider the bar as a finite section of an infinitely long bar, along which two stress waves are running in opposite directions. At the end of the finite bar section, the two waves of equal magnitude, one tensile and the other compressive, approach each other and cross. At this free end, the stress must be zero, as shown in Figure A.3. For the compressive wave, the wavespeed and particle velocity are in the same direction (towards the free end). For the other wave to be tensile, however, its particle velocity must be in the opposite direction to its direction of travel. The two waves have the same stress magnitude; as such, when they cross at the free end, their resultant stress cancels to zero. Their velocities, however are of equal magnitude and the same direction so the end of the bar experiences twice the velocity of a single wave.

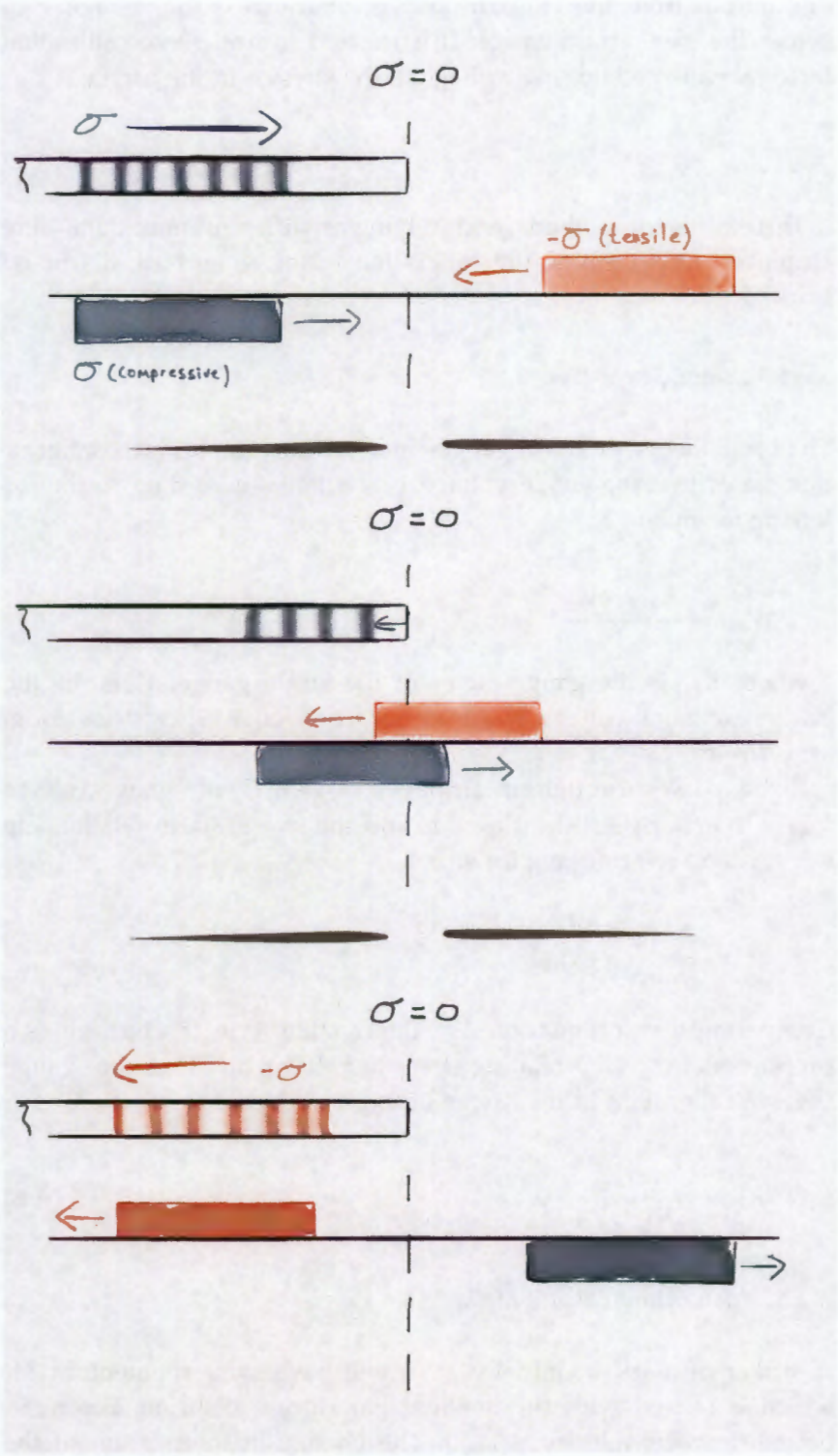

Figure A.3 Stress wave reflection modelled as superposition of waves

A.4 CALIBRATION

The output from the Hopkinson bar apparatus is the voltage V_{read} across the axial strain gauge. It is desired to find some calibration factor K which relates this voltage to the stress σ in the bar, i.e.:

$$\sigma = KV_{read} \tag{A.7}$$

Three different methods, each relying on different input data, were employed to determine the calibration factor K, and are discussed below.

A.4.1 *Strain Gauge Theory*

The basic theory of strain gauges in a Wheatstone bridge configuration states that the gauge voltage V_{out} behaves according to the following formula:

$$V_{out} = \frac{K_{gf} N \epsilon V_{ex}}{4}$$

where K_{gf} is the gauge factor of the strain gauge, $V_{ex}$is the the bridge excitation voltage, N is the number of active Wheatstone bridge arms (in this case, N =4).

If this passes through an amplifier of gain G, the gauge voltage $V_{out} = v_{read}/G$. By substituting this and the stress/strain relationship $\epsilon = \sigma/E$, and re-arranging for stress:

$$\sigma = \frac{4E}{GK_{gf}NV_{ex}} V_{read}$$

Comparing this to Equation A.7, the fraction term can be seen as a proportional constant relating stress to voltage, and thus the "gauge theory" calibration factor K_1 can be expressed as:

$$K_1 = \frac{4E}{GK_{gf}NV_{ex}} \tag{A.8}$$

A.4.2 *Momentum Balance Method*

A striker of mass m_s initially at v_0 will have some momentum M_s which is shared with the incident bar during collision, before rebounding with velocity $v_{rebound}$. The change in momentum of the striker is equal to the impulse given to the incident bar, thus:

$$I = \Delta M_s = m_s \Delta v_s = m_s(v_0 - v_{rebound}) \tag{A.9}$$

where the rebound velocity can be found by considering relative areas thus:

$$v_{rebound}\left(1+\frac{A_s}{A_b}\right)=v_0\left(\frac{A_s}{A_b}-1\right)$$

Total impulse I is equal to the applied constant force F multiplied by the time t for which the force is applied, so for every infinitesimal time period dt we can calculate the change in impulse dI:

$$dI = Fdt = A_b\sigma dt$$

Therefore, by integrating both sides:

$$I=\int_0^T A_b\sigma\left(t\right)dt$$

and substituting Equation A.7, we yield:

$$I=\int_0^T A_bKV_{read}dt$$

Simplifying and using Equation A.9:

$$m_s(v_0-v_{rebound})=A_bK\int_0^T V_{read}dt$$

Which, solving for the calibration factor, gives the "momentum balance" calibration factor K_2 as:

$$K_2=\frac{m_s(v_0-v_{rebound})}{A_b\int_0^T V_{read}dt} \tag{A.10}$$

The integral $\int_0^T V_{read}dt$ is computed numerically using the time-discrete voltage data points captured during the experiment, where $t=0$ is the beginning of the experiment and $t=T$ is the time taken for the initial compressive pulse to pass the strain gauge.

A.4.3 *Maximum Stress/Maximum Signal Ratio*

The calibration factor of the apparatus can also be calculated by comparing the maximum voltage output V_{read}^{max} from the Wheatstone bridge to the maximum stress in the bar. Equation A.2 gives us the stress in the bar as a function of its density and the particle velocity of the

stress wave. The stress in the bar is maximal at the moment of impact; considering this, Equation A.6 can be re-written as:

$$\sigma_b^{max} = \frac{A_s}{A_s + A_b} c\rho v_0 \tag{A.11}$$

(derived in A.2 by combining Equation A.4 with Equation A.2

Following this, the "maximum stress" calibration factor K_3 is as follows:

$$K_3 = \frac{\sigma_b^{max}}{V_{read}^{max}} \tag{A.12}$$

A.5 RESULTS AND DISCUSSION

This section shows only the results of the calibration experiment; when the Hopkinson bar apparatus is used in the main body of the dissertation, it is simply quoted and presupposes these findings.

Figure A.4 shows an example of the raw voltage outputs captured by the data capture hardware. The two light gates are seen closing (their output voltage rapidly decreasing to zero) as the striker bar passes them. Immediately after passing the last light gate, the striker impacts the incident bar and this causes a stress wave in the incident bar - seen here ringing back and forth in the bar multiple times as the wave reflects off the ends of the bar. Each reflection inverts the sense of the stress wave, so it is seen first as compressive, then tensile, then compressive, and so forth.

Following the procedures outlined above, the three calibration factors were found. Figure A.5 shows the final stress history in the bar as calculated by the three different calibration factors. In this particular instance, the maximum stresses are 58.8, 67.9, and 65.6 MPa respectively.

The "Strain Gauge Theory" calibration factor, K_1, underestimates the data somewhat when compared to the other two methods; it differs by 11.9% from the mean of the other two. This is due to its accuracy being strongly dependent on the accuracy with which we can measure the bridge excitation voltage. The excitation voltage V_{ex}in this case is only known by reading from the display on the bench power supply used to generate said voltage, so it is expected to be somewhat unreliable - however it is useful as a method of 'sanity checking' the other methods.

The other two factors, which rely on more accurately measurable (yet different) data are much closer together - within 3.4% of their mean. It is possible, however, that the measured maximum voltage used to calculate K_2 could be subject to electrical noise which would affect the accuracy of K_2, as it relies on only a single data point. Equally, there is no clear plateau in the stress readings so this measurement essentially relies on a very narrow peak point. K_3 relies on

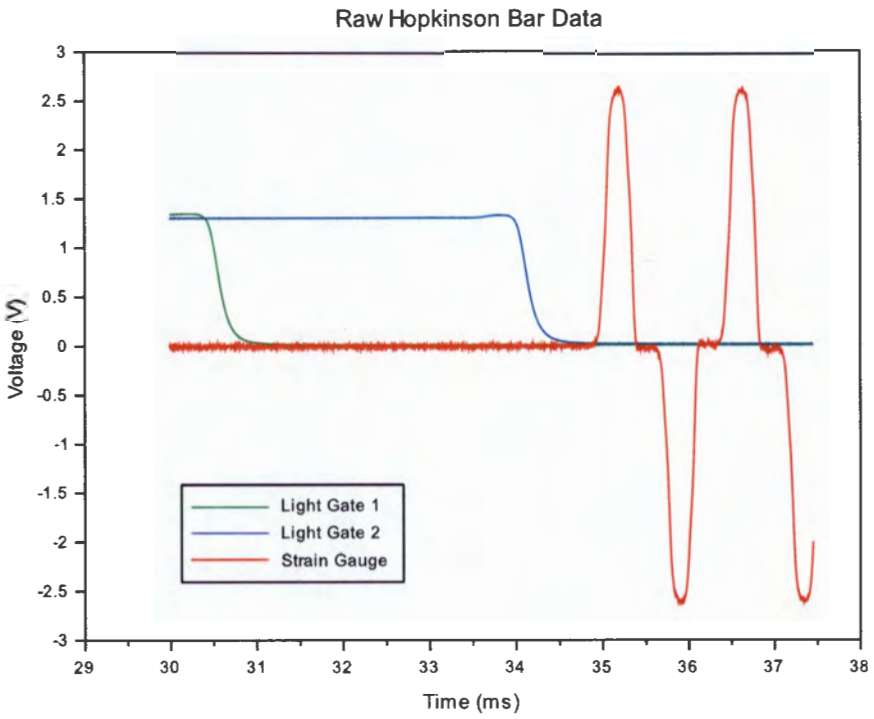

Figure A.4 Example of Raw Voltages from data capture during an experiment

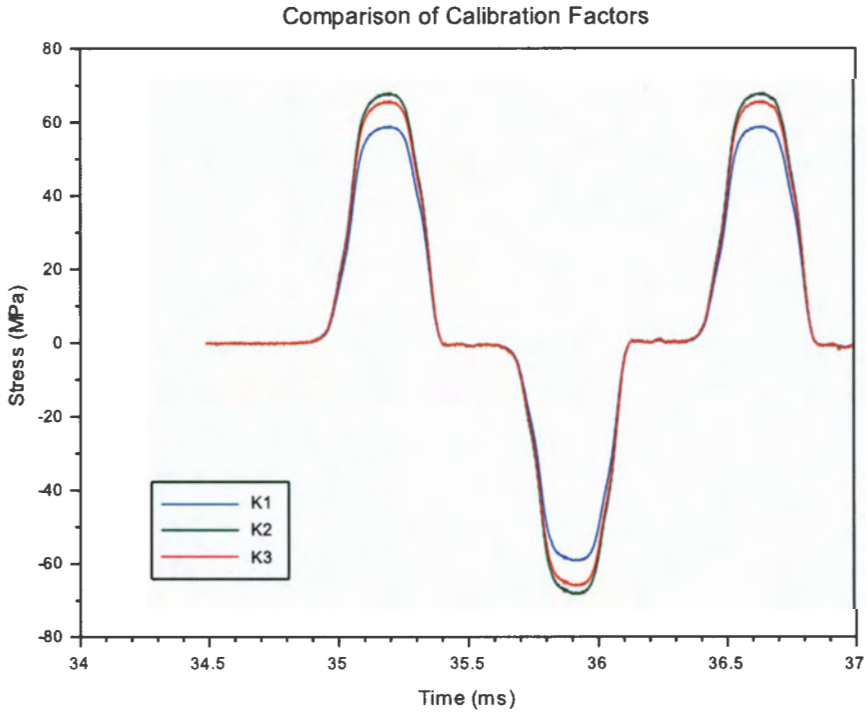

Figure A.5 Stress history in the incident bar as calculated with three different calibration factors

the rebound velocity calculated, which assumes a perfect ideal collision that, due to manufacturing inaccuracies in the bars, may well not be the case. To compensate for this (although the difference is almost negligible) we take K to be the average of K_2 and K_3.

B

DROP TESTING RESULTS

Date	#	Wheel Type	Diameter	Height (mm)	G	Disp. (cam)	Disp. (est.)	Disp error factor
31-Jul	a	curve	200	2700	40	N/A	135.00	N/A
31-Jul	b	curve	200	2800	45	N/A	124.44	N/A
31-Jul	c	curve	200	2800	80	56.00	70.00	1.25
22-Aug	a	curve	200	2700	80	54.00	67.50	1.25
22-Aug	b	curve	200	2700	80	54.00	67.50	1.25
22-Aug	c	curve	200	2700	70	54.00	77.14	1.43
22-Aug	d	composite	200	3000	70	43.70	85.71	1.96
22-Aug	e	dreamcatcher	200	3000	75	40.83	80.00	1.96
22-Aug	f	dreamcatcher	200	3000	75	33.00	80.00	2.42
09-Dec	a	solid	200	3000	90	N/A	66.67	N/A
09-Dec	b	solid	200	3000	90	N/A	66.67	N/A
10-Dec	a	solid	200	3000	100	38.00	60.00	1.58
10-Dec	b	solid	200	3000	80	39.15	75.00	1.92
17-Dec	a	solid	200	1000	100	N/A	20.00	N/A
17-Dec	b	solid	200	2000	135	N/A	29.63	N/A
17-Dec	c	solid	200	3000	150	N/A	40.00	N/A
17-Dec	d	solid	200	3000	150	N/A	40.00	N/A
17-Dec	e	solid	200	3000	145	N/A	41.38	N/A
22-Dec	a	solid	200	3000	170	28.60	35.29	1.23
22-Dec	b	grip (240mm)	240	1000	90	14.50	22.22	1.53
22-Dec	c	grip (240mm)	240	1500	120	18.86	25.00	1.33
22-Dec	d	grip (240mm)	240	2000	125	21.20	32.00	1.51
22-Dec	e	grip (240mm)	240	2500	135	28.35	37.04	1.31
22-Dec	f	grip (240mm)	240	3000	150	31.66	40.00	1.26
22-Dec	g	grip (240mm)	240	3000	130	34.66	46.15	1.33

C

WORKSHOP DRAWINGS

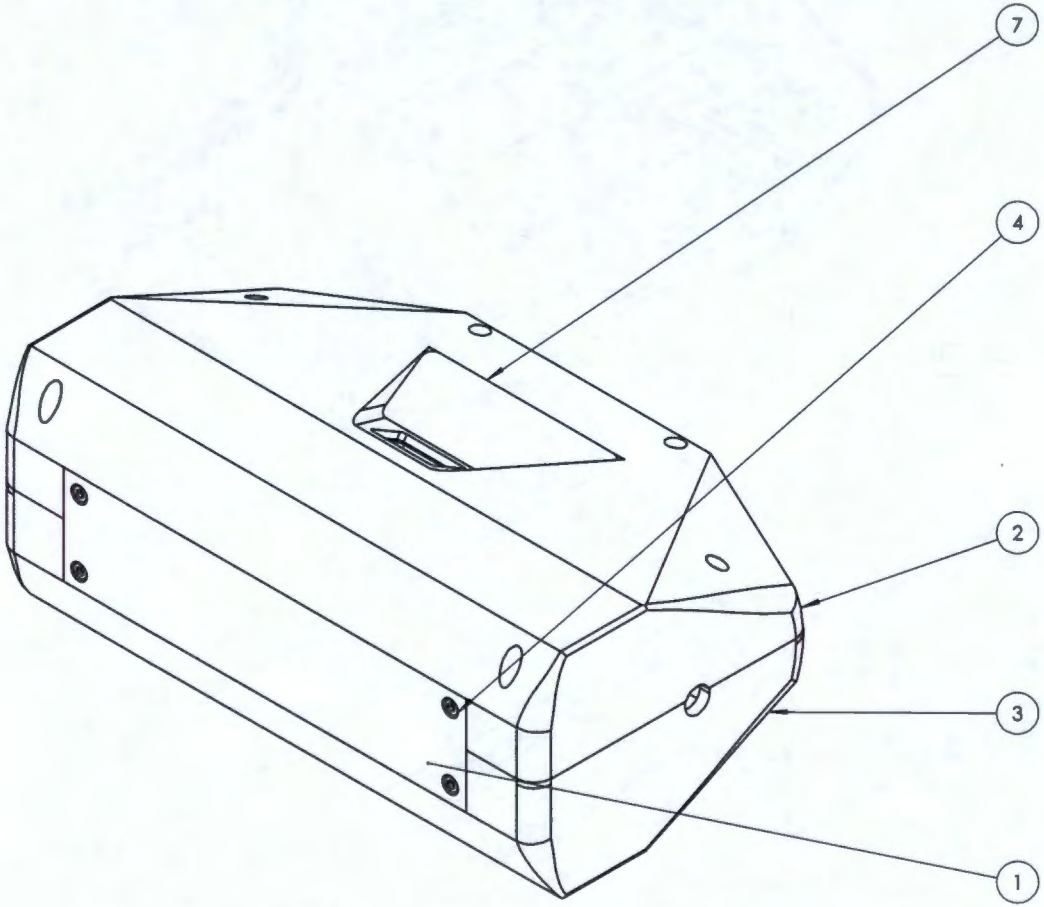

ITEM NO.	PART NUMBER	DESCRIPTION	QTY.
1	Shell_front		1
2	Shell_top		1
3	Shell_bottom		1
4	ISO 4762 M3 x 12 - – 12C	M3x12mm Socket Head Cap Screw	4
5	ISO 4762 M3 x 25 - – 18N	M3x25 Socket Head Cap Screw	4
6	ISO 4762 M3 x 30 - – 18N	M3x30mmm Socket Head Cap Screw	2
7	Heatsink_bottom		2
8	ISO 7046-1 - M2 x 6 - Z — 6N	M2x6mm CSK	8
9	Tail		1

A3 Landscape	University of Cape Town Department of Mechanical Engineering			
	Title: Shell_asm			
Assembly Drawing	Scale: 2:3	Date: 2014/05/02	Sheet 1	of 9
	Drawn By: Thomas J. Mather		Drawing Number TJM_Robot_asm	

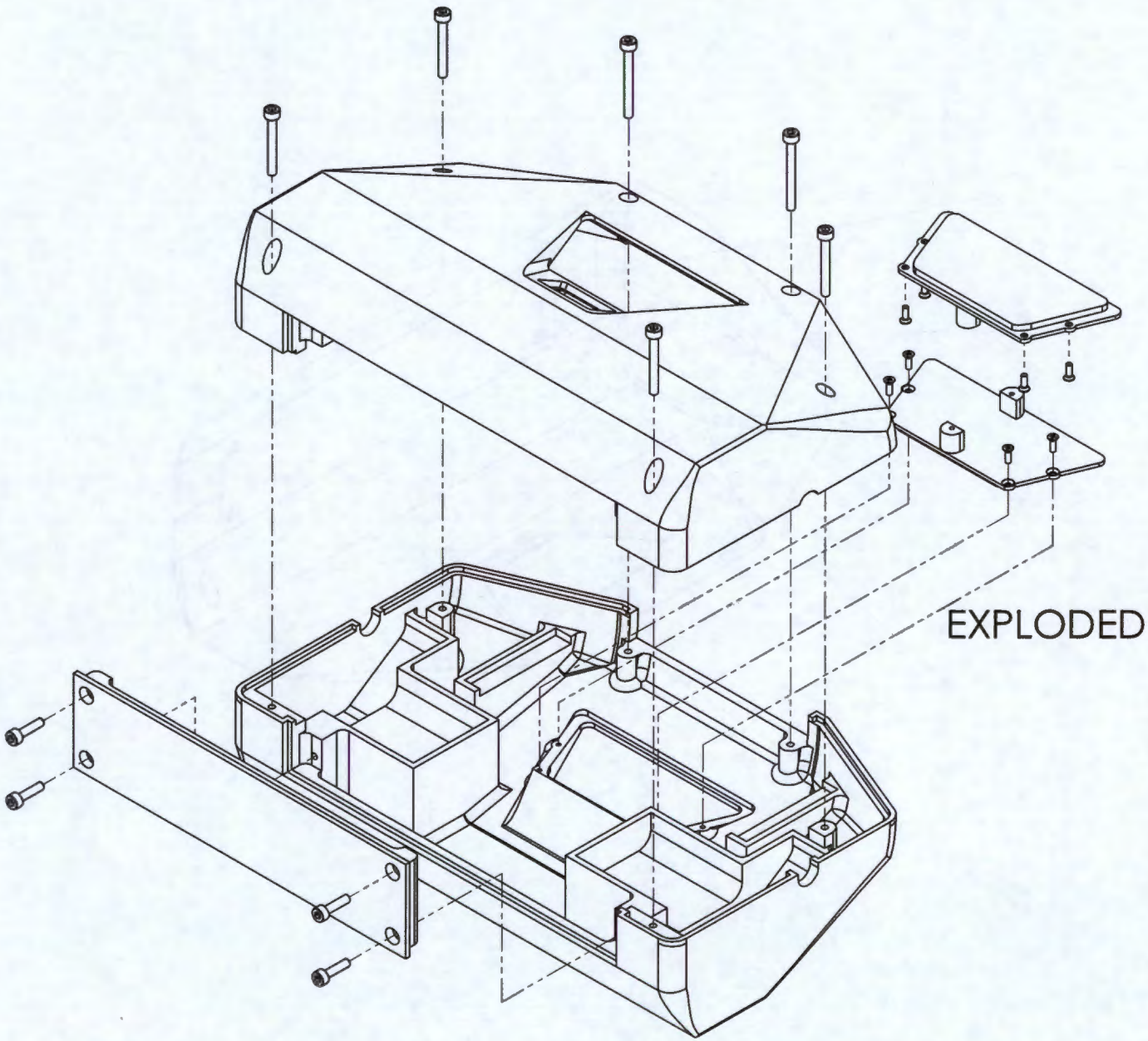

EXPLODED VIEW

A3 Landscape	University of Cape Town Department of Mechanical Engineering			
	Title: Shell_asm			
Assembly Drawing	Scale: 2:3	Date: 2014/05/02	Sheet 2	of 9
	Drawn By: *Thomas J. Mathew*		Drawing Number TJM_Robot_expl	

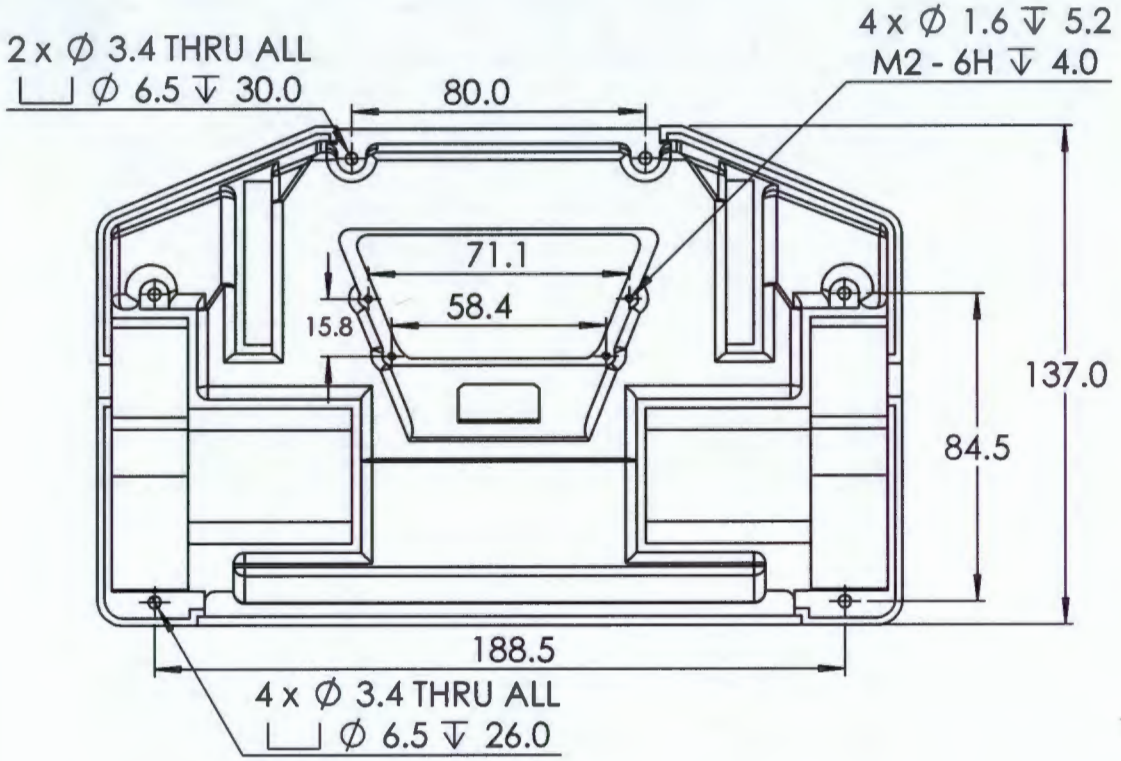

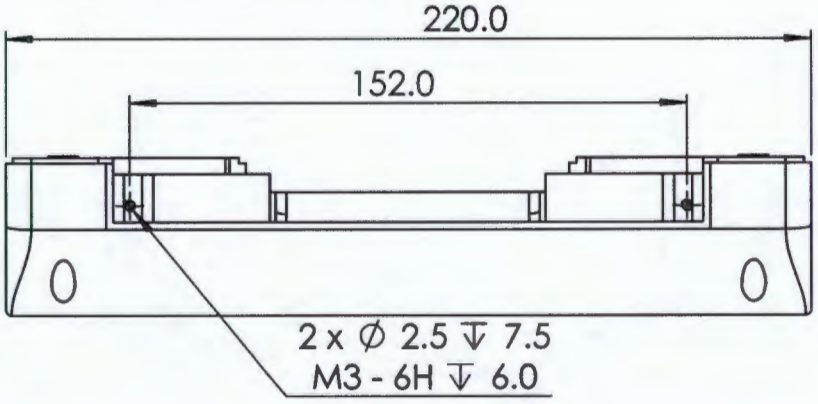

3D VIEW

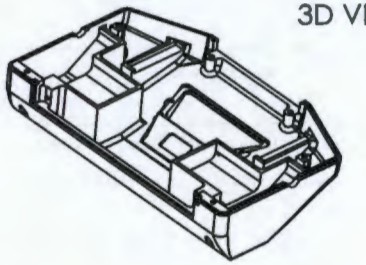

DETAIL of
Auxiliary View A
(parallel with face)

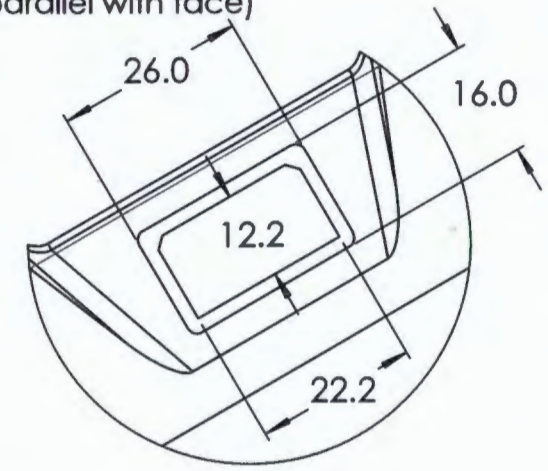

QUANTITY: 1off
To be machined from HDPE stock 220x44x137mm
Other dimensions for inspection purposes
Contact: Thomas Mathew (072 755 4007)

A4 Landscape	University of Cape Town Department of Mechanical Engineering			
	Title: Shell_top			
Part Finish	Scale: 1:2	Date: 2014/05/02	Sheet 3	of 9
Material: HDPE	Drawn By: Thomas J. Mathew		Drawing Number	

This drawing for reference and box dimension only.
(To be CNC machined from original CAD file)

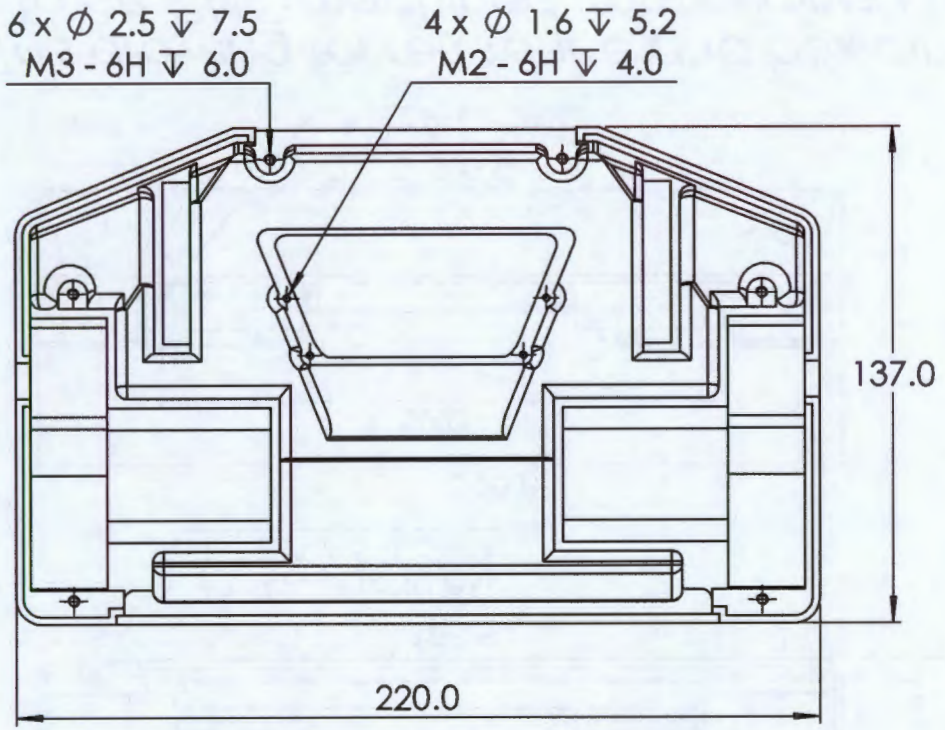

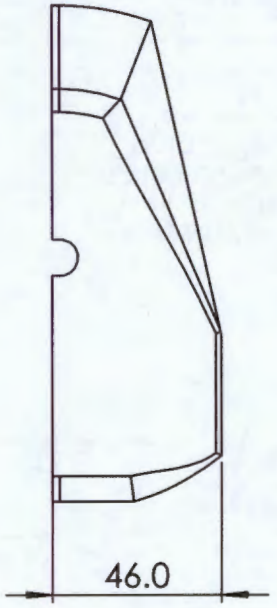

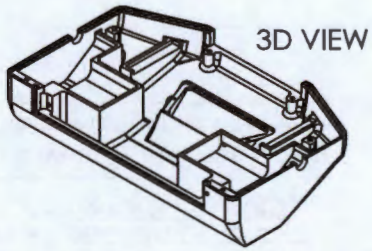

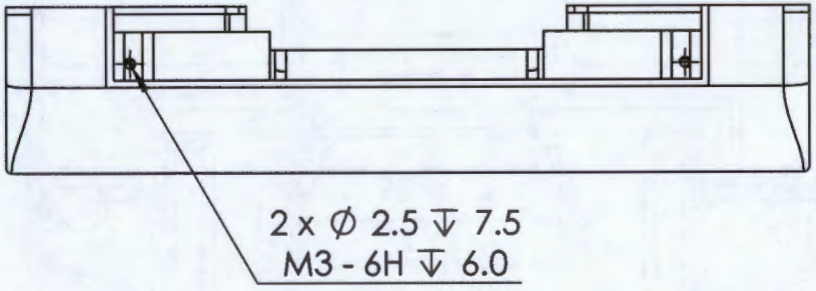

QUANTITY: 1off
To be machined from HDPE stock 220x46x137mm
Other dimensions for inspection purposes
Contact: Thomas Mathew (072 755 4007)

A4 Landscape	University of Cape Town Department of Mechanical Engineering			
	Title: Shell_bottom			
Part Finish	Scale: 1:2	Date: 2014/05/02	Sheet 4	of 9
Material: HDPE	Drawn By: Thomas J. Mathew		Drawing Number	

This drawing for reference and box dimension only.
(To be CNC machined from original CAD file)

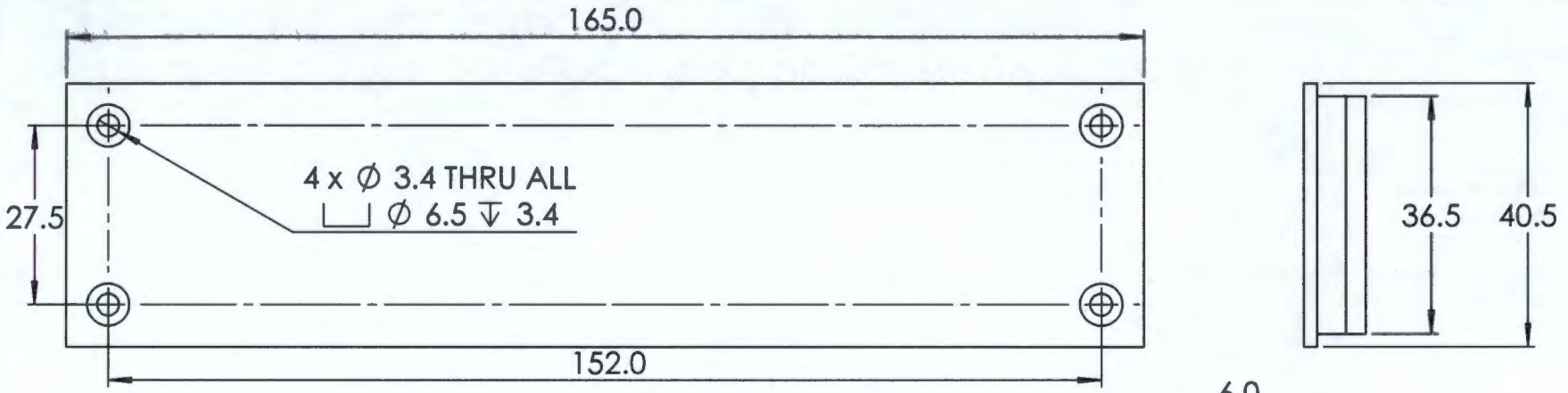

TO BE UPDATED - NOT FOR MANUFACTURE

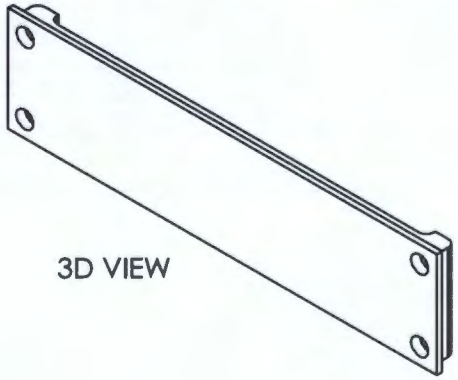

3D VIEW

QUANTITY: 1off
To be machined from aluminium stock 165x10x41mm
Other dimensions for inspection purposes
Contact: Thomas Mathew (072 755 4007)

A4 Landscape	University of Cape Town Department of Mechanical Engineering			
	Title: Shell_front			
Part Finish	Scale: 1:1	Date: 2014/05/02	Sheet 5	of 9
Material: Aluminium	Drawn By: Thomas J. Mathew		Drawing Number	

This drawing for reference and box dimension only.
(To be CNC machined from original CAD file)

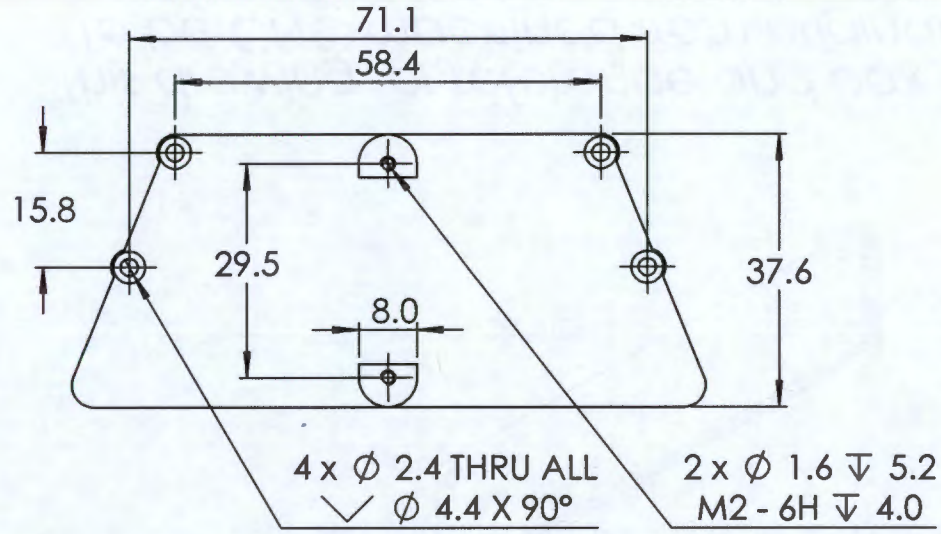

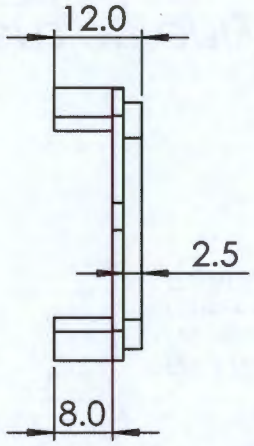

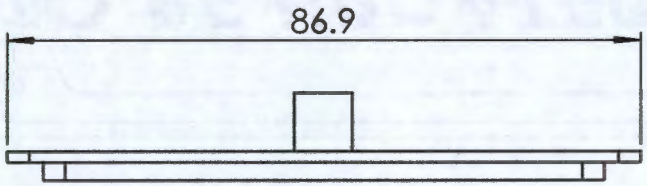

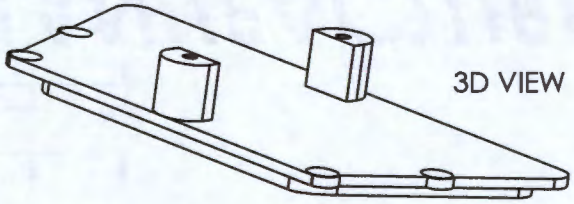

QUANTITY: 1off
To be machined from aluminium stock 87x12x38mm
Other dimensions for inspection purposes
Contact: Thomas Mathew (072 755 4007)

A4 Landscape	University of Cape Town Department of Mechanical Engineering			
	Title: Heatsink_bottom			
Part Finish	Scale: 1:1	Date: 2014/05/02	Sheet 6	of 9
Material: 6061 Alloy	Drawn By: Thomas J. Mathew		Drawing Number	

This drawing for reference and box dimension only.
(To be CNC machined from original CAD file)

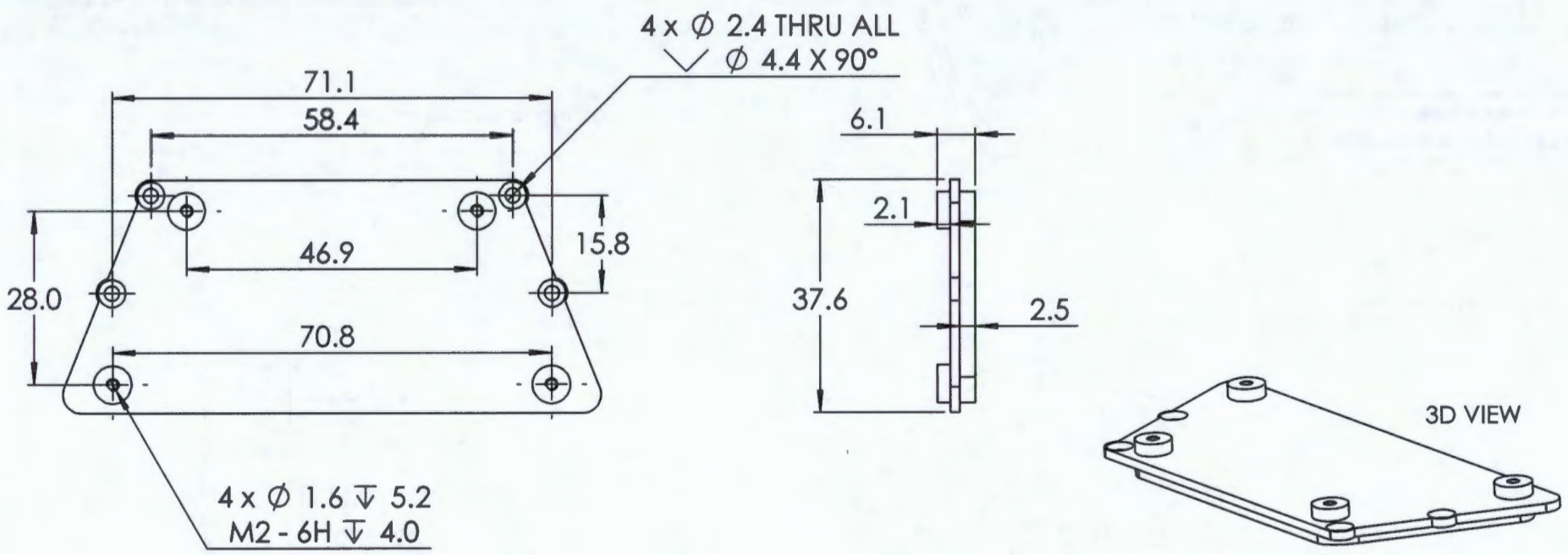

QUANTITY: 1off
To be machined from aluminium stock 87x6.1x38mm
Other dimensions for inspection purposes
Contact: Thomas Mathew (072 755 4007)

A4 Landscape	University of Cape Town Department of Mechanical Engineering			
	Title: Heatsink_top			
Part Finish	Scale: 1:1	Date: 2014/05/02	Sheet 7	of 9
Material: 6061 Alloy	Drawn By: Thomas J. Mathew		Drawing Number	

This drawing for reference and box dimension only.
(To be CNC machined from original CAD file)

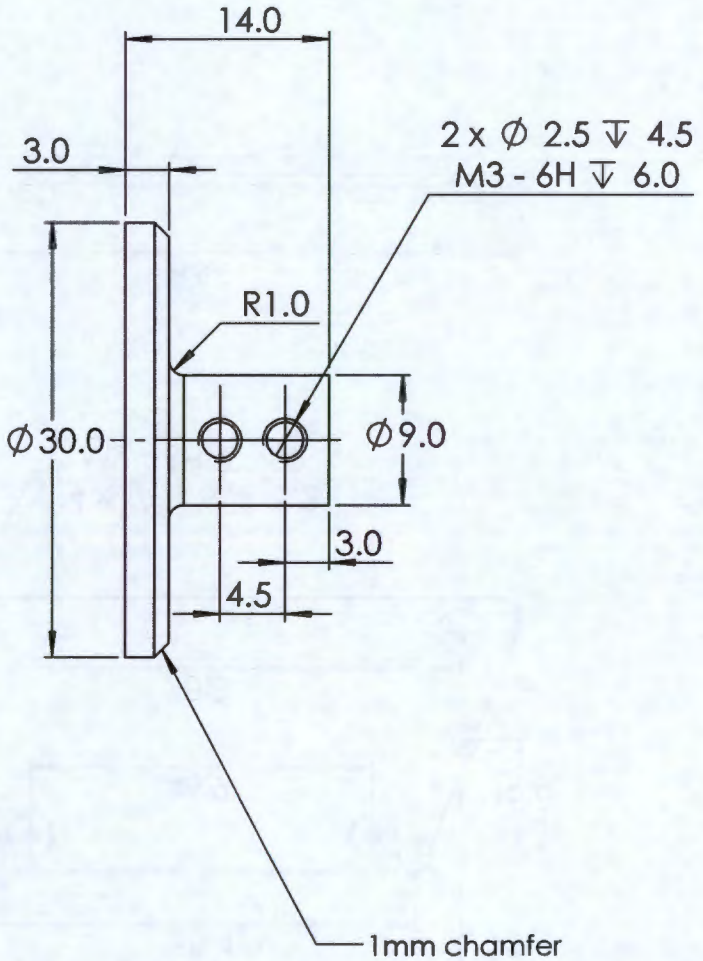

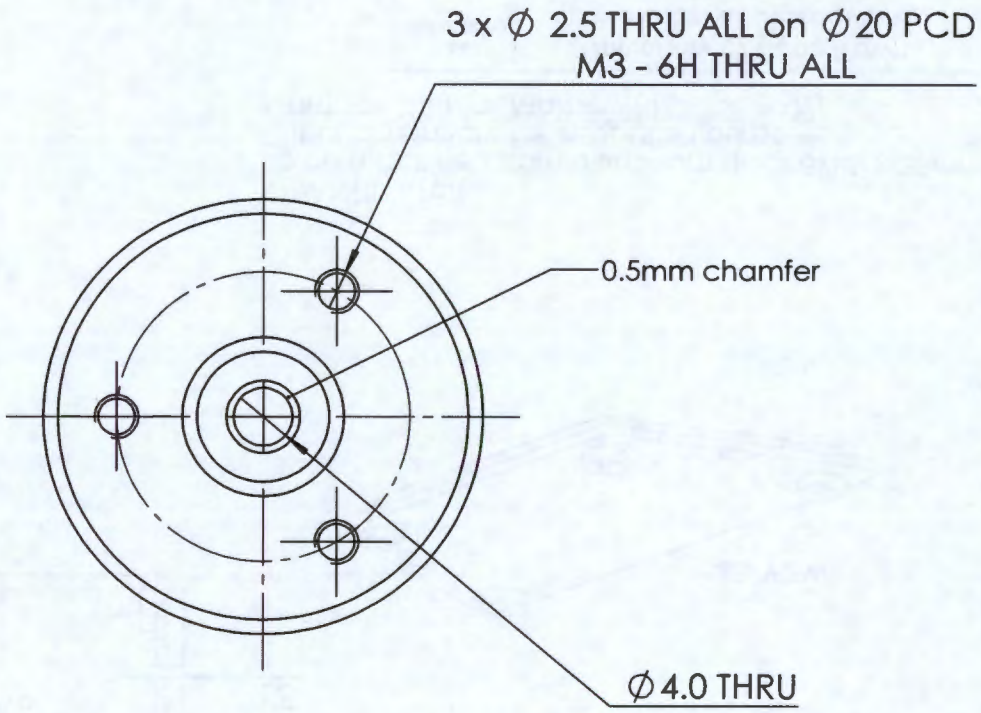

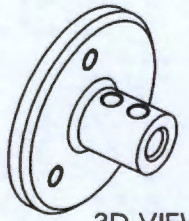

3D VIEW

- QUANTITY: 2off
- Part to be clean and free of burrs
- Please do not measure or infer dimensions from drawing
- Contact: Thomas Mathew (072 755 4007)

A4 Landscape	University of Cape Town Department of Mechanical Engineering			
	Title: Hub			
Part Finish	Scale: 2:1	Date: 2014/05/02	Sheet 8	of 9
Material: Brass	Drawn By: Thomas J. Mathew		Drawing Number	

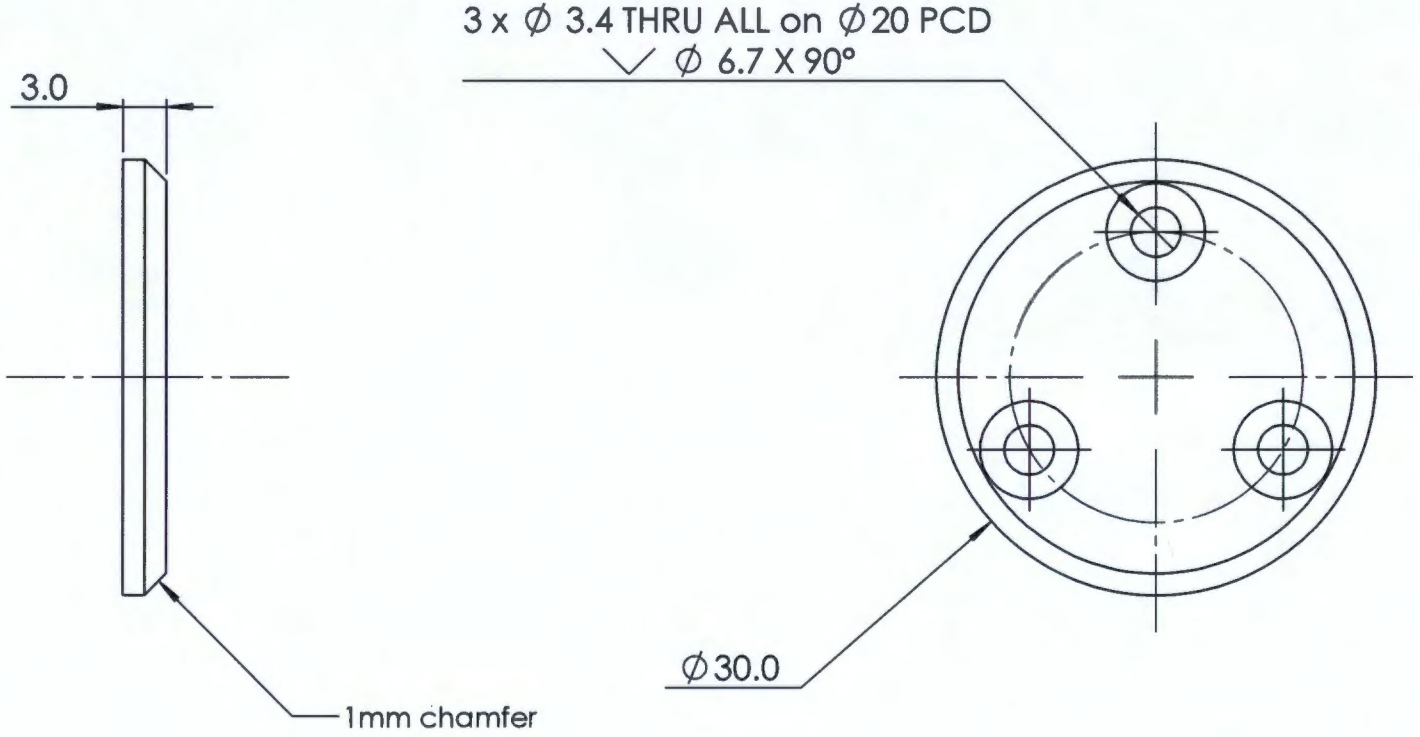

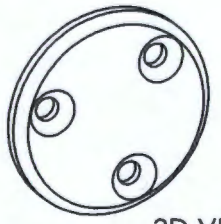

3D VIEW

- QUANTITY: 2off
- Part to be clean and free of burrs
- Please do not measure or infer dimensions from drawing
- Contact: Thomas Mathew (072 755 4007)

A4 Landscape	University of Cape Town Department of Mechanical Engineering			
	Title: Outer Hub			
Part Finish	Scale: 2:1	Date: 2014/05/02	Sheet 9	of 9
Material: Brass	Drawn By: Thomas J. Mathew		Drawing Number	

D

ELECTRICAL DOCUMENTATION

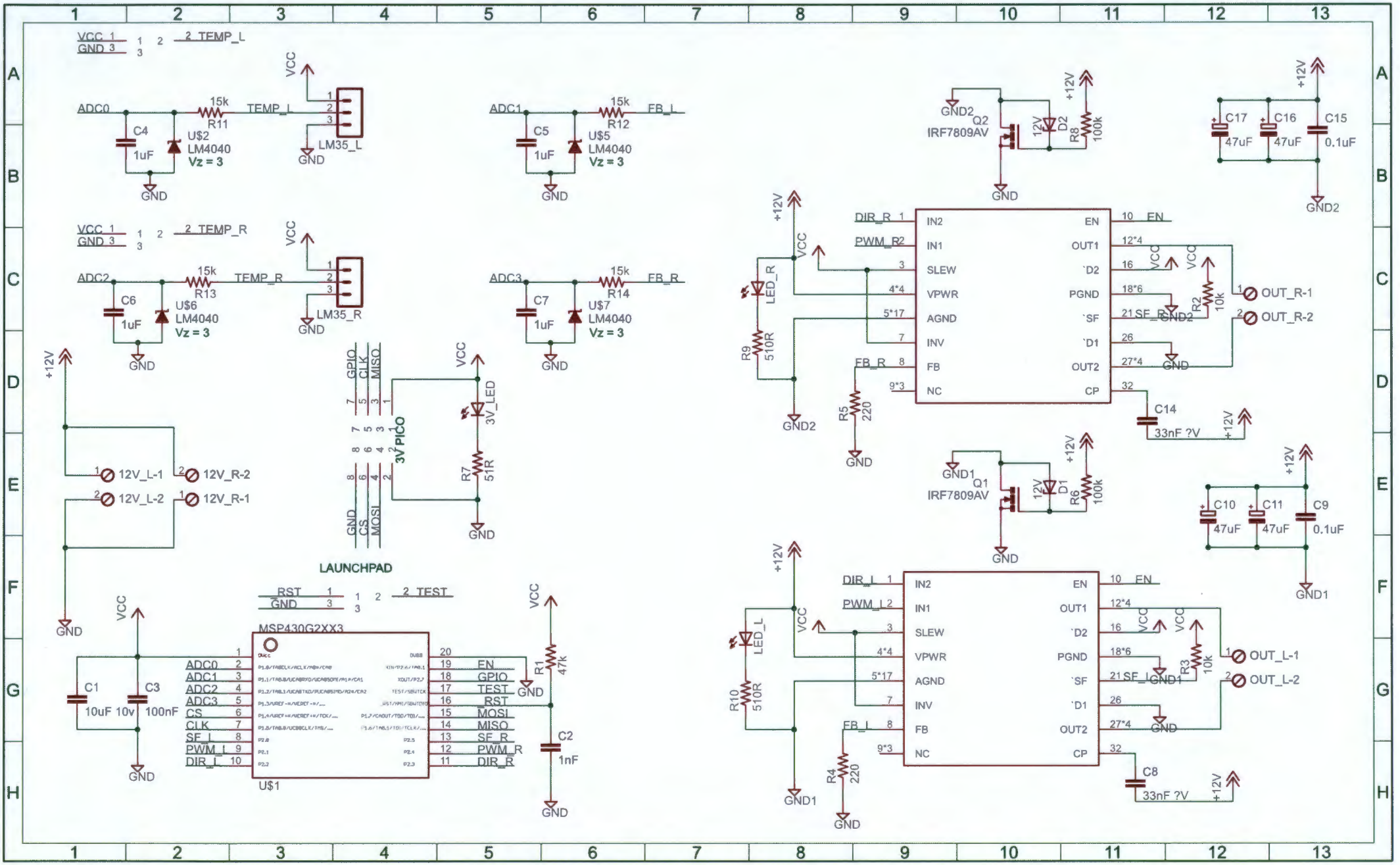
VCC 1
GND 3
2 TEMP_L
ADC0
15k
R11
TEMP_L
C4
1uF
U$2
LM4040
Vz = 3
LM35_L
ADC1
R12
FB_L
C5
U$5
VCC 1
GND 3
2 TEMP_R
ADC2
R13
TEMP_R
C6
U$6
LM35_R
ADC3
R14
FB_R
C7
U$7
+12V
12V_L-1
12V_R-2
12V_L-2
12V_R-1
GPIO
CLK
MISO
GND
CS
MOSI
3V PICO
3V_LED
R7
51R
LAUNCHPAD
RST 1
GND 3
2 TEST
MSP430G2XX3
ADC0
ADC1
ADC2
ADC3
CS
CLK
SF_I
PWM_I
DIR_I
EN
GPIO
TEST
RST
MISO
SF_R
PWM_R
DIR_R
R1
47k
C2
1nF
U$1
C1
10uF 10v
C3
100nF
GND2
Q2
IRF7809AV
12V
D2
R8
100k
C17
47uF
C16
47uF
C15
0.1uF
DIR_R
PWM_R
IN2
IN1
SLEW
VPWR
AGND
INV
FB
NC
EN
OUT1
`D2
PGND
`SF
`D1
OUT2
CP
LED_R
R9
510R
R5
220
R2
10k
OUT_R-1
OUT_R-2
C14
33nF ?V
GND1
Q1
D1
R6
C10
C11
C9
DIR_L
PWM_L
LED_L
R10
R4
R3
OUT_L-1
OUT_L-2
C8

E

BUDGET

The table below lists the costs of the materials and components required to manufacture a single platform. Most of the items listed below could be purchased at a reduced price at higher volume; however this estimate does not account for overhead costs such as electricity and labour which would increase with scaling.

Item	Cost (ZAR)
Motors	R1896
PCB Manufacture	R183
Motor Drivers	R225
Electrical Components	R150
HDPE stock	R309
Foam stock	R234
Brass stock	R75
Connectors	R58
Seal material	R23
Fasteners	R150
Wiring, misc	R100
TOTAL (ZAR)	R3353
Total (USD conversion 14/02/2014)	*US $287*

F

ETHICS CLEARANCE

EBE Faculty: Assessment of Ethics in Research Projects

Any person planning to undertake research in the Faculty of Engineering and the Built Environment at the University of Cape Town is required to complete this form before collecting or analysing data. When completed it should be submitted to the supervisor (where applicable) and from there to the Head of Department. If any of the questions below have been answered YES, and the applicant is NOT a fourth year student, the Head should forward this form for approval by the Faculty EIR committee: submit to Ms Zulpha Geyer (Zulpha.Geyer@uct.ac.za; Chem Eng Building, Ph 021 650 4791). Students must include a copy of the completed form with the thesis when it is submitted for examination.

Name of Principal Researcher/Student: Thomas J. Mathew Department: Mech Eng

If a Student: Degree: M.Sc (Eng) Supervisor: Trevor Cloete/Tracy Booysen

If a Research Contract indicate source of funding/sponsorship:

Research Project Title: SCARAB: Development of a Rugged, Low-Cost, Inspection-Class Robotic Platform

Overview of ethics issues in your research project:

Question 1: Is there a possibility that your research could cause harm to a third party (i.e. a person not involved in your project)?		**NO**
Question 2: Is your research making use of human subjects as sources of data? If your answer is YES, please complete Addendum 2.		**NO**
Question 3: Does your research involve the participation of or provision of services to communities? If your answer is YES, please complete Addendum 3.		**NO**
Question 4: If your research is sponsored, is there any potential for conflicts of interest? If your answer is YES, please complete Addendum 4		**NO**

If you have answered YES to any of the above questions, please append a copy of your research proposal, as well as any interview schedules or questionnaires (Addendum 1) and please complete further addenda as appropriate.

I hereby undertake to carry out my research in such a way that

- there is no apparent legal objection to the nature or the method of research; and
- the research will not compromise staff or students or the other responsibilities of the University;
- the stated objective will be achieved, and the findings will have a high degree of validity;
- limitations and alternative interpretations will be considered;
- the findings could be subject to peer review and publicly available; and
- I will comply with the conventions of copyright and avoid any practice that would constitute plagiarism.

Signed by:

	Full name and signature	Date
Principal Researcher/Student:	Thomas J. Mathew	16th February 2015

This application is approved by:

Supervisor (if applicable):		2015/02/16
HOD (or delegated nominee): Final authority for all assessments with NO to all questions and for all undergraduate research.		2015/02/16
Chair : Faculty EIR Committee For applicants other than undergraduate students who have answered YES to any of the above questions.		

BIBLIOGRAPHY

[1] T. Booysen and T. J. Mathew, "The Case for a General Purpose, First Response Rescue Robot," in *Proceedings of the 2014 PRASA, RobMech and AfLaT International Joint Symposium*, 2014. (Cited on pages iii and 9.)

[2] T. J. Mathew, G. Knox, W. K. Fong, T. Booysen, and S. Marais, "The Design of a Rugged, Low-Cost, Man-Packable Urban Search and Rescue Robotic System," in *Proceedings of the 2014 PRASA, RobMech and AfLaT International Joint Symposium*, 2014. (Cited on pages iii and 27.)

[3] Energia, "Energia Reference - Serial." [Online]. Available: http://energia.nu/Serial.html (Cited on pages xxi and 49.)

[4] iRobot Corporation, "iRobot FirstLook Media Kit." [Online]. Available: http://media.irobot.com/download/Firstlook_PR.jpeg (Cited on pages xxi and 62.)

[5] Faulhaber, "FAULHABER Miniature Drive Systems - Recon Scout IR." [Online]. Available: http://www.faulhaber.com/n810343/n.html (Cited on pages xxi, 63, and 115.)

[6] Tower Hobbies, "GWS 3.35" Shock Absorbing Wheel," 2015. [Online]. Available: http://www3.towerhobbies.com/cgi-bin/wtio001p?&I=LXHHZ4 (Cited on pages xxi and 63.)

[7] Wired4Space, "MSL Curiosity Rover wheel," 2012. [Online]. Available: http://www.wired4space.com/space/building-the-msl/attachment/msl-curiosity-rover-wheel (Cited on pages xxi and 64.)

[8] MFA Como Drills, "940D Series Datasheet." (Cited on pages xxiii, 113, and 114.)

[9] N. Tesla, "Method of and apparatus for controlling mechanism of moving vessels or vehicles," 1898. (Cited on pages 2 and 3.)

[10] L. C. B. J. Segovia, "IED Detonator," 2005. [Online]. Available: http://upload.wikimedia.org/wikipedia/commons/a/a5/IED_detonator.jpg (Cited on page 4.)

[11] L. D. Moore, "Roomba original," 2006. [Online]. Available: http://upload.wikimedia.org/wikipedia/commons/f/f5/Roomba_original.jpg (Cited on page 4.)

[12] B. KUKA Roboter GmbH, "Automation of Foundry with Robot." [Online]. Available: http://upload.wikimedia.org/wikipedia/commons/8/8a/Automation_of_foundry_with_robot.jpg (Cited on page 4.)

[13] FEMA 9356.1-PR, "Urban Search and Rescue Response System In Federal Disaster Operatios: Operations Manual," 2000. (Cited on page 3.)

[14] J. L. Casper, M. Micire, and R. R. Murphy, "Issues in intelligent robots for search and rescue," *Proc. SPIE*, vol. 4024, pp. 292–302, 2000. (Cited on page 3.)

[15] J. Blitch, "Artificial Intelligence Tecghnologies for Robot Assisted Urban Search and Rescue," *Expert Systems With Applications*, vol. 11, no. 2, pp. 109–124, 1996. (Cited on page 5.)

[16] R. G. Snyder, "Robots assist in search and rescue efforts at WTC," *IEEE Robotics and Automation Magazine*, vol. 8, no. 4, pp. 26–28, 2001. (Cited on page 5.)

[17] J. L. Casper and R. R. Murphy, "Human-robot interactions during the robot-assisted urban search and rescue response at the world trade center," *Systems, Man, and Cybernetics, Part B: ...*, vol. 33, no. 3, pp. 367–85, 2003. [Online]. Available: http://www.ncbi.nlm.nih.gov/pubmed/18238185http://ieeexplore.ieee.org/xpls/abs_all.jsp?arnumber=1200160 (Cited on pages 5, 10, and 18.)

[18] M. MacRae, "Rescue Robots Aid Japanese Recovery - ASME," 2011. [Online]. Available: https://www.asme.org/engineering-topics/articles/global-impact/rescue-robots-aid-japanese-recovery (Cited on page 5.)

[19] A. Boyle, "How high-tech is coming to the rescue," 2005. [Online]. Available: http://www.nbcnews.com/id/9131498/ns/technology_and_science-science/t/how-high-tech-coming-rescue/ (Cited on page 5.)

[20] G. Anthes, "Robots Gear Up for Disaster Response," *Communications of the ACM*, vol. 53, no. 4, 2010. (Cited on page 5.)

[21] A. Jacoff, E. Messina, H. Huang, and A. Virts, "Standard Test Methods For Response Robots," 2010. [Online]. Available: http://scholar.google.com/scholar?hl=en&btnG=Search&q=intitle:Standard+Test+Methods+For+Response+Robots#0 (Cited on pages 5, 24, and 100.)

[22] J. MacMillan, "Dawn, September 12th," 2001. [Online]. Available: http://trimdownglobal.com/trimdownlara/wp-content/uploads/sites/48/2014/09/11-settembre_6.jpg (Cited on page 10.)

[23] R. Murphy, "Trial by Fire - Activities of the Rescue Robots at the World Trade Center from 11-21 September 2001," *IEEE Robotics and Automation Magazine*, 2004. (Cited on page 11.)

[24] M. J. Micire, "Evolution and Field Performance of a Rescue Robot," *Journal of Field Robotics*, 2007. (Cited on page 10.)

[25] T. Linder, V. Tretyakov, S. Blumenthal, P. Molitor, H. Holz, R. Murphy, S. Tadokoro, and H. Surmann, "Rescue Robots at the Collapse of the Municipal Archive of Cologne City: a Field Report," 2010. (Cited on page 11.)

[26] T. Yoshida, K. Nagatani, T. S, T. Nishimura, and E. Koyanagi, "Improvements to the Rescue Robot Quince Toward Furure Indoor Surveillance Missions in the Fukushima Daiichi Nuclear Power Place," in *Robotics and Mechatronics Conference of South Africa (ROBOMECH)*, 2014. (Cited on page 11.)

[27] *United States Fire Administration and National Fire Association, Rescue Systems I*, 1993. (Cited on pages 11 and 12.)

[28] E. Dreyer and S. Marais, "Development of the RATEL UGV Platform." (Cited on page 13.)

[29] P. Henson and S. Marais, "The Utilization of Duplex Worm Gears in Robot Manipulator Arms: A Design, Build and Test Approach," in *Robotics and Mechatronics Conference of South Africa (ROBOMECH)*, 2012. (Cited on page 13.)

[30] Recon Robotics, "Recon Scout Throwbot LE Specification Sheet," 2011. [Online]. Available: http://www.reconrobotics.com/pdfs/REcon-Scout_Throwbot_Patrol_10-12.pdf (Cited on pages 14 and 15.)

[31] ——, "Recon Robotics - Throwbot XT with Audio." [Online]. Available: http://www.reconrobotics.com/products/Throwbot_XT_audio.cfm (Cited on pages 14 and 15.)

[32] ——, "Recon Scout XL Specification Sheet," 2013. [Online]. Available: http://www.recon-scout.com/pdfs/ReconRobotics_ReconScout_XL_4-13-v106.pdf (Cited on pages 14, 15, and 16.)

[33] ——, "Recon Scout IR Specification Sheet," Tech. Rep. 1, 2011. [Online]. Available: http://www.reconrobotics.com/pdfs/Recon_Scout_IR_LawEnf_Spec_Sheet.pdf (Cited on page 15.)

[34] ——, "Throwbot XT Specification Sheet," 2012. [Online]. Available: http://www.reconrobotics.com/pdfs/Recon_Robotics_Throwbot_Audio_XT_10-12.pdf (Cited on page 15.)

[35] P&R Infrared, "Recon Scout Throwbot - P&R Infrared." [Online]. Available: http://www.pr-infrared.com/shop/recon-scout-throwbot/ (Cited on page 15.)

[36] U.S. General Services Administration, "GSA Advantage! Store," 2013. [Online]. Available: https://www.gsaadvantage.gov/advantage/s/search.do?searchType=0&db=0&q=0:oreconrobotics&p=3 (Cited on page 15.)

[37] iRobot Corporation, "iRobot FirstLook Specifications," Tech. Rep., 2012. [Online]. Available: http://www.irobot.com/us/robots/defense/firstlook/~/media/Files/Robots/Defense/FirstLook/iRobot-110-FirstLook-Specs.ashx (Cited on page 17.)

[38] RecceRobotics, "RecceRobotics Products." [Online]. Available: http://www.recce-robotics.com/index-4.html#Adf (Cited on pages 17 and 18.)

[39] The Haddam Volunteer Fire Company, "What's It Weigh? Firefighter gear, piece by piece | The Haddams-Killingworth, CT Patch," 2013. [Online]. Available: http://patch.com/connecticut/thehaddams-killingworth/bp--whats-it-weigh-firefighter-gear-piece-by-piece (Cited on page 22.)

[40] International Association of Athletics Federations, "IAAF: Athletics Discipline - Hammer Throw - Disciplines - iaaf.org." [Online]. Available: http://www.iaaf.org/disciplines/throws/hammer-throw (Cited on page 22.)

[41] National Electrical Manufacturers Association, "ANSI/IEC 60529-2004: Degrees of Protection Provided by Enclosures (IP Code)," 2004. (Cited on page 24.)

[42] Crouzet, "DC geared motors - datasheet." (Cited on page 48.)

[43] RS Components, "Buy DC Geared Motors DC Geared Motor, Brushed, 12 V dc, 0.5 Nm, 54 rpm, 3 W Crouzet 82 861 010 online from RS for next day delivery." [Online]. Available: http://za.rs-online.com/web/p/dc-geared-motors/1784759/ (Cited on page 48.)

[44] Texas Intruments, "MSP430 Ultra-Low Power Microcontrollers Brochure." (Cited on page 49.)

[45] ——, "MSP430G2x53 / 2x13 Datasheet," 2013. (Cited on page 49.)

[46] Parallax Inc., "Pololu Dual MC33926 Motor Driver Carrier," 2011. (Cited on page 50.)

[47] Freescale Semiconductor, "MC33926 5.0A Throttle Control H-Bridge," pp. 2007–2009, 2009. (Cited on page 50.)

[48] ——, "Power Quad Flat No-Lead (PQFN) Package Design Guidelines AN2467," 2007. (Cited on page 54.)

[49] FLIR, "Quark LWIR Camera Cores | FLIR Systems." [Online]. Available: http://www.flir.com/cvs/cores/view/?id=51266 (Cited on page 60.)

[50] Recon Robotics, "Recon Scout - Robot Performance," 2015. [Online]. Available: http://www.reconrobotics.com/products/performance.cfm (Cited on page 62.)

[51] Innovative Industrial Solutions Inc., "Zistos Recon Scout Robot," 2012. [Online]. Available: http://i-i-s.net/alara-mobile-robotic-inspection/zistos-recon-scout-robot (Cited on page 63.)

[52] SoftWheel, "The Fluent Wheel," 2014. [Online]. Available: http://www.softwheel.technology/#!fluent/czgx (Cited on pages 64 and 65.)

[53] Jelly Products Ltd, "Loopwheels: bicycle wheels with integral suspension," 2015. [Online]. Available: http://www.loopwheels.com/about-loopwheels/ (Cited on page 64.)

[54] C. Baigh, "The ShockWheel invention by Chet Baigh," 2013. [Online]. Available: http://www.youtube.com/watch?v=O11hFiu43RQ (Cited on page 65.)

[55] Jelly Products Ltd, "loopwheels-25581.jpg," 2015. [Online]. Available: http://www.loopwheels.com/wp-content/uploads/2013/05/loopwheels-25581.jpg (Cited on page 65.)

[56] Measurement Specialities, "Model 834M1 Accelerometer Datasheet," 2011. (Cited on page 73.)

[57] H. Kolsky, "An Investigation of the Mechanical Properties of Materials at very High Rates of Loading," *Proceedings of the Physical Society. Section B*, vol. 62, no. 11, pp. 676–700, 1949. (Cited on page 121.)

[58] B. Hopkinson, "A Method of Measuring the Pressure Produced in the Detonation of High Explosives or by the Impact of Bullets," *Philosophical Transactions of the Royal Society of London.*

Series A, Containing Papers of a Mathematical or Physical Character, vol. 213, pp. 437–456, 1914. [Online]. Available: http://www.jstor.org/stable/91070?seq=1#page_scan_tab_contents (Cited on page 121.)

[59] T. J. Cloete and D. Bonorchis, "Stress Wave Propagation in Uniform Bars Impact Loading of a Uniform Bar," *Lecture Notes*, 2007. (Cited on page 121.)

[60] M. F. Spotts, *Mechanical Design Analysis*, 1st ed. Prentice-Hall, 1964. (Cited on page 121.)